Master's thesis

NTNU
Norwegian University of Science and Technology
Faculty of Information Technology and Electrical Engineering
Department of Electric Power Engineering

Ingvild G. Birkeland
Kristian Bjørgve

Reactive Power Considerations in Reliability Assessment of Power Systems

Master's thesis in Energy and Environmental Engineering
Supervisor: Vijay Venu Vadlamudi
June 2021

NTNU
Norwegian University of
Science and Technology

Ingvild G. Birkeland
Kristian Bjørgve

Reactive Power Considerations in Reliability Assessment of Power Systems

Master's thesis in Energy and Environmental Engineering
Supervisor: Vijay Venu Vadlamudi
June 2021

Norwegian University of Science and Technology
Faculty of Information Technology and Electrical Engineering
Department of Electric Power Engineering

NTNU
Kunnskap for en bedre verden

Abstract

The objective of this thesis is to implement a non-sequential Monte Carlo Simulation method with an AC optimal power flow approach in Python, for assessing the reliability of composite power systems. Further, the work concerns the implementation of a suitable method to account for reactive power considerations in composite system adequacy assessment in power system reliability studies.

Voltage issues in the power system are a growing concern due to, among other reasons, an increase in renewable power sources and heavier loaded systems. Voltage and reactive power are tightly interleaved, and little attention has been paid to the reactive power aspect in the field of power system reliability. Only a few publicly available sources investigate the topic, and even fewer provide a transparent method for replication that can enable further improvements. As such, one of the goals of this thesis work is to synthesise a reproducible method that distinctly differentiates between the curtailment due to active power shortage and the curtailment due to reactive power shortage in power system reliability studies. This includes presenting additional reliability indices based on an analytical method utilising optimal power flow, which takes reactive power considerations into account. A detailed description of the methodological approach with the necessary adaptations and assumptions is presented. In addition, a duplicate contingency state filtering technique is developed to increase the efficiency of the simulations.

Two scripts are developed in Python from the ground up to assess the so-called reactive power considerations (RPC) method. The first one relates to the standard composite system adequacy assessment, applied to the Roy Billinton Test System (RBTS) and the IEEE-Reliability Test System (IEEE RTS). The second one relates to the incorporation of exclusive reactive power considerations in the first one, and is applied to a modified IEEE 30-bus system. The validation is done through investigation of the results as well as a comparison of the obtained reliability indices with the ones available from respective methodological sources in the literature.

In the standard composite system adequacy assessment, the success of the developed Python scripts was verified. In-house composite system adequacy scripts in MATLAB,

available at the Department of Electric Power Engineering, were used in the development and verification of the Python code. A difference in the contingency solver routine was observed. However, the overall similarities between the reliability indices provide a proof of reproducibility of the adapted method.

The active power curtailment due to active power shortage was found to be differentiable from the curtailment caused by reactive power shortage.

It was also found that the reactive power considerations method could identify optimal locations for additional reactive power sources in the power system, ultimately giving valuable information to system planners and system operators.

The duplicate contingency state filter technique was implemented on all the three test systems, where it was found that it is possible to reduce the number of states considered by the contingency solver. As a consequence, a decrease in computational time was observed.

Sammendrag

Formålet med denne avhandlingen er å implementere en ikke-sekvensiell Monte Carlo-simuleringsmetode med bruk av AC optimal lastflyt i Python. Videre implementeres en metode som tar hensyn til reaktiv effekt i pålitelighetsstudier for kraftsystemer.

Spenningsproblemer er en økende utfordring i kraftsystemet, blant annet grunnet mer fornybar energiproduksjon, samt økt belastning i nettet generelt. Spenning og reaktiv effekt interagerer tett, og lite oppmerksomhet har blitt gitt dette aspektet i pålitelighetsstudier. Kun et fåtall offentlig publiserte kilder undersøker temaet, der enda færre presenterer metodologien på en transparent måte. Et formål med arbeidet utført i forbindelse med denne masteroppgaven er å bidra med en reproduserbar metode for å differensiere lastkutt forårsaket av mangel på aktiv effekt, fra lastkutt forårsaket av mangel på reaktiv effekt. Dette er representert av pålitelighetsindekser som spesifikt tar hensyn til reaktiv effekt. En detaljert beskrivelse av den metoden er også presentert, med nødvendige endringer og antagelser. I tillegg er en filtreringsmetode utviklet, der identiske systemtilstander filtreres ut for å effektivisere simuleringene.

To dataverktøy er utviklet i Python fra grunnen av til formålet. Den første for å validere den grunnleggende metoden for pålitelighetsanalyse, anvendt på testsystemene *Roy Billinton Test System (RBTS)* og *IEEE-Reliability Test System (IEEE RTS)*. Den andre er utviklet for å validere metoden for pålitelighetsanalyse med hensyn på reaktiv effekt, og er anvendt på det modifiserte testsystemet *IEEE 30-bus System*. Valideringen er utført ved analyse av resultater, og ved direkte sammenligning av pålitelighetsindekser fra de respektive metodologiske kildene i litteraturen.

Det utviklede dataverktøyet til den grunnleggende metoden for pålitelighetsanalyse i Python ble verifisert. Tilsvarende dataverktøy i MATLAB, tilgjengelig ved Institutt for elkraftteknikk på NTNU, er brukt til utvikling og verifisering av Python-koden. En rutineforskjell mellom verktøyene brukt til å løse systemtilstandene ble observert. Likevel er de gjennomgående likhetene mellom resultatene et bevis på at den adapterte metoden er reproduserbar.

I tillegg ble det verifisert at aktivt lastkutt forårsaket av mangel på aktiv effekt kan

differensieres fra aktivt lastkutt forårsaket av mangel på reaktiv effekt.

Pålitelighetsanalyse med hensyn på reaktiv effekt viste seg også å kunne identifisere optimal plassering av reaktiv kompensering i kraftsystemet. Dette bidrar med verdifull informasjon til systemplanleggere og systemoperatører.

Metoden for å filtrere ut identiske systemtilstander ble implementert på alle tre testsystemer. Det ble observert at antall systemtilstander som ble vurdert av systemløsningsverktøyet ble redusert merkbart.

Acknowledgement

We would like to thank our supervisor, Associate Professor Vijay Venu Vadlamudi at the Department of Electric Power Engineering, NTNU, for inspirational guidance throughout this Masters project work. We would especially like to thank him for introducing us to the interesting and fascinating field of power system reliability and Monte Carlo simulations. He has also always been available for discussions and inputs, which has been of great value to us.

Ingvild G. Birkeland Kristian Bjørgve

Trondheim, June 2021

Contents

List of Figures

List of Tables

Abbreviations

AC	Alternating Current
COPT	Capability Outage Probability Table
CV	Coefficient of Variation
CYPL	Constant Yearly Peak Load
DC	Direct Current
DPL	Daily Peak Load
EDLC	Expected Duration of Load Curtailments
EENS	Expected Energy Not Supplied
$EENS_P$	Expected Energy Not Supplied due to Active Power Shortages
$EENS_Q$	Expected Energy Not Supplied due to Reactive Power Shortages
EFLC	Expected Frequency of Load Curtailments
ELC	Expected Load Curtailment
ELC_P	Expected Active Power Curtailments due to Active Power Shortages
ELC_Q	Expected Active Power Curtailments due to Reactive Power Shortages
EQC_P	Expected Reactive Power Curtailments due to Active Power Shortages
EQC_Q	Expected Reactive Power Curtailments due to Reactive Power Shortages
EVarS	Expected Var Shortage due to voltage violation
$EVNS_P$	Expected Var Not Supplied due to Active Power Shortages
$EVNS_Q$	Expected Var Not Supplied due to Reactive Power Shortages
FOR	Forced Outage Rate

HLI	Hierarchical Level I
HLII	Hierarchical Level II
HLII RPC	Composite System Adequacy Assessment with Reactive Power Considerations
HLIII	Hierarchical Level III
HPL	Hourly Peak Load
IEAR	Interrupted Energy Assessment Rate
IEEE	Institute of Electrical and Electronics Engineers
IEEE RTS	IEEE-Reliability Test System
LDC	Load Duration Curve
LOL	Loss of Load
LOLE	Loss of Load Expectation
LOLF	Loss of Load Frequency
LOLP	Loss of Load Probability
MCS	Monte Carlo Simulation
NTNU	Norwegian University of Science and Technology
OPF	Optimal Power Flow
PLC	Probablity of Load Curtailments
PSR	Power System Reliability
RBTS	Roy Billinton Test System
SD	Standard Deviation
TTF	Time To Fail
TTR	Time To Repair

WPL	Weekly Peak Load
YPL	Yearly Peak Load

1 Introduction

1.1 Background

The structure of the power systems is changing. The ongoing electrification will lead to higher energy demand [1], again leading to heavier loaded power systems. The heavily loaded systems tend to have high reactive power demand and high reactive power loss in the transmission network [2]. Without adequate reactive power reserve, in the worst case, there could be blackouts.

There is also an increase in the penetration of renewable power sources, such as wind power and solar power [3]. These are stochastic sources of generation and often inverter-based, consequently providing limited reactive power generation and limited reactive power reserves. Reactive power plays a vital role in power system operation, especially concerning voltage stability. The increase of the converter based renewable power sources can therefore lead to lack of sufficient reactive power and, thus can lead to voltage stability issues [4].

Even though reactive power support and voltage control is a well-established ancillary service, little attention has been paid to reactive power aspects in power system reliability (PSR) studies [2]. In the present PSR methods, it is common to shed active power to alleviate the violated limits, even though this could have been mitigated by reactive power rescheduling or compensation [5]. Thus, it is valuable to be able to differentiate between the curtailments due to active power shortage and the curtailments due to reactive power shortage. The implementation of a tool that includes reactive power considerations in PSR assessment is therefore an important building block towards a more realistic representation of the planning and operation of the power system.

1.2 Scope

The overall objective of the thesis is to contribute to an in-house power system reliability tool in Python that evaluates composite power system adequacy by also taking reactive power considerations into account. This includes developing a tool to evaluate composite system adequacy in Python using the Monte Carlo Simulation (MCS) State Sampling method and an Optimal Power Flow (OPF) approach based on the framework developed by a previous Masters student Øystein Stake Laengen [6]. The code is further developed to include reactive power considerations in order to obtain a comprehensive picture of power system adequacy. This is done by adapting the method developed by Qin and Wang [2]. This development is also meant to investigate if it is possible differentiate the energy not supplied due to active power shortage from the energy not supplied due to reactive power shortage.

A justification for developing this tool in Python is that NTNU has started a transition to Python in the programming introductory courses. An adaptation to Python will create a foundation that will ensure the continuation of research in the field of PSR in a programming language the students are familiar with.

The work of this thesis is divided into two parts. The first part consists of implementing a composite system adequacy tool in Python using the non-sequential State Sampling method. The second part consists of further development of the code created in the first part to include reactive power considerations. Both parts are tested and verified using different test systems.

Contributions:

1. A composite system adequacy assessment software utilising MCS and AC-based OPF has been developed using an objective oriented approach in Python. This has been done as an adaptation of a methodological framework developed in a previous Masters thesis at NTNU [6], with suitable extensions. One extension is the implementation of Jacobian matrices in the OPF contingency solver, which increases the code efficiency. The software has also been generalised to allow for implementation on other real-life and test systems.

2. The composite system adequacy software has been extended to include reactive power considerations, by implementing the method presented in [2]. The software allows for differentiating the curtailments caused by active power shortage from the ones caused by reactive power shortage. In addition, the optimal location of reactive power compensation can be identified, giving valuable insight to system planners and system operators.

   An adaptation of the analytical method in [2] was necessary to fit the MCS and AC OPF approach used in this thesis, the adaptation being a restructuring of the algorithmic approach. The resulting framework and the reactive power-specific reliability indices have also been presented in a transparent and pedagogical manner to allow for the reproduction of the results of the thesis. In addition, the tool has been generalised to allow for implementation on other test systems.

3. A duplicate contingency state filtering technique has been proposed, implemented and validated. The duplicate state filter showed itself to be a valuable complement to the previous filter routines in [6], reducing the number of contingency states investigated in the OPF solver by up to 50 %.

4. The software is developed for in-house educational and research uses at the Department of Electric Power Engineering at NTNU. All the underlying approaches and results are presented in an as transparent manner as possible to allow for replication.

1.3 Structure of Thesis

Chapter 1 - *Introduction*: This chapter provides background, scope and structure of the thesis.

Chapter 2 - *Fundamentals of Power System Reliability*: Fundamental power system reliability theory is briefly presented in this chapter as a prelude to the thesis work.

Chapter 3 - *Power System Reliability Assessment*: This chapter complements the reliability theory presented in Chapter 2. In this chapter, standard power system reliability assessment methods are explained, focusing on Monte Carlo simulation methods. The

chapter presents the State Sampling method and the State Transition method, as well as convergence criteria of the Monte Carlo simulation methods.

For establishing narrative clarity and with an aim to make this thesis a complete and independent unit in and of itself, much of the content from Chapter 2 and Chapter 3 is a replication of the specialisation project work, with suitable extensions where deemed necessary.

The core of the thesis work is presented in Chapters 4 through 8.

Chapter 4 - *Composite System Adequacy Assessment*: This chapter explains the methodology for implementing HLII reliability assessment using Python, including the elements needed to build the HLII reliability assessment tool. The algorithmic approach is presented in a step-by-step representation. It is an important building block for later implementation of reactive power considerations in PSR.

Chapter 5 - *Reactive Power Considerations in Composite System Adequacy Assessment*: The reactive power considerations method originally put forward in [2] is presented, as well as an explanation of the adaptations and assumptions made to fit the MCS and OPF approach. This is followed by a step-by-step explanation of the applied methodological approach.

Chapter 6 - *Code Development and Programming*: The important aspects of the code development are presented in this chapter. This includes programming language and contingency state filtering application, as well as OPF solver options and parameter descriptions.

Chapter 7 - *Case Studies*: In this chapter, the developed standard HLII reliability assessment software is implemented and validated using the RBTS and the IEEE RTS test systems. Further, the developed reactive power considerations (RPC) tool at HLII is tested and validated using the IEEE 30-Bus System.

Chapter 8 - *Conclusions and Further Work*: A summary of the findings of this thesis work are presented in this chapter, followed by a suggestion of ideas for future work.

2 Fundamentals of Power System Reliability

In general, the function of power systems is to satisfy the load requirement, meaning that at all times there should be enough available capacity to meet the load demand of the consumers. This is somewhat the same as the definition of PSR, which can be defined as the ability of the system to provide an adequate supply of electrical energy. PSR assessment investigates all the aspects of the ability of the system to provide sufficient energy to the consumer [7].

PSR can be categorised into system adequacy and system security, as shown in Figure 2.1. System adequacy is about having sufficient facilities in the power system to satisfy the load demand and system operational constraints [8]. This includes generating facilities, transmission facilities and distribution facilities. System adequacy is therefore associated with the static conditions of the system, taking into account scheduled and unscheduled outages of the components of the system [9].

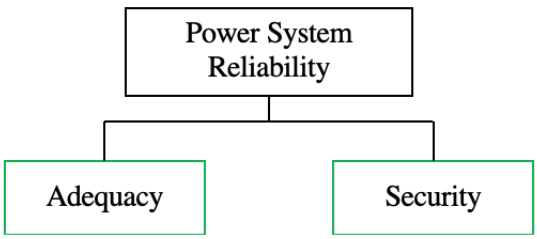

Figure 2.1: *Power system reliability. Figure adapted from [10].*

System security, on the other hand, is defined as the ability of the system to respond to disturbances within the system [7], e.g. short circuit events or sudden loss of components. This is associated with the dynamic conditions of the system, such as transients.

The thesis work will only cover the system adequacy and will therefore not cover transient conditions.

2.1 Hierarchical Levels

In the studies of power system reliability it is common to categorize the different parts of the power system in hierarchical levels based on their function [7]. The hierarchical structure is shown in Figure 2.2, where HLI covers the capability of the system to generate the energy demand in the system. HLII covers the ability of the system to supply the load demand in addition to the generation capability in HLI. HLIII includes both HLI and HLII, but also covers the distribution of energy and the end consumer loads [7].

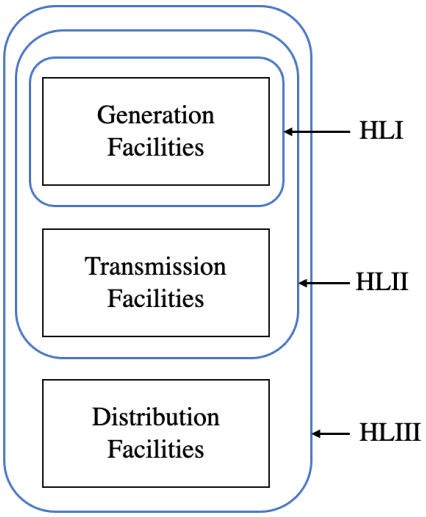

Figure 2.2: *Hierarchical levels in PSR. Figure adapted from [8].*

2.1.1 HLI

The HLI studies are covering the energy generation and the energy demand of the power system. It is assumed that the transmission and distribution of energy in the system have perfect reliability [7]. This means that the ability to meet the system energy demand is only depending on the reliability of the generation system, not considering any transmission or transformation constraints.

2.1.2 HLII

HLII also considers the transmission system, in addition to the generation capability. Several constraints covering the steady-state stability need to be included, such as voltage limits and line loading constraints [7]. In order to determine these aspects, power flow calculations of the different system states need to be conducted. Depending on the wanted accuracy, a DC approach or an AC approach can be used to solve the power flow of each system state. The DC approach neglect the reactive power flows and voltage limits of the system, but will in return simplify the calculations. The AC calculations take all previously neglected aspects into account, which increases the complexity [8]. As well as including deterministic data for the system, such as line impedances and voltage inputs, stochastic data for the failure and repair rates of the components are also taken into account.

2.1.3 HLIII

HLIII includes both hierarchical levels HLI and HLII as well as covering the distribution part of the network. HLIII studies are rarely conducted as a whole because of the large number of components and aspects that need to be included. In addition to generators and transmission lines, the HLIII studies include components such as transformers, switches, breakers and fuses. This increases the number of system states to an almost incomprehensible level. Thus, it is common to divide the analysis into separate entities [8]. The approach is often to analyse several sub parts of the system individually at the HLII level and combine the indices into a larger model with the specific HLIII studies [10].

The HLIII studies will not be investigated further in this thesis.

2.2 Two-state Model and Multi-state Model

In reliability assessment there are two state models that can be implemented: a two-state model and a multi-state model. The two-state model is defined so that each component

is either fully available or fully unavailable. The availability is given by the forced outage rate (FOR), which is the probability that the generator is fully unavailable, also written as p_{down}. If FOR is equal to 0.02, there is a 2 % probability that the generator is on outage and 98 % probability that it is available, written as p_{up}. The concept is also shown in Figure 2.3a

A multi-state model, on the other hand, has more than two states. These states are called derated states and are described by having partial availabilities, denoted p_i. An example of this is shown in Figure 2.3b. In the case shown in the figure, the system can be fully available, fully unavailable or derated with half the capacity available.

This thesis work will only cover the two-state model.

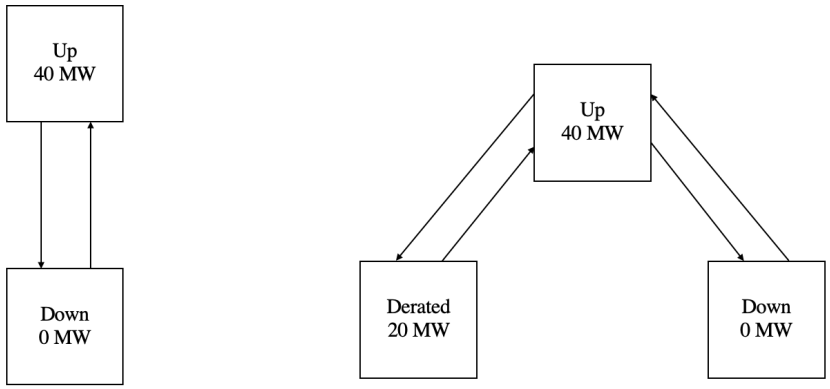

(a) *Two-state model.* **(b)** *Multi-state model.*

Figure 2.3: *Example of two-state model and multi-state model. Figure adapted from [11].*

2.3 Generation Model: Capability Outage Probability Table

The Capability Outage Probability Table (COPT) consists of all possible states of a generation system. Each state is represented by a given number of MW on outage, x_j, and its probability of occurrence. This include the individual probability, which is the probability that x_j MW is on outage, as well as the cumulative probability, which is the probability that x_j MW or more is on outage. The expressions for the individual

probability and the cumulative probability are shown in Equation (2.1) and Equation (2.2), respectively. $p(X)$ is the probability that there is X MW on outage and C is the total available generation capacity.

$$P(X = x_j) = p(X) \tag{2.1}$$

$$P(X \geq x_j) = \sum_{X=x_j}^{C} p(X) \tag{2.2}$$

To illustrate the COPT an example is made, shown in Table 2.1. The system consists of four generators of 10 MW, 10 MW, 20 MW and 30 MW. All the generators have a FOR value of 0.02. The table shows all the states the system can be in, j, as well as the capacity on outage at each state, x_j, individual probability, $P(X = x_j)$, and cumulative probability, $P(X \geq x_j)$. The individual probabilities are calculated for each state. The cumulative probability is calculated using Equation (2.2).

In Table 2.1 it can be observed that increasing capacity on outage corresponds to a decreasing individual probabiliy. This, however, does not account for state 4 with 40 MW on outage. This is due to the topology of the system, where there are several combinations that result in an outage of 40 MW. More combinations will therefore result in a higher probability.

A recursive algorithm can also be used to develop the COPT, where units are added sequentially [8]. It is then possible to directly calculate the cumulative probability without having to calculate the individual probabilities. It is therefore a more efficient way of calculating the elements of the COPT. The expression used to calculate cumulative probability using the recursive algorithm is shown in Equation (2.3). $P^{old}(X \geq x_j)$ is the cumulative probability of the outage state before the current generator is added. This way of calculating the cumulative can be done when evaluating both the two-state and multi-state model.

$$P(X \geq x_j) = (1 - FOR) \cdot P^{old}(X \geq x_j) + FOR \cdot P^{old}(X \geq x_j) \tag{2.3}$$

Table 2.1: *Example of a COPT. System consisting of* 4 *generators of* 10 MW, 10 MW, 20 MW *and* 30 MW, *where all have a FOR value of* 0.02.

State	Capacity outage	Individual probability	Cumulative probability
j	x_j	$p(X = x_j)$	$P(X \geq x_j)$
1	0	0.92236816	1.00000000
2	10	0.03764768	0.07763184
3	20	0.01920800	0.03998416
4	30	0.01959216	0.02077616
5	40	0.00077616	0.00118400
6	50	0.00039200	0.00040784
7	60	0.00001568	0.00001584
8	70	0.00000016	0.00000016

Furthermore, large systems usually have a large number of states, which again requires a large amount of calculations. This can be decreased by not including states with negligible probabilities of occurrence, e.g. if the probability is less that 10^{-8} [8]. In addition, it will reduce the computational time significantly.

2.4 Load Model

The load variations in the course of a certain time period, usually one year, can be represented through a load model. The time period can be divided into time increments depending on the wanted accuracy of the model. The simplest one is the constant yearly peak load (CYPL), which is represented by the peak load demand during a year. However, the accuracy of the model is low because CYPL is representative for only a few days of the year. A more accurate model is the weekly peak load (WPL), followed by the even more accurate models of daily peak load (DPL) and hourly peak load (HPL). Using DPL model and HPL model result in increased computational time, but they have a more accurate representation of the load variations during the year.

Chronological representations of CYPL, WPL, DPL and HPL are shown for the last 1000 hours of the year in Figure 2.4. It can be seen that each time increment is represented

by a specific load level. In addition, it should be noted that the CYPL is represented by the peak value of all weeks of WPL. WPL is then represented by the peak value of DPL for each week. The same accounts for HPL. Consequently, CYPL and WPL will give significantly more pessimistic load levels than DPL and HPL.

Another way of representing the load model is in descending order, often referred to as load duration curve (LDC) [8]. Figure 2.5 shows the LDC of each of the different load models. It can seen that the CYPL model is at constant 185 MW, whereas the load demand for HPL spans from 185 MW to 57 MW. Again, it is clear that CYPL is a much more pessimistic model than using e.g. HPL model.

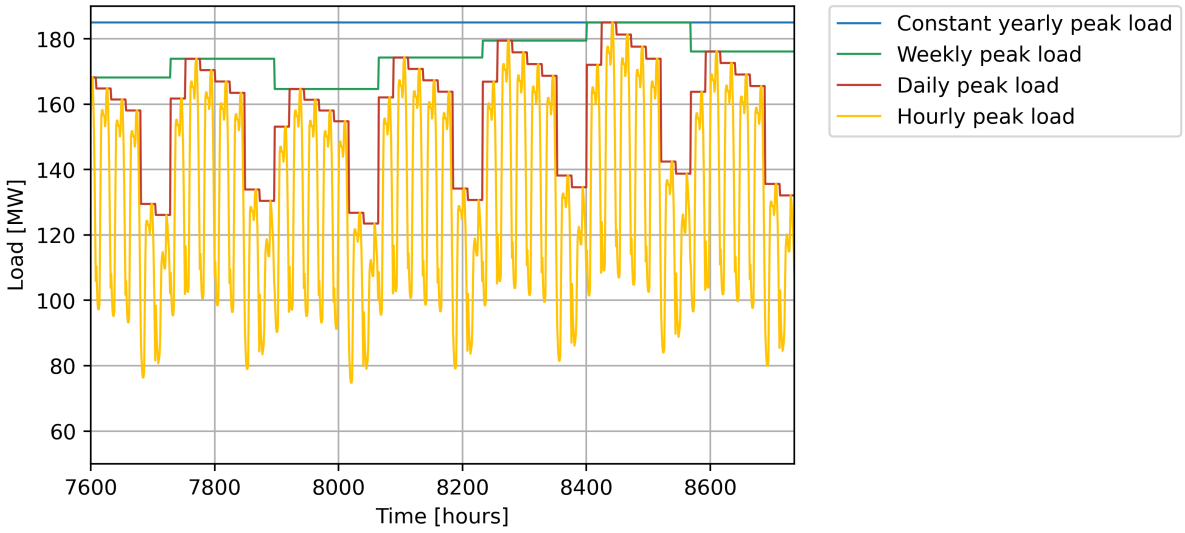

Figure 2.4: *Chronological load representation for the last 1000 hours of the year. Figure based on data from [12].*

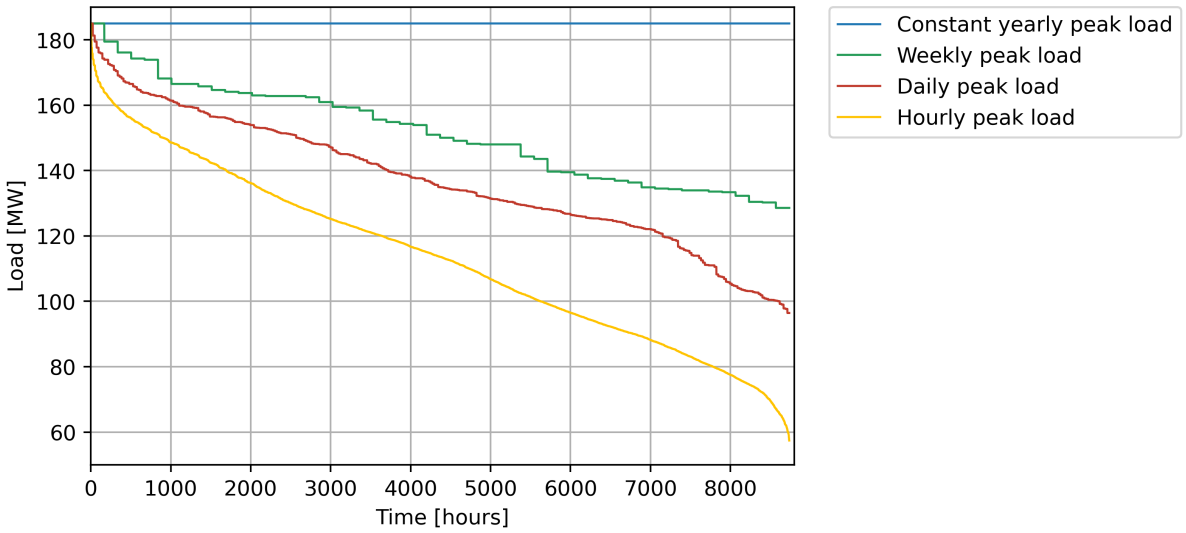

Figure 2.5: *Load duration curve representation of one year. Figure based on data from [12].*

2.5 Probabilistic Indices in HLI Assessment

The probabilistic indices used in PSR are based on loss of load (LOL) situations, and give adequacy indicators that describe the availability of the components of the power system and the whole system itself [10]. A LOL event is defined as a situation where the total demand is larger than the generation capacity [8]. For HLI assessment this is when the load demand is larger than the available generation capacity. In HLII assessment, on the other hand, this also includes insufficient transfer capability to meet the demand. A LOL situation can be caused by generation unit outages, transmission line failures or unexpected increase in demand. Also a combination of these causes can lead to LOL situations.

It should be noted that a LOL event does not mean that the load is actually lost and is not the same as a blackout. Usually when there is a capacity deficit, the system operator will perform mitigating actions in order to keep the power system balanced [13].

Another thing to note is that the reliability indices give indications and do not reflect e.g. the the ability of the system to withstand transients. It is only an indicator of the ability of the system to meet the given requirements [7].

The probabilistic indices can be divided into basic indices and severity based indices [14]. The basic indices reflect the frequency of the LOL events, but do not consider the severity. This is why the severity based indices are introduced. The result of these indices depends on the chosen model, whether it is CYPL model, WPL model, DPL model or HPL model [8].

In the following, the analytical indices will be explained first. Then, the Monte Carlo simulation indices are presented.

2.5.1 Loss of Load Probability (LOLP)

The loss of load probability (LOLP) is the probability of a LOL situation during a certain time period. In other words, the probability that the demand exceeds the available generation capacity. The LOLP index can be calculated using Equation (2.4), and is done by combining the COPT and the load model. In practice, it calculates the probability that the number of MW on outage, X, is larger than the installed capacity, C, minus the load at a specific time increment, L_t. Further, the LOLP can be used to calculate loss of load expectation (LOLE), which will be described later.

$$LOLP_t = P(X > C - L_t) \tag{2.4}$$

As an example to illustrate LOLP, a system equal to the one used to calculate the COPT in Table 2.1 is considered. The CYPL is set to 40 MW. The total capacity installed is 70 MW, so if more than 30 MW is on outage there will be a LOL situation. LOLP will in this case be equal to $P(X \geq 40) = 0.00118400$. In other words, the probability that the load demand will exceed the generation capacity is 0.00118400.

2.5.2 Loss of Load Expectation (LOLE)

The loss of load expectation (LOLE) is defined as the expected number of time increments there will be capacity shortage in a time period. LOLE is usually given in the units days per year or hours per year, depending on the model used. Equation (2.5) shows the

LOLE for the HPL model, where the probability of a LOL situation is multiplied by the time increment, ΔT. It can be seen that the probability in the expression is the same as LOLP, so that the expression can be rewritten as shown in Equation (2.6).

$$LOLE = \sum_{t=1}^{8760} P(X > C - L_t) \cdot \Delta T \Big[\frac{hours}{year}\Big] \tag{2.5}$$

$$LOLE = \sum_{t=1}^{8760} LOLP \cdot \Delta T \Big[\frac{hours}{year}\Big] \tag{2.6}$$

It should be noted that neither LOLP nor LOLE include the severity of the outage, which means a deficit of 5 MW will be treated the same way as a deficit of 50 MW. This is why the index expected energy not supplied (EENS) is introduced, which will be explained in the following section.

2.5.3 Expected Energy Not Supplied (EENS)

As mentioned, the expected energy not supplied (EENS) also defines the severity of the LOL events. It can be calculated using Equation (2.7), where the expression between the brackets gives the capacity deficit, which is multiplied with the probability of being in the specific outage state. This is calculated for each time increment and then summed to obtain the total energy deficit during a year. To obtain an accurate result, hourly time increments should be used. In literature, this index is also referred to as loss of energy expectation (LOEE) [8, 10].

$$EENS = \sum_{t=1}^{8760} \sum_{x_j=C-L_t}^{C} [x_j - (C - L_t)] \cdot p(X = x_j) \; [MWh/year] \tag{2.7}$$

EENS can be illustrated through a simple example where the EENS of one time increment is to be calculated. The load for a specific time increment is set to 40 MW and the total generation capacity is 70 MW, using the same system as in the COPT in Table 2.1. If there is an outage of 40 MW or more, there will be a capacity deficit. To calculate the EENS, each of the deficits caused by outages are multiplied with the individual probability, which

results in $EENS_t = 10\,\text{MW} \cdot 0.00077616 + 20\,\text{MW} \cdot 0.00039200 + 30\,\text{MW} \cdot 0.00001568 + 40\,\text{MW} \cdot 0.00000016 = 0.0160784\,\text{MWh}$.

2.5.4 Loss of Load Frequency (LOLF)

The loss of load frequency (LOLF) is defined as the number of times there is a transition from available state to unavailable state during a time period, usually a year. The expression is shown in Equation (2.8). x_t is equal to 1 if the previous state is available and the current state is unavailable. Otherwise, x_t is equal to 0.

$$LOLF = \sum_{t=1}^{3760} x_t \left[\frac{occ.}{year}\right], \; x_t = \begin{cases} 1 \text{ if } (x_t = 1) \cap (x_{t-1} = 0) \\ 0 \text{ if } (x_t = 1) \cap (x_{t-1} = 1) \\ 0 \text{ if } (x_t = 0) \cap (x_{t-1} = 1) \\ 0 \text{ if } (x_t = 0) \cap (x_{t-1} = 0) \end{cases} \tag{2.8}$$

LOLF can be described through an example, where the situation is shown in Figure 2.6. In the figure, the black areas define LOL events where generation capacity is lower than the demand. It can be seen that in $t = 3$ there will be a LOL event, so that $x_t = x_3 = 1$. This is also the situation in $t = 8$. In $t = 9$ the LOL situation is still present, but since $x_{t-1} = x_8 = 1$; $x_9 = 0$. For this small time period, the total LOLF is equal to 2 occurrences.

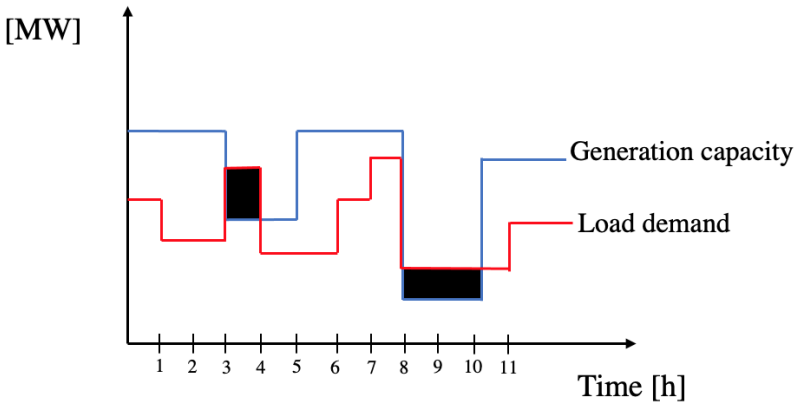

Figure 2.6: *Demand and available generation capacity during a time period of 11 hours.*

2.5.5 Probability Indices in Monte Carlo Simulations

In MCS the system is evaluated for each time increment during a period, usually a year. Since this is done by sampling random numbers from a probability distribution, the simulations should be executed for a significant number of years. Calculating average value will then be representative for evaluating the indices of the system .

When analysing the probability indices analytically, LOLE is usually calculated based on the calculations of LOLP. When executing MCS, on the other hand, the LOLP will be a "re-engineered" version. This is because in MCS the LOLP is calculated based on the simulated number of LOL events. The MCS method of calculating LOLE is therefore explained first in this section.

Equation (2.9) shows the expression for LOLE. It is executed for N years, and each year is divided into M time increments, usually hourly time increments. Each time increment will have an outcome x_j, which is equal to 1 if there is a LOL event and 0 if not. x_j is then multiplied with the time increment.

$$LOLE^{MCS} = \frac{\sum_{i=1}^{N}(\sum_{j=1}^{M} x_j \cdot \Delta T)}{N} \tag{2.9}$$

The LOLP index for MCS is, as mentioned, a "re-engineered" version. As shown in Equation (2.10), the LOLP can be obtained by dividing the LOLE by the number of time increments during the chosen period of time.

$$LOLP^{MCS} = \frac{\sum_{i=1}^{N}(\sum_{j=1}^{M} x_j \cdot \Delta T)}{N \cdot M} \tag{2.10}$$

MCS EENS is defined as shown in Equation (2.11). Compared to the expression of LOLE, there is an additional part Z_j. This is the energy deficit when the load demand is larger than the generating capacity. As for LOLE, x_j is equal to 1 if there is a deficit and 0 if not.

$$EENS^{MCS} = \frac{\sum_{i=1}^{N}(\sum_{j=1}^{M} x_j \cdot Z_j \cdot \Delta T)}{N} \tag{2.11}$$

In MCS, LOLF can be found by dividing the total number of occurrences by the number of years simulated, as shown in Equation (2.12). The number of occurrences are found by summing the occurrences of each time increment for all the simulations years and then dividing by the number of years.

$$LOLF^{MCS} = \frac{\sum_{i=1}^{N}(\sum_{j=1}^{M} x_j)}{N} \tag{2.12}$$

2.6 Probabilistic Indices in HLII Assessment

In literature, several variations of HLII indices are provided [8, 10, 15, 16, 17]. However, the descriptions, abbreviations and notations used for the indices differ. This is because the indices serve to give a variety of information depending on the objective of the assessment.

The indices used in HLI assessment can be extended to composite system adequacy indices [10]. As mentioned earlier, transmission lines are included in the HLII assessment in addition to generating capacity and load. This means that the LOL events do not only depend on the generators and the loads, but also on the capacity limits of the transmission lines.

The probabilistic indices of HLII can be divided into individual load point indices and system indices [15]. The individual load point indices are found by evaluating each load bus, whereas the system indices evaluates the overall adequacy of the system. The indices presented in this thesis work can be applied to both categories. Since there is a large variety of HLII indices, this thesis will only cover the ones that are considered the most general, which are found in [10, 15].

2.6.1 Probability of Load Curtailments (PLC)

Probability of Load Curtailments (PLC) gives the probability of load curtailment. This includes all states where there is load curtailment, given as S. The expression for PLC is shown in Equation (2.13), where x_i is the curtailment of system state i. It is represented

as a sum of all the states where there are curtailments.

$$PLC = \sum_{i \in S} P(x_i) \tag{2.13}$$

2.6.2 Expected Load Curtailments (ELC)

Expected Load Curtailments (ELC) gives the expected capacity deficit. This is given by Equation (2.14), where C_i is the curtailment of state i and F_i is the frequency of state i. F_i can be further explained through Equation (2.15), where N is the set of all possible departure rates corresponding to state i, p_i is the probability of state and δ_k is the departure rate.

$$ELC = \sum_{i \in S} C_i F_i \left[\frac{MW}{year}\right] \tag{2.14}$$

$$F_i = p_i \sum_{k \in N} \delta_k \tag{2.15}$$

2.6.3 Expected Frequency of Load Curtailments (EFLC)

Expected Frequency of Load Curtailments (EFLC) is defined as the sum of all occurrences of load curtailment over a chosen time period, usually a year. This is shown in Equation (2.16), where the chosen model is HPL. x_t is equal to 1 if there is a load curtailment in time t that was not present in time $t-1$, and equal to 0 otherwise.

$$EFLC = \sum_{t=1}^{3760} x_t \left[\frac{occ.}{year}\right], \; x_t = \begin{cases} 1 \text{ if } (x_t = 1) \cap (x_{t-1} = 0) \\ 0 \text{ if } (x_t = 1) \cap (x_{t-1} = 1) \\ 0 \text{ if } (x_t = 0) \cap (x_{t-1} = 1) \\ 0 \text{ if } (x_t = 0) \cap (x_{t-1} = 0) \end{cases} \tag{2.16}$$

2.6.4 Expected Duration of Load Curtailments (EDLC)

Expected Duration of Load Curtailments (EDLC) is defined as the expected number of hours or days where there are load curtailments during a year, depending on the model used. This is shown in Equation (2.17) and Equation (2.18) where HPL and and DPL are used, respectively.

$$EDLC = PLC \cdot 8760 \left[\frac{hours}{year}\right] \tag{2.17}$$

$$EDLC = PLC \cdot 365 \left[\frac{days}{year}\right] \tag{2.18}$$

2.6.5 EENS

EENS is an important index in composite system adequacy assessment [10]. It is more or less the same as for HLI, which is given analytically in Equation (2.7) and for MCS in Equation (2.11). The difference between HLI and HLII is that transmission lines are taken into account and can therefore be a source of failure, so that the EENS for composite systems is as shown in Equation (2.19). x_j is the curtailment in MW, and $p(X = x_j)$ is the probability that the curtailment is x_j.

$$EENS = \sum_{t=1}^{8760} \sum_{x_j=C-L_{tot}}^{C} [x_j - (C - L_{tot})] \cdot p(X = x_j) \left[\frac{MWh}{year}\right] \tag{2.19}$$

3 Power System Reliability Assessment

In general, PSR adequacy assessment can be divided into deterministic and probabilistic methods, as shown in Figure 3.1. The deterministic methods estimate the generation capacity and the network capacity needed in the system. However, they do not take into account the random behavior of the system such as uncertainty of load variations and random failures [18]. Probabilistic reliability assessment, on the other hand, deals with the stochastic nature of the power system.

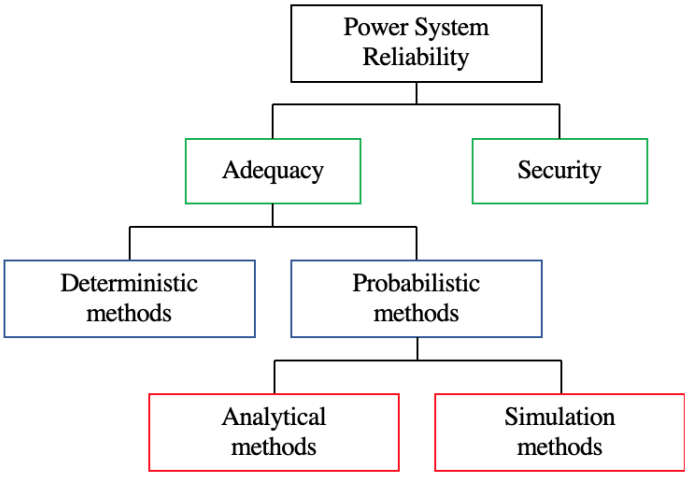

Figure 3.1: *Power system reliability methods. Figure drawn based on theory from [7, 19].*

The probabilistic methods can further be divided into analytical techniques and simulation techniques [19]. The analytical techniques use mathematical equations to evaluate the adequacy of the system, while the simulation techniques simulate the random behaviour of the system. Monte Carlo simulation (MCS) is an example of a simulation technique commonly used to evaluate PSR, which will be described later in this chapter.

Similar for the two techniques is that they require good understanding of the system evaluated. According to [10], when evaluating the reliability of a system it is important to:

- *"Understand the way in which the components and system operate.*
- *Identify the way in which they can fail.*
- *Deduce the consequences of the failures.*

– *Derive models to represent these characteristics.*

– *Then select the evaluation technique."*

Analytical reliability methods will not be treated in this thesis, and will not be further discussed. The focus will instead be on simulation methods, more specifically on MCS methods, which will be explained in the following section.

3.1 Monte Carlo Simulation Methods

In reliability assessment, Monte Carlo Simulation (MCS) is a method used to sample system states. This is done by using random numbers from probability distributions. With this method it is possible to simulate the random behavior of a system. The simulations are often conducted over a large number of years, which treat the problem as a series of a real experiments [8]. It is then possible to obtain realistic index values.

In practice, MCS is done by generating random numbers and then deciding the system state of the components at a specific time. There are several advantages of MCS compared to analytical methods. One advantage is that it is possible to include certain processes that must be approximated analytically. Also, MCS is not dependent on the size of the system, and works better than analytical methods when evaluating larger systems. Another advantage is that MCS can simulate the probability distributions of the failure events and the repair events, which in general is difficult to manage with analytical methods.

The MCS methods can be divided into sequential and non-sequential simulation methods. The non-sequential MCS methods sample a set of system states through generating random variates, where the system states are independent of each other. The sequential MCS methods generate a sequence of system states, where the current state depends on the previous state. The methods that will be explained later in this chapter are the State Sampling method and the State Transition method, where the explanations are based on the approach of [10].

Before explaining the MCS methods, it is necessary to obtain mathematical understand-

ing of the random variates and probability distributions. In addition, after the MCS methods are explained, the convergence criteria of the MCS will be presented.

3.1.1 Random Variate Generation in MCS

The definition of a random variate is a random variable that follows a given distribution [10]. One common distribution is the uniform distribution. This usually has range [0,1], where any interval of the same length have the same probability of occurrence.

Another distribution that is commonly used is the exponential distribution, given by the expression in Equation (3.1). X is the random variate and λ is the shape parameter.

$$f(X) = \lambda \cdot e^{-\lambda \cdot X} \tag{3.1}$$

However, when generating random variates using most programming languages it is only possible to generate numbers with a uniform distribution. It is therefore necessary to define the inverse transform of the exponential distribution to be able to obtain variables with exponential distribution. This is done by defining the cumulative distribution function of the exponential function, given in Equation (3.2).

$$F(X) = 1 - e^{-\lambda \cdot X} \tag{3.2}$$

The inverse transform is then obtained by setting Equation (3.2) equal to U, a number that is uniformly distributed. The equation is then solved for X. This is shown in Equation (3.3). The distributions of U and $1 - U$ are equal when the range of U is [0,1] [10].

$$X = F^{-1}(U) = -\frac{1}{\lambda} \cdot \ln(1 - U) = -\frac{1}{\lambda} \cdot \ln(U) \tag{3.3}$$

The method of obtaining random variates with an exponential distribution is used for example in the State Transition method, where time to failure and time to repair follow this distribution.

3.1.2 State Sampling Method

The first method to be explained is the State Sampling method. This is a non-sequential method, meaning that it is chronologically and sequentially independent. Each component of the system is sampled, where the components can be described by a uniform distribution function with a range [0,1]. A random variate U is generated for each system component, and is then compared against the FOR value of the components. If U is larger or equal to the FOR value, the component is available. If U i smaller, the component is unavailable. The total available capacity gives the state of the whole system. When executing the sampling over a large number of simulation years, realistic indices can be obtained. However, it is not possible to obtain the frequency and duration, which is the main disadvantage of the method.

The method can be explained through an example system of four generators of 40 MW with FOR values equal to 0.3. In this example 5 samples are obtained, where U_1, U_2, U_3 and U_4 are the random variates of each generator. S_1, S_2, S_3 and S_4 are the states of the components, where 0 means it is available and 1 means it is unavailable. The resulting available capacity of each sample is shown in Table 3.1.

Table 3.1: *Example of State Sampling Method for a system with four generators.*

Sample	Generated numbers $\{U_1\ U_2\ U_3\ U_4\}$	System state $\{S_1\ S_2\ S_3\ S_4\}$	Available capacity [MW]
1	{0.9 0.3 0.6 0.7}	{0 0 0 0}	160
2	{0.2 0.4 0.7 0.1}	{1 0 0 1}	80
3	{0.5 0.8 0.3 0.1}	{0 0 0 1}	120
4	{0.1 0.1 0.2 0.1}	{1 1 1 1}	0
5	{0.2 0.8 0.8 0.4}	{1 0 0 0}	120

3.1.3 State Transition Method

The State Transition method is a sequential method, meaning that the next step is dependent of the previous. Therefore, the simulations must be performed in chronological

order. Unlike the State Sampling method, this method focuses on the state transitions of the whole system instead of at component level. By utilising the State Transition method it is also possible to obtain the frequency and duration of the states, so that e.g. the LOLF index can be calculated.

The method is based on generating a random number to obtain the time to the next event. The event is in this case the change of state of a component. This can be either time to fail (TTF) or time to repair (TTR), depending on the current state of the system. It is important to note that TTF and TTR have exponential distributions, as shown in Equation (3.1). This also accounts for the total transition time T. The shape parameter, λ, of T is the sum of TTF and TTR of each component, depending on the state of the components. This is shown in Equation (3.4), where m is the total number of components. T can also be defined as in Equation (3.5), where the transition to the next state for the whole system is the transition time of the component that changes state earliest.

$$\lambda = \sum_{i=1}^{m} \lambda_i \tag{3.4}$$

$$T = min\{T_i\} \tag{3.5}$$

To explain the method, the current state can be defined as $S^{(k)}$. There is a transition from this state to the next state, which can be defined as $S^{(k+1)}$. This happens in time equal to 0, which is defined as t_0. The probability that the system state $S^{(k+1)}$ is a result of a transition of component j can be explained through the conditional probability $P_j = P(T_j = t_0 | T = t_0)$. Equation (3.6) shows the the derived expression, where the right hand side of the equation can be explained as the probability that the system reaches state j. A more thorough mathematical proof of Equation (3.6) can be found in [10].

$$P_j = P(T_j = t_0 | T = t_0) = \frac{P(T_j = t_0 \cap T = t_0)}{P(T = t_0)} = \frac{\lambda_j}{\sum_{i=1}^{m} \lambda_i} \tag{3.6}$$

The sum of the probability of all the states can be expressed by Equation (3.7) and is equal to 1. This means that when sampling the next state it is certain that a transition

will be a result of reaching one of the m states.

$$\sum_{j=1}^{m} P_j = \sum_{j=1}^{m} \frac{\lambda_j}{\sum_{i=1}^{m} \lambda_i} = \frac{\sum_{j=1}^{m} \lambda_j}{\sum_{i=1}^{m} \lambda_i} = 1 \tag{3.7}$$

When sampling, a uniformly distributed random number U_1 is generated, which falls into one of the m possible intervals. This is shown in Figure 3.2, and gives the next system state. If U_1 falls into interval j, it means that the next system transition is a result of a transition of component j. In practice, if component j is available, the state will change to unavailable, and vice versa.

Then, a new number U_2 is generated to find the time until next state transition. This is exponential distributed, and therefore Equation (3.3) should be used, with shape parameter equal to the sum of either TTF or TTR of each component, depending on the state.

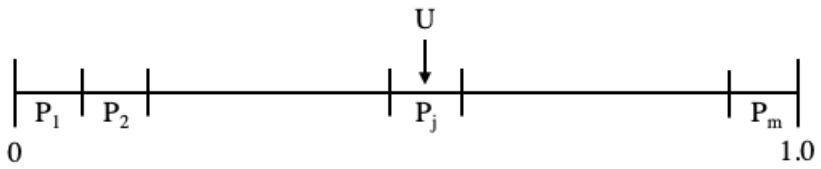

Figure 3.2: *Probability of state intervals. Figure adapted from [10].*

The method can be further explained using an example system of four generators that are all initially available. Each of them has a transition rate, λ_i, given as number of transitions per year. The probability of state, P_j, is calculated using Equation (3.6). The upper limit interval defines the intervals, as shown in Figure 3.2.

A random number U is generated, $U = 0.50$. This number is a part of the interval of the third generator, G_3. The current state of G_3 is available, so the state will change to unavailable. The transition rate is now changed to TTR. The transition probabilities and upper limits are updated, as shown in Table 3.3. It can be seen that the probability of a transition of G_3 is significantly higher than the possibilities of other transitions, because the repair rate is much higher than the failure rate.

To obtain the time to the next event, i.e. time to next transition, a new number is

Table 3.2: *$S^{(k)}$ for the state transition example.*

Generating Unit	State	λ_i [#/year]	P_j	Upper Limit of Interval
G_1	Up	2.0	0.2000	0.2000
G_2	Up	2.0	0.2000	0.4000
G_3	Up	2.0	0.2000	0.6000
G_4	Up	4.0	0.4000	1.0000

generated using Equation (3.3) and the updated λ based on the new system state. By repeating this over a total time of e.g. a year and again repeating for a large number of years, it is possible to obtain representative values of the indices.

Table 3.3: *$S^{(k+1)}$ for the state transition example.*

Generating Unit	State	λ_i [#/year]	P_j	Upper Limit of Interval
G_1	Up	2.0	0.0294	0.0294
G_2	Up	2.0	0.0294	0.0588
G_3	Down	100.0	0.8824	0.9412
G_4	Up	4.0	0.0588	1.0000

3.2 Convergence Criteria of MCS

Since the MCS is based on generating random numbers, the convergence is a fluctuating process. This means that adding a few more samples will not necessarily lead to better accuracy [10]. However, the range errors will be smaller as the number of samples increase. This is called the law of large numbers, and can be defined as follows: The sample mean approaches the true mean when the number of samples tends towards infinity. This means that having a large number of samples will decrease the variance and the value will approach the true mean. Therefore, the variance can be used to find the convergence criteria of the MCS.

The coefficient of variation (CV) is a good measure of the precision and is given by

Equation (3.8). This can be used as a convergence criterion in reliability assessment using MCS. s(X) is the standard deviation (SD) of a sample, N is the number of samples, and E(X) is the population mean. A more thorough explanation of standard deviation and population mean can be found in books on statistics, eg. in [20]. It can be seen from the expression that in order to minimize the CV, the variance should be decreased or the number of samples should be increased.

$$\beta = \frac{s(X)}{\sqrt{N} \cdot E(X)} \tag{3.8}$$

It should also be noted that there is a difference in convergence speed of the different indices used in PSR adequacy assessment. The convergence speed of EENS is the slowest, and therefore this index should be used when calculating the CV to find the number of required simulation years or required number of samples [10]. In this way it is possible to obtain accuracy in the evaluation of the reliability of a system.

3.2.1 Deciding the Appropriate CV

As mentioned, the convergence criteria of MCS decides how many samples or how many simulation years are needed in order to get an accurate evaluation of the reliability of a system. The decided CV will essentially be a compromise between the accuracy of the evaluation and the computational time of the MCS. In [10] it is written *"A reasonable stopping criterion should be specified for a particular system in order to provide a compromise between the accuracy and the computing time. This may need to be examined in some detail for the configuration in question."*. Thus, the chosen CV should also be based on the system that is used.

There are different methods of using the CV to decide how many years are sufficient to get an accurate reliability evaluation [10]. The first one is to end the simulations when the CV reaches a given tolerance value. In practice the CV is calculated after each sampled state, and when the CV is below a set value the simulations terminate and the final indices are calculated. Another method is to decide a fixed amount of simulation years or a fixed amount of samples and then calculate the CV. If convergence is not reached,

the amount of years simulated should be set higher. This means that in some cases more years are simulated than necessary, leading to an unnecessarily high computational time.

4 Composite System Adequacy Assessment

As a stepping stone towards implementing reactive power considerations in HLII assessment, an adaptation of the MCS State Sampling method for composite system adequacy assessment in [6] is considered necessary.

The composite system adequacy assessment, or HLII assessment for short, described in Section 2.1, includes the availability of both generators and transmission lines. This causes the need for a power flow based analysis, to more accurately represent the behaviour and the physical limitations of the power system considered. This can either be done with a DC-based approach or an AC-based approach. In this thesis only the AC-based power flow analysis is utilised, due to the reactive power considerations implementation later on.

There are numerous methodological approaches in the field composite system adequacy, where the most suited approach for any given case depends on which aspects are applied, or what numerical accuracy is desired. The applied method of [6] used in this thesis, encompasses the aforementioned MCS State Sampling method. The sampled contingency states are represented as OPF problems, where the solutions to these contribute to the expectancy of the behaviour of the investigated system. This expectancy is represented by a selected set of composite system PSR indices.

This chapter aims to gather the key aspects and building blocks used in the utilised composite system assessment method of [6], including necessary adaptations and expansions. The algorithmic approach describes the overall application when developing the code utilising an object oriented approach in Python.

4.1 Network Model and Network Equations

When defining the composite system adequacy formulation and simulation process, the network model should be presented briefly. This is so in order to have a clear view of the power system theory needed when defining the OPF problems and the system constraints later in this chapter.

There are several ways of representing a network model, and in this thesis the bus injection model is utilised. It focuses on nodal variables, i.e. variables at each bus such as voltages, currents and power injections. The advantage of using this model is that the power flow equations can be given in a compact form [21]. It should, however, be noted that it does not directly deal with power flow on the individual branches [22].

Further, a branch between two buses can be represented by the π-model, shown in Figure 4.1. It consists of a series impedance, y_{ij}, and a shunt susceptance, y_{ij}^{sh}. The shunt susceptance is equally divided between the two buses. The power flow of a line can be calculated using the parameters of the π-model.

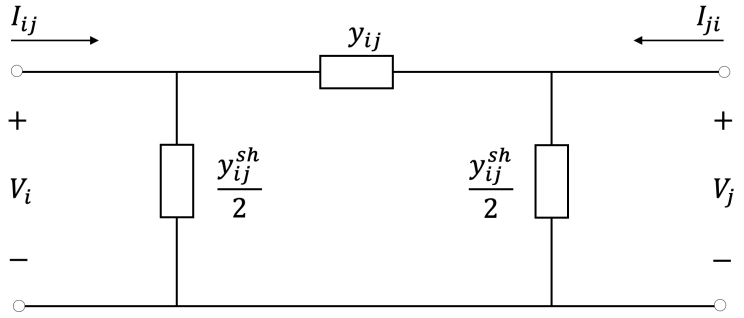

Figure 4.1: *Nominal π model for a medium length line. Figure adapted from [23].*

Equation (4.1) shows the bus admittance matrix of the system in Figure 4.1. A diagonal element of the matrix is a sum of the admittances of the lines connected to the bus under consideration as well as the shunt admittance(s) connected to the bus. An off-diagonal element of the matrix is the negative value of the total admittance of the line(s) connected between the two buses under consideration. It can also be noted that the admittance matrix can be represented by a conductance matrix and a susceptance matrix, as shown in Equation (4.2).

$$Y_{bus} = \begin{bmatrix} Y_{ii} & Y_{ij} \\ Y_{ji} & Y_{jj} \end{bmatrix} = \begin{bmatrix} y_{ij} + \frac{y_{ij}^{sh}}{2} & -y_{ij} \\ -y_{ij} & y_{ij} + \frac{y_{ij}^{sh}}{2} \end{bmatrix} \tag{4.1}$$

$$[Y_{bus}] = [G_{bus}] + j[B_{bus}] \tag{4.2}$$

The active and reactive power injections at each bus can be described through AC power

flow equations, shown in Equation (4.3) and Equation (4.4). These are the equations used in the bus injection model. A more thorough explanation and derivation of the power flow equations can be found in books on Power Flow Analysis, such as [23]. The presented equations are used later when defining the OPF problem, including the Jacobian matrices.

$$P_i(V,\delta) = V_i \cdot \sum_{j=1}^{k} V_j \Big[G_{ij}\cos(\delta_i - \delta_j) + B_{ij}\sin(\delta_i - \delta_j) \Big] \tag{4.3}$$

$$Q_i(V,\delta) = V_i \cdot \sum_{j=1}^{k} V_j \Big[G_{ij}\sin(\delta_i - \delta_j) - B_{ij}\cos(\delta_i - \delta_j) \Big] \tag{4.4}$$

Further, the current on a line between two buses can be described using Equation (4.5). However, it is desirable to formulate the current using nodal variables [24]. By using Euler's identity, $e^{j\phi} = \cos\phi + j\sin\phi$, the absolute value of the current can be written as shown in Equation (4.6). This will also be used when defining the OPF problem.

$$|I_{ij}| = |V_i - V_j| \cdot |y_{ij}| \tag{4.5}$$

$$|I_{ij}| = \sqrt{\Big(V_i \cdot \cos\delta_i - V_j \cdot \cos\delta_j\Big)^2 + \Big(V_i \cdot \sin\delta_i - V_j \cdot \sin\delta_j\Big)^2} \cdot |y_{ij}| \tag{4.6}$$

4.2 Elements of HLII Assessment

4.2.1 Sampling of System States

When sampling each system state using the State Sampling method, random numbers, U, with a uniform distribution in the interval [0,1] are generated to evaluate whether the generators and lines can be considered available or unavailable. Unlike the most common sampling approaches, the system states can be sampled using a simultaneous sampling approach instead of looping through each hour of each year. This is done by initially sampling all generator and line states, saving them in a $n_{components} \times n_{states}$ matrix,

shown in Equation (4.7). The subscript values describe the component number and the state number.

Another matrix of the same size is then made, consisting of the FOR values of each component, shown in Equation (4.8). The subscript value is the component number. It can be noted that the FOR values of the components are the same for all generated states. The corresponding elements of the state matrix and the FOR matrix are compared to decide whether the components of each state, S, are available (0) or unavailable (1), represented by Equation (4.9).

$$M_{samples} = \begin{bmatrix} U_{1,1} & U_{1,2} & \cdots & U_{1,n_{states}} \\ U_{2,1} & U_{2,2} & \cdots & U_{2,n_{states}} \\ \vdots & & \ddots & \vdots \\ U_{n_{comp.},1} & U_{n_{comp.},2} & \cdots & U_{n_{comp.},n_{states}} \end{bmatrix} \tag{4.7}$$

$$M_{FOR} = \begin{bmatrix} FOR_1 & FOR_1 & \cdots & FOR_1 \\ FOR_2 & FOR_2 & \cdots & FOR_2 \\ \vdots & & \ddots & \vdots \\ FOR_{n_{comp}} & FOR_{n_{comp}} & \cdots & FOR_{n_{comp}} \end{bmatrix} \tag{4.8}$$

$$M_{states} = \begin{bmatrix} S_{1,1} & S_{1,2} & \cdots & S_{1,n_{states}} \\ S_{2,1} & S_{2,2} & \cdots & S_{2,n_{states}} \\ \vdots & & \ddots & \vdots \\ S_{n_{comp.},1} & S_{n_{comp.},2} & \cdots & S_{n_{comp.},S_{states}} \end{bmatrix} \tag{4.9}$$

To further explain the sampling approach, an example is made, where 3 system states are investigated. The system consists of 3 buses, where Bus 1 has 2 generators, and 3 lines are connecting the buses. This is shown in Figure 4.2. The FOR values of each component, given in the figure, are used to make M_{FOR}, shown in Equation (4.10). Random numbers are generated to make the 3 system states, and the corresponding $M_{samples}$ can also be seen in Equation (4.10). The M_{FOR} matrix is compared against $M_{samples}$ element-wise to check if each component is available or not. The resulting matrix, M_{states}, shows the

availability of the components for the 3 system states.

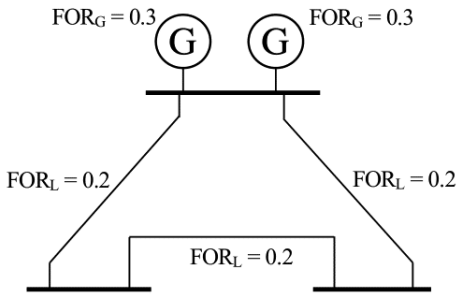

Figure 4.2: *Example system with 2 generators and 3 lines.*

$$M_{samples} = \begin{bmatrix} 0.8 & 0.1 & 0.4 \\ 0.5 & 0.7 & 0.2 \\ 0.2 & 0.3 & 0.9 \\ 0.5 & 0.1 & 0.8 \\ 0.4 & 0.2 & 0.6 \end{bmatrix}, \quad M_{FOR} = \begin{bmatrix} 0.3 & 0.3 & 0.3 \\ 0.3 & 0.3 & 0.3 \\ 0.2 & 0.2 & 0.2 \\ 0.2 & 0.2 & 0.2 \\ 0.2 & 0.2 & 0.2 \end{bmatrix} \Rightarrow \quad M_{states} = \begin{bmatrix} 0 & 1 & 0 \\ 0 & 0 & 1 \\ 0 & 0 & 0 \\ 0 & 1 & 0 \\ 0 & 0 & 0 \end{bmatrix} \tag{4.10}$$

A high number of simulation years creates an immense number of states to be evaluated to obtain convergence. Therefore, filtering techniques are crucial in order to decrease the number of states investigated in the contingency solver. The screening and filtering techniques applied in the HLII assessment of this thesis will be thoroughly explained in Chapter 6.

4.2.2 Isolated Buses

When evaluating the sampled system states, there is a need of investigating whether the contingencies cause isolation of buses or parts of the system being islanded. This can be the case when one or more lines are on outage; isolation (or islanding) is said to occur when a bus or a set of buses does not have a line connection to the rest of the system. It is important to take this into consideration because of the complete cut-off of the loads at the buses that are isolated [2].

It can be noted that there are two ways of evaluating the isolated buses or the islanded parts of the system. The first is to define all load at the isolated buses as lost, which is the approach utilised in this thesis. The second is to look at the islanded part or parts of the system as individually functioning systems. The load shedding of each islanded part of the system is then given by the difference of the generation capacity and the demand. If there is no generation at the islanded part of the system, all load is considered lost. It is important to know what method is applied, since different load shedding approaches ultimately affects the reliability indices.

It has been investigated if there is any literature that explains algorithms identifying isolated buses. It seems like there is a common opinion that an algorithm that identifies isolated buses is necessary to obtain an accurate representation of the system [8, 25]. However, no one suggests a specific algorithm. Therefore, it has been chosen to implement the algorithm developed by [6] without much adaptation.

The approach of [6] will only be briefly explained in this thesis. For an extensive step-by-step explanation of the algorithmic approach, the reader is referred to [6]. In short, the lines and generators on outage in a contingency are first removed from the system under consideration. Then, the conductance and the susceptance matrices are used to check if any buses (or set of buses) do not have a line connection to the rest of the system. If so, the buses are marked as isolated.

To ensure no buses are falsely marked as isolated, the algorithm consists of two parts. The first part iterates through each bus and checks if there are any line connections to buses of a lower number. If not, the bus is marked as isolated. The next step checks if the buses that are marked as isolated are falsely marked. If so, these buses are changed to not isolated. The isolated buses are then removed from the conductance and susceptance matrices.

In the approach of [6], all contingency states are tried to check if there are any isolated buses or if a part of the system is islanded. It is, however, only necessary to check the states where one or more lines are on outage. Therefore, an additional criterion should be added. Only if there are one or more lines on outage, the state is tested for isolated buses.

4.2.3 Convergence Criteria

In the simulation approach of this thesis, the CV is calculated at the end of the simulations to evaluate whether the indices have converged. Thus, it is not used as a stopping criterion, which is the most common utilisation. It is done in this manner due to the simultaneous sampling approach. This is so to obtain lower computational time.

As explained in Section 3.2.1, choosing an appropriate CV will be based on a compromise between accuracy and computational time. As an example, Figure 4.3 is made to show the CV for different number of simulation years; in this case the RBTS is used. It can be seen that reaching a CV of 1 % requires around 1000 simulation years. However, this might be computationally time consuming. Instead, a CV of, say, 500 years increases the CV only by a little, while the computational time decreases significantly. In addition, in [26] the following is stated: *"The ability to include a high degree in corrective calculations will never override the inherent uncertainties in the forecast data including load, failure rates, repair rates and in the Monte Carlo Simulation"*. Due to the these uncertainties, a small decrease in convergence can be beneficial when performing MCS over a large number of years.

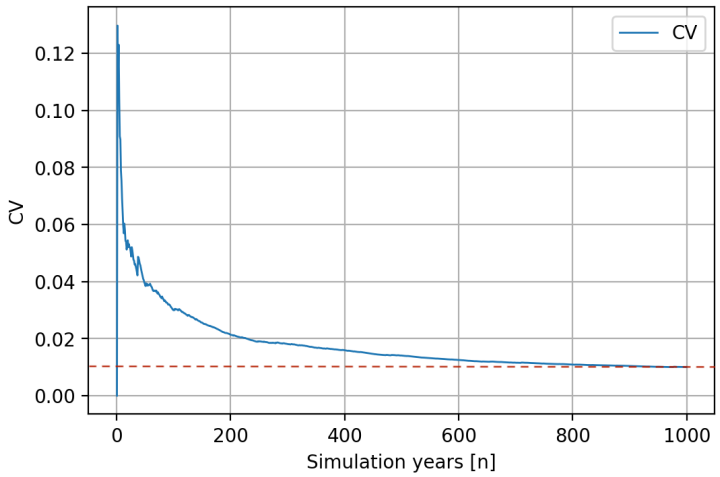

Figure 4.3: *CV for an increasing number of years using the RBTS. The red dotted line represents a CV of* 1 %.

In literature, the CV used in case studies varies between 1 % and 10 % [10, 27], depending on the wanted accuracy of the results. Thus, a CV in the lower end of this interval can

be considered to be indicative of successful convergence. In this thesis, the simulations are considered to be converged if the CV is approximately 1-2 %.

4.3 Optimal Power Flow in HLII Assessment

OPF is used in composite system adequacy to find a feasible operating point within safe operating limits. This section describes the general definition of OPF, followed by composite system adequacy specific description of the OPF problem that is solved for each contingency state.

4.3.1 General OPF Definition

OPF is commonly used in power system planning and operation because of its ability to integrate both economic and security aspects of a power system into a mathematical formulation [28]. In practice, OPF combines an objective function with the power flow equations to form an optimisation problem [21]. Its objective is in most cases to minimise the total cost while maintaining the electric power within safe operating limits [29], meaning that the solver tries to find a feasible operating point without violating any of the defined system constraints. If one or more constraints are violated, measures are taken to restore operation without any violations. There are several ways of defining an OPF problem, based on how the objective function is defined. Some examples of objectives are:

- Minimising generation costs.
- Minimising rescheduling costs
- Minimising curtailment costs.

The general formulation of OPF can be described through Equation (4.11) [24]. u is the set of controllable decision variables and x is the set of dependent decision variables, also called state variables. The first is typically the controllable bus power injections and the latter is typically the voltage magnitudes and angles. $g(u, x)$ and $h(u, x)$ are the system

constraints. The equalities represented by $g(u, x)$ include the power flow equations and the inequalities represented by $h(u, x)$ are the physical limits of the control variables and the operating limits of the power system.

$$\begin{aligned} \text{Minimise} \quad & f(u, x) \\ \text{Subject to} \quad & g(u, x) = 0 \\ & h(u, x) \geq 0 \end{aligned} \tag{4.11}$$

4.3.2 OPF in PSR Assessment

Since composite adequacy assessment aims to minimise the curtailment during possible contingencies, the OPF objective function in this thesis is based on minimising the costs of curtailment. As it is desirable to reschedule generation first, the costs of rescheduling are set to zero. In this way it is certain that rescheduling is performed first and curtailments are executed as the last option. This decision is based on the work of [6], where the OPF problem is solved in the same manner. The objective function of the analysis in this thesis can therefore be described by Equation (4.12), where C_i is the cost of changing the decision variables, X.

$$\min \text{ f} = \sum_i C_i(X) \quad [\$/\text{kWh}] \tag{4.12}$$

As mentioned earlier, an OPF problem is represented by a vector of independent decision variables, u, and another vector of dependent decision variables, x. In this thesis, however, both vectors are gathered in one vector including all desicion variables, as shown in Equation (4.13). Compared to traditional OPF, active and reactive curtailment are included in the decision variable vector in this thesis. The variables considered are therefore active and reactive power generation at each bus, active and reactive load curtailment at each bus, voltage magnitude at each bus and voltage angle at each bus. All the decision variables have a corresponding cost variable, and are optimised with the goal of minimising the overall cost.

$$X = [\ P_{g1} \quad \dots \quad Q_{g1} \quad \dots \quad C_P \quad \dots \quad C_Q \quad \dots \quad V_1 \quad \dots \quad \delta_1 \quad \dots\ ] \tag{4.13}$$

The costs can be represented by a vector, shown in Equation (4.14). This is the cost of increasing a decision variable at each bus, so that every element of the vector corresponds to a decision variable. Since the only costs are costs of active and reactive curtailment, these are the only non-zero elements in the cost vector.

$$W = [\ w_1 \quad w_2 \quad \dots \quad w_{6k-1} \quad w_{6k}\ ]^T \tag{4.14}$$

4.3.3 Constraints

The constraints of an OPF problem can be divided into equality constraints and inequality constraints. The equality constraints considered in the OPF problem of this thesis are the active and reactive power flow constraints as well as the constraint concerning the power factor. The inequality constraints are the current rating as well the operating limits of the system.

In this section, constraints will be listed and explained in order to get a good overview for later implementation. It should be noted that all quantities must be in per unit and angles in radians in order to solve the OPF problem.

By combining Equation (4.13) and Equation (4.14), the objective function used in the OPF problem of this thesis can be written as shown in Equation (4.15). The cost vector, W, is multiplied with the decision variable, X. In this way, the objective function is on a suitable form for the OPF solver.

$$\min \mathrm{f} = [W] \cdot [X] \tag{4.15}$$

Equality Constraints

The first equality constraint is the active power flow constraint. In practice, at each node the active generation capacity of the system must be equal to the total active power

demand and losses. If there is not enough generation capacity, active power curtailment might be necessary, written as C_{P_i}. $P_i(V, \delta)$ is represented by Equation (4.3).

$$[\mathbf{P}] = P_{gi} + C_{P_i} - P_{load_i} - P_i(V, \delta) = 0 \tag{4.16}$$

Similarly, as regards the reactive power flow constraint, the total reactive power generation must be equal to the the total reactive power demand and losses. If there is insufficient generation capacity, curtailments are necessary, represented by C_{Q_i}. $Q_i(V, \delta)$ is given by Equation (4.4).

$$[\mathbf{Q}] = Q_{gi} + C_{Q_i} - Q_{load_i} - Q_i(V, \delta) = 0 \tag{4.17}$$

Further, the power factors of the loads are at all times fixed. H_{load_i} gives the ratio between active and reactive power load curtailments at each bus, as shown in Equation (4.18). This constraint makes sure the power factor is constant at all times. However, in order to implement this constraint in the OPF solver, it must be represented in matrix form to comply with the decision vector, X. Therefore, a matrix A is introduced in order to get the constraint in a suitable form. This decision is based on the approach of [6]. The power factor constraint is written as K_{pf} in Equation (4.19).

$$H_{load_i} \cdot C_{P_i} - C_{Q_i} = 0 \tag{4.18}$$

$$K_{pf} = [A] \cdot [X] = \begin{bmatrix} 0 \\ \vdots \\ 0 \end{bmatrix} \tag{4.19}$$

Inequality Constraints

Equation (4.20) presents the line rating constraint. The current of a line is a function of the bus voltages, as shown in Equation (4.5). However, this should be represented using the decision variables in the vector X so that it is suitable for implementation in the OPF

solver. By using Equation (4.6), the expression can be rewritten as shown in Equation (4.21). It can be seen that the element on the right side is moved to the left side of the inequality.

$$I_{ij} \leq I_{ij}^{max} \tag{4.20}$$

$$\Big(V_i \cdot \cos\delta_i - V_j \cdot \cos\delta_j\Big)^2 + \Big(V_i \cdot \sin\delta_i - V_j \cdot \sin\delta_j\Big)^2 - \Big(\frac{I_{ij}^{max}}{y_{ij}}\Big)^2 \leq 0 \tag{4.21}$$

The following inequality constraints represent the operating limits of the system. Equation (4.22) shows that the active power generation cannot be negative and must be lower than the maximum active power capability of the bus. Similarly, as shown in Equation (4.23), the reactive power generation must be larger than the minimum reactive power capability of the bus and lower than the maximum capability.

$$0 \leq P_{gi} \leq P_{gi}^{max} \tag{4.22}$$

$$Q_{gi}^{min} \leq Q_{gi} \leq Q_{gi}^{max} \tag{4.23}$$

Further, the active load curtailment cannot be negative and must be lower than the active power load of the bus under consideration. Since the reactive power curtailment is a function of the active power, this cannot be lower than zero either, as shown in Equation (4.25). It must also be lower than the reactive power load of the bus.

$$0 \leq C_{Pi} \leq P_{load_i} \tag{4.24}$$

$$0 \leq C_{Qi} \leq Q_{load_i} \tag{4.25}$$

The voltage level at each bus must also be within the given limits, as shown in Equation (4.26). This constraint can be further divided into the voltage limits of the PV buses and

the limits of the PQ buses, but that will not be taken into consideration in this thesis. Also the voltage angles of each bus must be within the limits shown in Equation (4.27).

$$V_i^{min} \leq V_i \leq V_i^{max} \tag{4.26}$$

$$-\pi \leq \delta_i \leq \pi \tag{4.27}$$

4.3.4 Implementing the Jacobian Matrices

The accuracy and efficiency of the optimisation method can be significantly improved by implementing the Jacobian matrices of the OPF problem. As a part of the optimisation method, the Jacobian serves several purposes. Mainly it provides a linearisation of the constraint equations used in the iterative process, but it also represents the sensitivities with the respect to the decision variables [21].

As shown in Equation (4.28), the Jacobian can be defined as a matrix with the first order partial derivatives of a vector-valued function. In the non-linear optimisation problem defined and utilised in this thesis, the objective function, the equality constraints and inequality constraints are partially derived by the decision variables, X. This section provides the deduction of the Jacobians on geometric form, where a thorough explanation is deemed necessary as it is an extension of the method used in [6].

$$\mathbf{J_f(x_{n-m})} = \begin{bmatrix} \frac{\partial f_n}{\partial x_n} & \cdots & \frac{\partial f_n}{\partial x_m} \\ \vdots & \ddots & \vdots \\ \frac{\partial f_m}{\partial x_n} & \cdots & \frac{\partial f_m}{\partial x_m} \end{bmatrix} \tag{4.28}$$

Jacobian of the Objective Function

The Jacobian of the objective function with respect to X is shown in Equation (4.15). It is represented by the gradient of the objective function, which is a linear function. By partial differentiation of the objective function with respect to the decision variables, X, the resulting Jacobian will be the same as the cost vector. Because the costs of

rescheduling and voltage adjustments are set to zero, the only non-zero elements are the active power curtailment cost and reactive power curtailment cost, as seen in Equation (4.29).

$$\begin{aligned}\mathbf{J}_{[\mathbf{f}]}([\mathbf{X}]) &= \nabla \mathbf{f}([\mathbf{X}]) \\ &= [\ W_{P_{g1}} \ \dots \ W_{Q_{g1}} \ \dots \ W_{C_{P1}} \ \dots \ W_{C_{Q1}} \ \dots \ W_{V_1} \ \dots \ W_{\delta_1} \ \dots\ ] \\ &= [\ 0 \ \dots \ 0 \ \dots \ W_{C_{P1}} \ \dots \ W_{C_{Q1}} \ \dots \ 0 \ \dots \ 0 \ \dots\ ]\end{aligned} \tag{4.29}$$

Jacobian of the Constant Power Factor Constraint

The constraint to keep the power factor constant during load shedding, can be seen in Equation (4.18). Since the equation is linear, the Jacobian based on the partial derivatives of the decision variables, X, is equal to matrix A deducted in Equation (4.30).

The diagonal governing the decision variable C_{P_i} for the active power curtailment is represented as the load ratio H_{load_i} from bus n to bus m. The diagonal governing the reactive power curtailment C_{Q_i} is -1, while the rest of the elements are zero.

$$\begin{aligned}&\mathbf{J}_{[\mathbf{K_{pf}}]}([\mathbf{X}]) \\ &= \begin{bmatrix} 0 & \cdots & 0 & H_{load_m} & \cdots & \cdot & -1 & \cdots & \cdot & 0 & \cdots & 0 \\ \vdots & \ddots & \vdots & \vdots & \ddots & \vdots & \vdots & \ddots & \vdots & \vdots & \ddots & \vdots \\ 0 & \cdots & 0 & 0 & \cdots & H_{load_n} & 0 & \cdots & -1 & 0 & \cdots & 0 \end{bmatrix}\end{aligned} \tag{4.30}$$

Jacobian of the Line Rating Constraint

The line rating inequality constraint, shown in Equation (4.21), is only dependent on the bus voltage, V, and the corresponding angle, δ. This means that the non-zero elements of the line rating inequality constraint are partial derviatives with respect to V and δ, as shown in Equation (4.31).

$$\mathbf{J}_{[\mathbf{I}]}([\mathbf{X}]) = \begin{bmatrix} \frac{\partial I_n}{\partial P_{g1}} & \cdots & \cdot & \frac{\partial I_n}{\partial Q_{g1}} & \cdots & \cdot & \frac{\partial I_n}{\partial C_{P1}} & \cdots & \cdot & \frac{\partial I_n}{\partial C_{Q1}} & \cdots & \cdot & \frac{\partial I_n}{\partial V_1} & \cdots & \cdot & \frac{\partial I_n}{\partial \delta_1} & \cdots & \cdot \\ \vdots & \ddots & \vdots & \vdots & \ddots & \vdots & \vdots & \ddots & \vdots & \vdots & \ddots & \vdots & \vdots & \ddots & \vdots & \vdots & \ddots & \vdots \\ \frac{\partial I_m}{\partial P_{g1}} & \cdots & \cdot & \frac{\partial I_m}{\partial Q_{g1}} & \cdots & \cdot & \frac{\partial I_m}{\partial C_{P1}} & \cdots & \cdot & \frac{\partial I_m}{\partial C_{Q1}} & \cdots & \cdot & \frac{\partial I_m}{\partial V_1} & \cdots & \cdot & \frac{\partial I_m}{\partial \delta_1} & \cdots & \cdot \end{bmatrix}$$

$$= \begin{bmatrix} 0 & \cdots & 0 & \frac{\partial I_n}{\partial V_1} & \cdots & \cdot & \frac{\partial I_n}{\partial \delta_1} & \cdots & \cdot \\ \vdots & \ddots & \vdots & \vdots & \ddots & \vdots & \vdots & \ddots & \vdots \\ 0 & \cdots & 0 & \frac{\partial I_m}{\partial V_1} & \cdots & \cdot & \frac{\partial I_m}{\partial \delta_1} & \cdots & \cdot \end{bmatrix} \tag{4.31}$$

The non-zero elements in the Jacobian matrix shown in Equation (4.31) are presented in Equations (4.32), (4.33), (4.34) and (4.35). The full derivation of the expressions can be found in Appendix A. n represents the line number, the subscripts i and j represent the buses the line is connected between.

$$\frac{\partial I_n}{\partial V_i} = 2\ \left[V_i - V_j\ \cos(\delta_i - \delta_j)\right] \tag{4.32}$$

$$\frac{\partial I_n}{\partial V_j} = 2\left[V_j\ \cos(2\delta_j) - V_i\ \cos(\delta_i - \delta_j)\right] \tag{4.33}$$

$$\frac{\partial I_n}{\partial \delta_i} = 2\,V_i\,V_j\ \sin(\delta_i - \delta_j) \tag{4.34}$$

$$\frac{\partial I_n}{\partial \delta_j} = 2\,V_i\,V_j\ \sin(\delta_j - \delta_i) \tag{4.35}$$

Jacobian of the Power Balance Constraints

The Jacobian matrix for the active power balance constraint, based on Equation (4.16), is shown in Equation (4.36). The active power constraint is partially differentiated with respect to the decision variables. The active power balance derived by the active power

generation, P_{gi}, and the active power curtailment, C_{Pi}, are equal to one at the diagonal. The elements of the matrix where active power balance is derived by V and δ are different from zero.

The Jacobian for the reactive power balance constraint is in a similar form as the active power constraint. The difference is that the derivation by Q_{gi} and C_{Qi} are equal to one at the diagonals. The elements of the reactive power balance derived by V and δ are also different from zero.

$$
\begin{aligned}
&\mathbf{J}_{[\mathbf{P}]}([\mathbf{X}]) \\
&= \begin{bmatrix}
\frac{\partial P_n}{\partial P_{g1}} & \cdots & \cdot & \frac{\partial P_n}{\partial Q_{g1}} & \cdots & \cdot & \frac{\partial P_n}{\partial C_{P1}} & \cdots & \cdot & \frac{\partial P_n}{\partial C_{Q1}} & \cdots & \cdot & \frac{\partial P_n}{\partial V_1} & \cdots & \cdot & \frac{\partial P_n}{\partial \delta_1} & \cdots & \cdot \\
\vdots & \ddots & \vdots & \vdots & \ddots & \vdots & \vdots & \ddots & \vdots & \vdots & \ddots & \vdots & \vdots & \ddots & \vdots & \vdots & \ddots & \vdots \\
\frac{\partial P_m}{\partial P_{g1}} & \cdots & \cdot & \frac{\partial P_m}{\partial Q_{g1}} & \cdots & \cdot & \frac{\partial P_m}{\partial C_{P1}} & \cdots & \cdot & \frac{\partial P_m}{\partial C_{Q1}} & \cdots & \cdot & \frac{\partial P_m}{\partial V_1} & \cdots & \cdot & \frac{\partial P_m}{\partial \delta_1} & \cdots & \cdot
\end{bmatrix} \\
&= \begin{bmatrix}
1 & \cdots & 0 & 0 & \cdots & 0 & 1 & \cdots & 0 & 0 & \cdots & 0 & \frac{\partial P_n}{\partial V_1} & \cdots & \cdot & \frac{\partial P_n}{\partial \delta_1} & \cdots & \cdot \\
\vdots & \ddots & \vdots & \vdots & \ddots & \vdots & \vdots & \ddots & \vdots & \vdots & \ddots & \vdots & \vdots & \ddots & \vdots & \vdots & \ddots & \vdots \\
0 & \cdots & 1 & 0 & \cdots & 0 & 0 & \cdots & 1 & 0 & \cdots & 0 & \frac{\partial P_m}{\partial V_1} & \cdots & \cdot & \frac{\partial P_m}{\partial \delta_1} & \cdots & \cdot
\end{bmatrix}
\end{aligned}
\tag{4.36}
$$

In the optimisation problem both active and reactive power constraints are combined, which gives the Jacobian matrix shown in Equation (4.37).

$$\mathbf{J}_{[\mathbf{P},\mathbf{Q}]}([\mathbf{X}]) = \begin{bmatrix} 1 & \cdots & 0 & 0 & \cdots & 0 & 1 & \cdots & 0 & 0 & \cdots & 0 & \frac{\partial P_n}{\partial V_1} & \cdots & \cdot & \frac{\partial P_n}{\partial \delta_1} & \cdots & \cdot \\ \vdots & \ddots & \vdots & \vdots & \ddots & \vdots & \vdots & \ddots & \vdots & \vdots & \ddots & \vdots & \vdots & \ddots & \vdots & \vdots & \ddots & \vdots \\ 0 & \cdots & 1 & 0 & \cdots & 0 & 0 & \cdots & 1 & 0 & \cdots & 0 & \frac{\partial P_m}{\partial V_1} & \cdots & \cdot & \frac{\partial P_m}{\partial \delta_1} & \cdots & \cdot \\ 0 & \cdots & 0 & 1 & \cdots & 0 & 0 & \cdots & 0 & 1 & \cdots & 0 & \frac{\partial Q_n}{\partial V_1} & \cdots & \cdot & \frac{\partial Q_n}{\partial \delta_1} & \cdots & \cdot \\ \vdots & \ddots & \vdots & \vdots & \ddots & \vdots & \vdots & \ddots & \vdots & \vdots & \ddots & \vdots & \vdots & \ddots & \vdots & \vdots & \ddots & \vdots \\ 0 & \cdots & 0 & 0 & \cdots & 1 & 0 & \cdots & 0 & 0 & \cdots & 1 & \frac{\partial Q_m}{\partial V_1} & \cdots & \cdot & \frac{\partial Q_m}{\partial \delta_1} & \cdots & \cdot \end{bmatrix} \tag{4.37}$$

The elements of the Jacobian for the active power balance constraint derived by the decision variables voltage magnitude, V, and voltage angles, δ, can be seen in Equation (4.38). G_{ij} and B_{ij} represent the real and imaginary parts of an element of the admittance matrix, *Y-bus*, for the system.

$$\begin{aligned} \frac{\partial P_i}{\partial V_i} &= -2\,V_i\,G_{ii} \;-\sum_{j\neq i} V_j\,(G_{ij}\cos(\delta_i-\delta_j)+B_{ij}\sin(\delta_i-\delta_j)) \\ \frac{\partial P_i}{\partial V_j} &= -V_i\,(G_{ij}\cos(\delta_i-\delta_j)+B_{ij}\sin(\delta_i-\delta_j)) \\ \frac{\partial P_i}{\partial \delta_i} &= V_i\sum_{j\neq i} V_j\,(G_{ij}\sin(\delta_i-\delta_j)-B_{ij}\cos(\delta_i-\delta_j)) \\ \frac{\partial P_i}{\partial \delta_j} &= -V_i\,V_j\,(G_{ij}\sin(\delta_i-\delta_j)-B_{ij}\cos(\delta_i-\delta_j)) \end{aligned} \tag{4.38}$$

The Jacobian elements for the reactive power derived by the same decision variables can be seen in Equation 4.39. The Jacobian elements for the active and reactive power equations are well known in the field of Power System Analysis, and a more thorough deduction can be found in [23].

$$\begin{aligned}
\frac{\partial Q_i}{\partial V_i} &= 2\,V_i\,B_{ii} - \sum_{j \neq i} V_j\,(G_{ij}\sin(\delta_i - \delta_j) - B_{ij}\cos(\delta_i - \delta_j)) \\
\frac{\partial Q_i}{\partial V_j} &= -V_i\,(G_{ij}\sin(\delta_i - \delta_j) - B_{ij}\cos(\delta_i - \delta_j)) \\
\frac{\partial Q_i}{\partial \delta_i} &= -V_i \sum_{j \neq i} V_j\,(G_{ij}\cos(\delta_i - \delta_j) + B_{ij}\sin(\delta_i - \delta_j)) \\
\frac{\partial Q_i}{\partial \delta_j} &= V_i\,V_j\,(G_{ij}\cos(\delta_i - \delta_j) + B_{ij}\sin(\delta_i - \delta_j))
\end{aligned} \tag{4.39}$$

4.3.5 Priority Order of Load Curtailment

As mentioned, if any of the system constraints are violated when performing OPF, measures must be taken. There are different policies of execution, which are often based on the respective costs of the different measures. In general, the cost of generation rescheduling is lower than the cost of load shedding at the buses, and therefore the load shedding measure should be performed first. If rescheduling is insufficient in alleviating the constraint violations, load curtailment might be necessary.

Since the overall goal of the OPF is to minimise the costs, the curtailments are performed based on the cost of curtailment at each of the buses. This creates a curtailment priority [30], where the most important load bus has the highest cost and the least important load bus has the lowest cost. In order to prioritise the load curtailment at the individual buses, the concept of interrupted energy assessment rate (IEAR) is used in this thesis. IEAR is defined as the cost of unsupplied energy due to power interruptions, given in \$/kWh [31]. A thing to note is that there are different IEAR policies defining the costs. One policy is that the costs are lower at the buses closest to the failed component, so that the load close to the failed component is curtailed first [30]. Another policy is to keep IEAR fixed, independent of the location of the failed component. In this thesis, the latter policy is used.

To show how the priority is decided, an example is provided in Table 4.1. The example

system considered consists of four buses with different IEAR values. It can be seen that Bus 3 has the highest priority since the cost is the highest, and Bus 2 has the lowest priority since the cost is the lowest. Bus 1 is defined as slack bus without load and is therefore not considered.

Table 4.1: *Example of curtailment priority of a system of 4 buses.*

Bus	IEAR [$/kWh]	Priority order
2	4.5	3
3	8.0	1
4	6.4	2

It can also be noted that the cost of curtailment can be equal and fixed at all buses. In these cases, the curtailment is rather based on the topology of the system. In practice, this means that curtailment is performed where it is the most efficient to alleviate the constraint violations in the system.

4.4 Algorithmic Approach

In this section, the algorithmic approach is explained. Figure 4.4 depicts the composite system adequacy assessment algorithm, and is the basis for the following step-wise explanation. It should be noted that the algorithmic approach using different test systems is the same, as the only differences pertain to the system data and the outage data. Any load curve/table can also be implemented.

In addition, it is important to note that the algorithmic description is based on an object oriented approach in Python, which is the language used in the code development in this thesis. In practice, this means using classes and objects to define parameters and functions.

4.4.1 Step-by-step Algorithmic Approach

Import data and define classes:

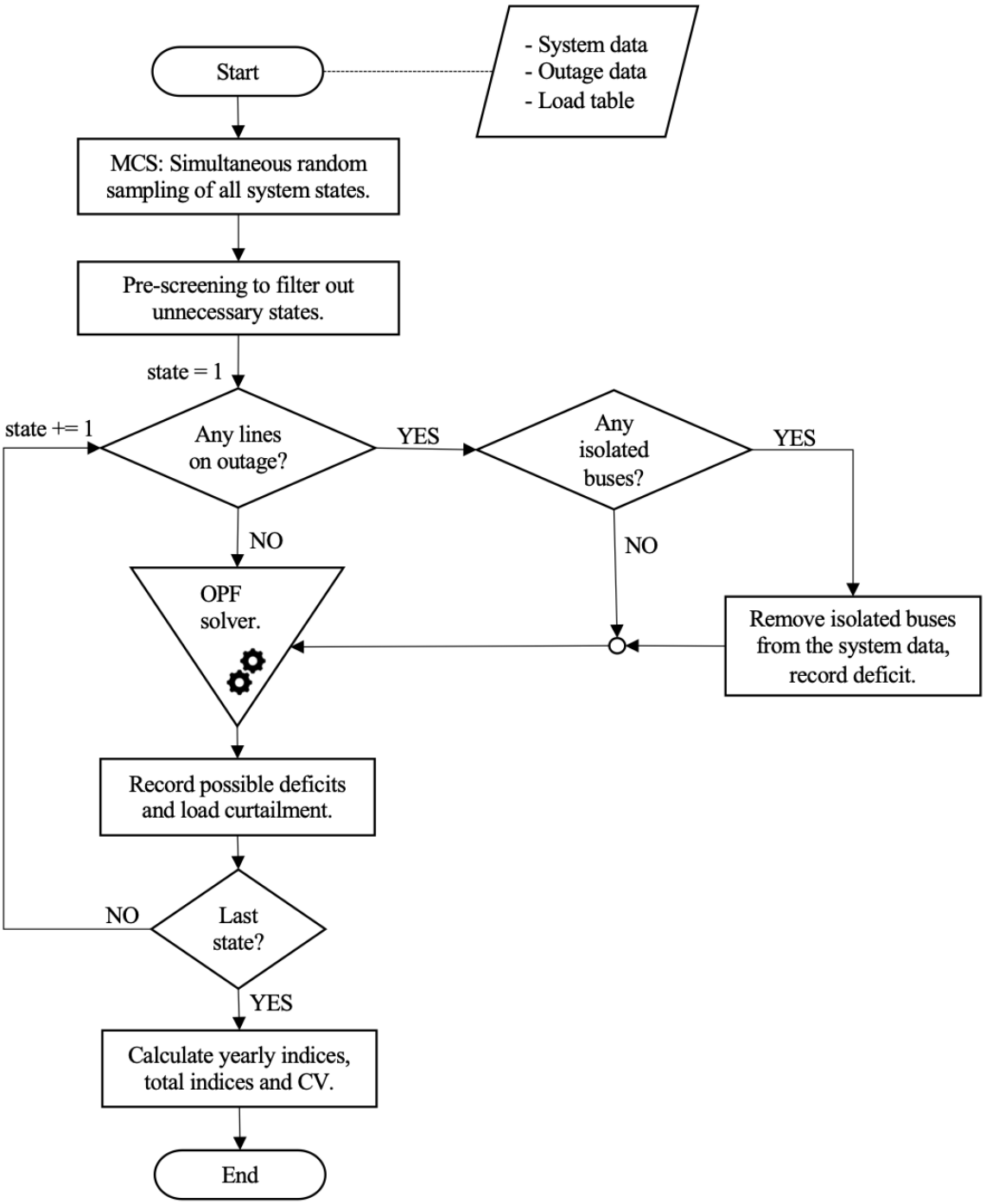

Figure 4.4: *Flow chart depicting the algorithmic approach of the HLII assessment.*

- Import system data, outage data and load table.
- Create a MCS data class, where generator and line objects are made based on the parameters of the data imported.
- Create an OPF data class, containing the system data used later in the OPF prob-

lem.

Sampling of states using the State Sampling method:

- Sample random uniformly distributed numbers in the interval [0,1] and save to a $(n_{components} \times n_{states})$ matrix, $M_{samples}$, as shown in Equation (4.7). Note that n_{states} is the number of time increments, and equals the number of hours in a year times the number of simulation years if a HPL model in utilised.
- Create another matrix, M_{FOR} of the same dimensions. Each column contains the FOR values of the components, as shown in Equation (4.8).
- The two matrices are compared index by index. If the element under consideration of $M_{samples} > M_{FOR}$, the component is available (0). If not, it is unavailable (1). The availability of each component each time increment is saved into a new matrix, M_{states}, also with the same dimensions as shown in Equation (4.9).
- To limit the number of considered curtailment states, the states that will not cause curtailment are removed from M_{states}. The exact filtering techniques used in this thesis will be explained in Chapter 6.
- The system states where at least one line is on outage is marked as "possible isolated". The marked states will be checked for isolated buses in the following step.

Checking for isolated buses:

- Each state is now considered one by one. A copy of the system data from the system objects is made for each state evaluated. The admittance matrix for the system state is made, based on Equation (4.1).
- If the state is marked as "possible isolated", it is checked if there are any isolated buses using the algorithm explained in Section 4.2.2.

  - If yes, the bus or buses are removed from the system data copy, and the deficit is recorded. The generators and lines on outage are also removed from the system data copy.
  - If no, only the generators and lines on outage are removed from the system data copy.

Solving the OPF problem:

- Elements needed to solve the OPF problem is defined:
  - Cost vector (defined in Equation (4.14)), vector of upper boundaries and vector of lower boundaries (defined in Equations (4.22-4.27)) are made using data from the OPF data object.
  - A matrix A, as defined in Equation (4.19), is made to keep the power factor fixed at each load bus.
  - Initial starting point of the decision variables, X_0. It is desirable to choose values as close to the solution as possible.
- An OPF problem class is defined, which saves values and contains functions used to calculate the equality- and inequality constraints, as well as the Jacobian matrices. The functions include:
  - OPF objective function, as shown in Equation (4.15), and its Jacobian matrix.
  - Non-linear inequality line rating constraint, as shown in Equation (4.21), and its Jacobian matrix.
  - Non-linear equality active power balance constraint, as shown in Equation (4.16), and its Jacobian matrix.
  - Non-linear equality reactive power balance constraint, as shown in Equation (4.17), and its Jacobian matrix.
  - Linear equality power factor constraint, as shown in Equation (4.19), and its Jacobian matrix.
- A minimisation function is used to find a solution to the OPF problem. The solution can either be successful or unsuccessful, depending on whether a solution is found:

  - Successful: The curtailment (if any) is saved.
  - Unsuccessful: Measures are made to find a solution, running the OPF problem over again. The exact measures used in this thesis are explained in Chapter 6. The curtailment (if any) is then saved.
  - Unsuccessful after measures: If no solution is found, the curtailment of the approximate solution is saved.

- If the last state is considered, proceed to calculating indices, SD and CV. If not, proceed to the next curtailment state.

Calculation of indices, SD and CV:

- The yearly bus and system indices are calculated using the expressions defined in Sections 2.5 and 2.6. This is based on all considered contingency states.
- The SD and CV are also calculated, as explained in Section 3.2.

5 Reactive Power Considerations in Composite System Adequacy Assessment

Reactive power has an impact on the voltage stability in power systems, especially in heavy loaded systems that have high reactive power demand and high reactive power losses [2]. During a contingency, the active power requirement does not change significantly, but the reactive power component changes substantially [32]. Consequently, it is important to implement reactive power considerations in PSR assessment.

The power system is transitioning towards having a larger share of inverter-based renewable power sources, such as solar and wind power production [3]. Since these do not necessarily provide reactive power, there is an increasing demand of reactive power support and voltage regulation [33]. Thus, there is a need for evaluating what impact the lack of reactive power sources has on the power system and in what way it affects the reliability of the system.

Historically, PSR assessments have most often been executed on the basis on DC power flow [34]. It is computationally more efficient than using AC power flow, but does not capture how reactive power affects the power system reliability [35]. In addition, network violations are often alleviated by active power load shedding, excluding the fact that reactive power might be the issue; dealing exclusively with reactive power requirements could be the best way to mitigate the violations [36]. Therefore, methods considering reactive power in PSR adequacy assessment have been developed in order to capture the influence and effects on the system [2, 34, 37].

The method of implementation by Qin and Wang [2] has been chosen as the preferred assessment method, which would be the basis of adaptation for developing the in-house framework for reliability assessment . The methodological description in [2] provides a clear approach of implementing reactive power considerations in PSR assessment. In addition, new indices are presented, which gives the possibility of a more detailed evaluation of composite system adequacy.

In this chapter, the indices developed by [2] are first presented, followed by a pedagogical description of the methodological approach. Then, the adaptations made to fit the MCS

and OPF approach are described, followed by an algorithmic explanation of the OPF problems used to evaluate reactive power considerations in composite system (HLII RPC) adequacy assessment.

5.1 Indices for Reactive Power Considerations in PSR

Additional indices should be introduced to be able to differentiate the curtailments due to active power shortage and curtailments due to reactive power shortage [2, 36]. This is so in order to give a more accurate evaluation of the energy and Var not supplied. This to properly evaluate the composite system adequacy of the power system.

The indices described in this chapter are the ones defined in [2], which is also the main resource if nothing else is specified. Thus, this section is devoted to retelling the important concepts regarding indices put forward in [2], with an aim to pedagogical clarity.

In addition, it should be noted that the indices presented in [2] are based on an analytical calculation using probability of state and frequency of state. Therefore, the calculation of the indices using MCS is also described in this section, followed by a comparison between indices for reactive power considerations and regular HLII indices.

Another thing to note, is that in many cases the power factor of the load is constant. In these cases the reactive power deficit is a function of the active power deficit.

5.1.1 Analytically Based Indices

First, the common terminology of the indices used should be defined. They are all described as the sum of the total number of considered contingencies, written as NC. As described in Chapter 2, the contingencies considered are often based on the probability of state, where states with probability lower than a certain limit are neglected.

Expected Active and Reactive Curtailment Due to Active Power Shortage

If the total demand, including load and system losses, is larger than the total generation capacity, the active and reactive capacity deficit should be calculated as shown in

Equation (5.1) and Equation (5.2). In practice, these indices give the average curtailed capacity at each bus or for the whole system.

The expression for expected active power curtailment due to active power shortage is shown in Equation (5.1), where LC_{Pi} is the active load curtailment due to active power shortage for state i. The expression for expected reactive power load curtailments due to active power shortage is shown in Equation (5.2), where QC_{Pi} is the reactive load curtailment due to active power shortage for state i. In both expressions, F_i is the frequency of state i, given by Equation (2.15).

$$ELC_P = \sum_{i=1}^{NC} LC_{Pi} \cdot F_i \; [MW/year] \tag{5.1}$$

$$EQC_P = \sum_{i=1}^{NC} QC_{Pi} \cdot F_i \; [MVar/year] \tag{5.2}$$

Expected Energy and Var Not Supplied Due to Active Power Shortage

The indices describing expected energy and Var not supplied due to active power shortage are based on the same contingency states as the previous indices, where the total demand is larger than the total generation capacity. In other words, it is the energy and the Var that have to be curtailed in order to have generation capacity equal to total demand.

The expression for expected energy not supplied due to active power shortage is given by Equation (5.3), where LC_{Pi} is the active load curtailment of state i. The expression for expected Var not supplied due to active power shortage can be written as shown in Equation (5.4), where QC_{Pi} is the reactive load curtailment due to active power shortage. In both expressions p_i is the probability of state i, multiplied with the number of hours in a year to obtain the denomination MWh/year.

$$EENS_P = \sum_{i=1}^{NC} LC_{Pi} \cdot p_i \cdot 8760 \; [MWh/year] \tag{5.3}$$

$$EVNS_P = \sum_{i=1}^{NC} QC_{Pi} \cdot p_i \cdot 8760 \; [MVarh/year] \tag{5.4}$$

Expected Active and Reactive Power Curtailment Due to Reactive Power Shortage

Expected curtailments due to reactive power shortage describe how much active and reactive power that must be curtailed in order to alleviate voltage violations at the buses or to ensure the available reactive power is equal to the reactive power demand. These indices are calculated after curtailments are made to obtain total generation capacity equal to total demand.

In the method developed by [2], these indices are recorded when active and reactive load curtailment is necessary to alleviate voltage violations at the buses.

The expression for expected active power curtailment due to reactive power shortage is given by Equation (5.5), where LC_{Qi} is the active load curtailment due to reactive power shortage for state i. Equation (5.6) shows the expression for expected reactive power curtailments due to reactive power shortage, where QC_{Qi} is the reactive load curtailment due to reactive power shortage for state i. In both expressions F_i is the frequency of state i, given by Equation (2.15).

$$ELC_Q = \sum_{i=1}^{NC} LC_{Qi} \cdot F_i \; [MW/year] \tag{5.5}$$

$$EQC_Q = \sum_{i=1}^{NC} QC_{Qi} \cdot F_i \; [MVar/year] \tag{5.6}$$

Expected Energy and Var Not Supplied Due to Reactive Power Shortage

Expected energy and Var not supplied due to reactive power shortage can be explained as the energy and Var that have to be curtailed in order to alleviate voltage violations, and is based on the same premise as the previously described capacity indices.

Equation (5.7) shows the expression for energy not supplied due to reactive power shortage, where LC_{Qi} is the reactive load curtailment. Equation (5.8) describes the expected Var not supplied due to reactive power shortage, where QC_{Qi} the reactive load curtailment due to reactive power shortage. p_i is the probability of state i, which is multiplied

with the number of hours in a year.

$$EENS_Q = \sum_{i=1}^{NC} LC_{Qi} \cdot p_i \cdot 8760 \; [MWh/year] \tag{5.7}$$

$$EVNS_Q = \sum_{i=1}^{NC} QC_{Qi} \cdot p_i \cdot 8760 \; [MVarh/year] \tag{5.8}$$

Expected Var Shortage Due to Voltage Violations (EVarS)

Expected Var shortage due to voltage violation is the the amount of reactive power needed to alleviate the voltage violations in the power system. This index is used in [2] when voltage violations are alleviated by injecting reactive power at the buses.

The expression is given in Equation (5.9), where $VarS_{Qi}$ is the Var shortage that causes the voltage violation for state i and p_i is the probability of state i.

$$EVarS = \sum_{i=1}^{NC} VarS_{Qi} \cdot p_i \cdot 8760 \; [MVarh/year] \tag{5.9}$$

A thing to note, is that the expected Var shortage at the buses can be used to determine where in the power system additional reactive power sources should be placed [2]. Thus, this index is especially valuable for system planners and system operators, in order to secure a stable and reliable power system.

5.1.2 MCS Based Indices

As explained in Chapter 3, when performing MCS the system is evaluated for each time increment during a period, usually a year. Therefore, the indices obtained are given in MWh/year or MVarh/year.

The method of calculating the energy and Var based indices is shown in Equations (5.10), (5.11), (5.12), (5.13) and (5.14). It is executed for N years, and each year is divided into M time increments, usually hourly increments. For each time increment M, the active or reactive curtailment or the injected reactive power is multiplied with the number of hours considered, ΔT. The indices are then divided by the number of years simulated.

$$EENS_P^{MCS} = \frac{\sum_{i=1}^{N}(\sum_{j=1}^{M} LC_{Pj} \cdot \Delta T)}{N} \, [MWh/year] \tag{5.10}$$

$$EVNS_P^{MCS} = \frac{\sum_{i=1}^{N}(\sum_{j=1}^{M} QC_{Pj} \cdot \Delta T)}{N} \, [MVarh/year] \tag{5.11}$$

$$EENS_Q^{MCS} = \frac{\sum_{i=1}^{N}(\sum_{j=1}^{M} LC_{Qj} \cdot \Delta T)}{N} \, [MWh/year] \tag{5.12}$$

$$EVNS_Q^{MCS} = \frac{\sum_{i=1}^{N}(\sum_{i=1}^{M} QC_{Qj} \cdot \Delta T)}{N} \, [MVarh/year] \tag{5.13}$$

$$EVarS^{MCS} = \frac{\sum_{i=1}^{N}(\sum_{j=1}^{M} VarS_{Qj} \cdot \Delta T)}{N} \, [MVarh/year] \tag{5.14}$$

The capacity based indices are calculated as shown in Equations (5.15), (5.16), (5.17) and (5.18). The average active or reactive capacity deficit is calculated for each year. It is done by calculating the sum of capacity deficit for the curtailment states of year i, divided by the number of curtailment states that year, NC_i. In practice, this gives yearly the average capacity deficit of the curtailment states. The sum is then divided by the number of years simulated, N.

$$ELC_P^{MCS} = \frac{\sum_{i=1}^{N}}{N}\left(\frac{\sum_{j=1}^{NC_i} LC_{Pj}}{NC_i}\right) \, [MW/year] \tag{5.15}$$

$$EQC_P^{MCS} = \frac{\sum_{i=1}^{N}}{N}\left(\frac{\sum_{j=1}^{NC_i} QC_{Pj}}{NC_i}\right) \, [MVar/year] \tag{5.16}$$

$$ELC_Q^{MCS} = \frac{\sum_{i=1}^{N}}{N}\left(\frac{\sum_{j=1}^{NC_i} LC_{Qj}}{NC_i}\right) \, [MW/year] \tag{5.17}$$

$$EQC_Q^{MCS} = \frac{\sum_{i=1}^{N}}{N}\left(\frac{\sum_{j=1}^{NC_i} QC_{Qj}}{NC_i}\right) \, [MVar/year] \tag{5.18}$$

5.1.3 Comparison of Indices

To summarize, it is useful to compare the indices that take reactive power considerations into account and the corresponding indices that are used in regular composite system PSR evaluation. This is shown in Table 5.1. It can be seen that taking reactive power into account provides a larger range of indices and thus it is possible to get a more detailed evaluation of PSR adequacy.

Table 5.1: *Comparison of HLII indices where reactive power considerations are taken into account and regular HLII indices without distinction.*

HLII indices due to active power shortage	HLII indices due to reactive power shortage	Regular HLII indices
$EENS_P$	$EENS_Q$	$EENS$
$EVNS_P$	$EVNS_Q$	
ELC_P	ELC_Q	ELC
EQC_P	EQC_Q	

It should also be mentioned that $EVarS$ has no equivalent in the regular HLII indices. This is because it is a case-specific index for injecting reactive power to alleviate voltage violations.

5.2 Methodological Description

As written in the introduction of this chapter, through an extensive literature survey in the field of reactive power considerations in PSR, it was found that the approach developed by Qin and Wang [2] is the preferred method of implementation. In this section, the methodology will be explained. A flowchart, shown in Figure 5.1, has been created to clearly depict each step of the method.

Based on Figure 5.1, the method developed by [2] can be explained as follows. First, all possible contingency states are defined, including the probability of state as well as a severity index. A filtering technique based on the probability of state and severity of state

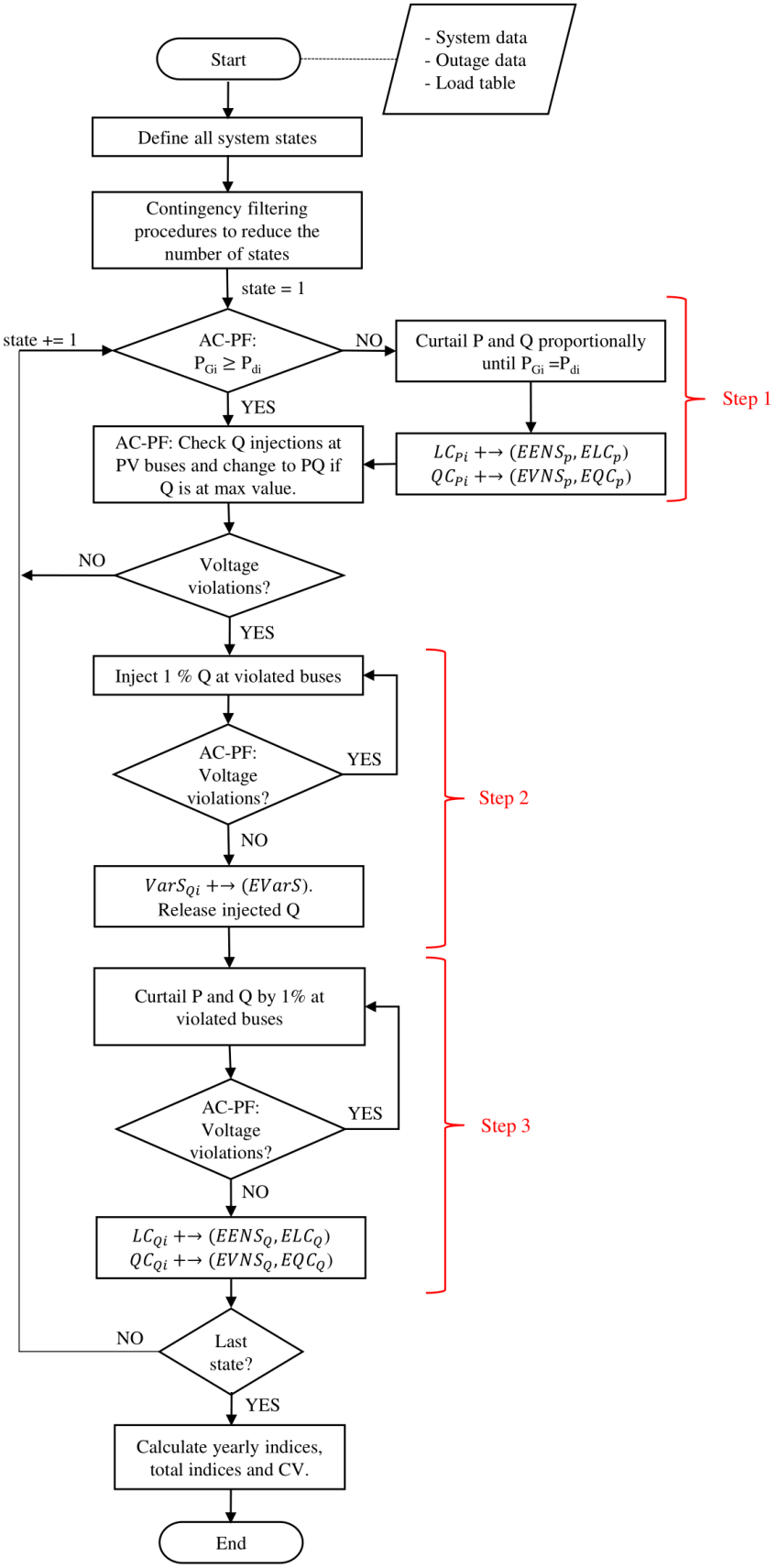

Figure 5.1: *Created flowchart describing the RPC method of [2].*

is then utilised to filter out states. In addition, only up to second-order contingencies are considered.

An AC power flow is performed on the system. If the total demand, including load and losses, is larger than the total generation capacity, active and reactive power is curtailed proportionally at all buses until total active generation is equal to total active demand. The active power curtailment and reactive power curtailment (LC_{Pi} and QC_{Pi}, respectively) are recorded. This step can be seen as Step 1 in Figure 5.1.

Another AC power flow is then performed, and it is checked if the reactive power injections at the PV buses are at the maximum level. If so, the PV bus is changed to a PQ bus. This step is followed by determining whether there are any voltage violations in the system, which can be related to local reactive power shortage [2]. If there are no voltage violations, no further injection or curtailment is necessary.

If there are voltage violations in the system, the reactive power shortage can be relieved using two different methods. The first one is to inject reactive power at the buses with voltage violations, which is presented as Step 2 in Figure 5.1. This is performed by injecting 1 % reactive power at these buses, followed by another AC power flow. If the voltage violations are not alleviated, another 1 % reactive power is injected. This is repeated until the bus voltages are within the set operational limits at all buses, and the total injected reactive power ($VarS_{Qi}$) is recorded. The resulting index gives an indication of the amount of reactive power compensation needed at the voltage violated buses to avoid active and reactive power curtailment. This step provides valuable information to system planners regarding local reactive power shortage [2] and potential placement of additional shunt capacitors.

The second method is to curtail active and reactive power by 1 % of the load at the voltage violated buses, which is Step 3 in Figure 5.1. This is followed by an AC power flow. Another 1 % of the active and reactive load is curtailed if the voltage violations are not alleviated. This is repeated until the voltages at all buses are within the set limits, and the total active power curtailment and reactive power curtailment (LC_{Qi} and QC_{Qi}, respectively) are recorded. Then the next curtailment state is considered.

When all states are considered, the cumulative indices are calculated using the expressions presented in Section 5.1.

5.3 Methodological Adaptations Made to Fit the MCS and OPF Approach

In order to implement the method of [2] using a MCS and OPF approach, some changes must be made to the methodological approach described in the previous section. To easily follow each step, Figure 5.2 is made.

First, some principal differences between the two approaches must be defined. In this thesis the considered system states are based on MCS approach, by simultaneously sampling random system states utilising the State Sampling method. An explanation of the sampling approach can be found in Section 4.2.1. This is different from the approach of [2], where each system state is only considered once and the calculation of indices are based on the probability of state and the frequency of state.

Also the screening and filtering techniques are different. The considered states are in this thesis not based on the quantification of the probability of state and the severity of state, but rather on which and how many of the components that are on outage. The filtering technique of [2] reduces the amount of states to a number significantly lower than the states considered in method of this thesis. The specific filtering techniques used in this thesis are explained further in Chapter 6.

The load model used in [2] is an approximate representation of the one presented in [38], using 14 different loads levels. In this thesis, however, the hourly load model described in [38] is utilised.

One considerable uncertainty when interpreting the method in [2], is how the reactive power injections are treated when PV buses are converted to PQ buses. It can either be interpreted as additional reactive power capacity available, or as fixed reactive power injections after the conversion. The first interpretation has been chosen as it will provide an increased reactive power capacity in the test system. This should reduce the amount

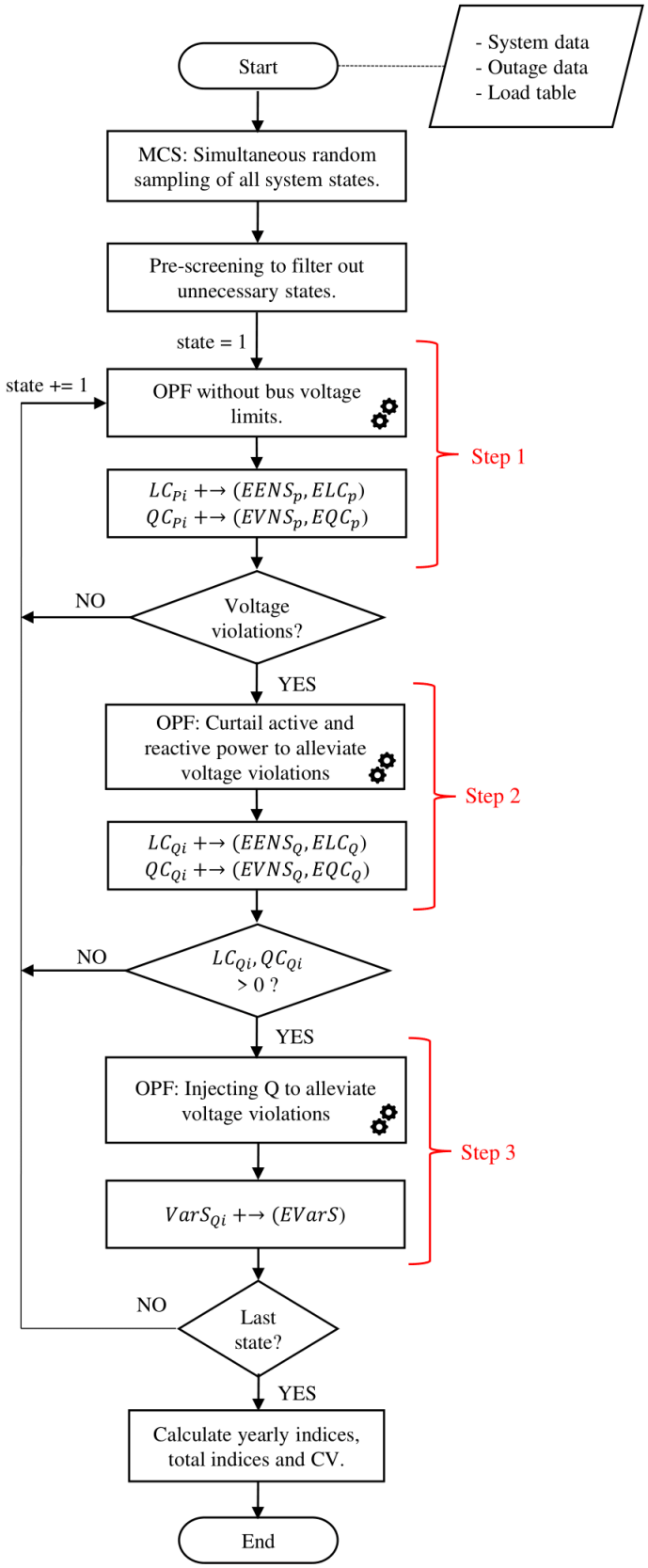

Figure 5.2: *Flowchart describing the adapted RPC method, based on the methdology of [2].*

of voltage issues in the system, with the goal to more easily identify the subtle nuances when changes are made in the case studies. The reactive power injections in this thesis are treated as additional shunt capacitors that are adjustable from zero to full capacity. They also have perfect reliability, which is similar to the synchronous condensers in the system.

In the HLII RPC approach developed to be used in this thesis, three OPF problems are defined and solved. One thing to note about the approach of [2], is that the curtailments and injections of the different steps are performed proportionally at all buses. This means that the curtailment in Step 1 corresponds to the share of load, which is shown in Table B.1 in Appendix B. With the OPF approach, on the other hand, injections and curtailments are performed with the goal of minimising the overall curtailment and therefore minimising the costs. Thus, the curtailments and injections are performed where it is necessary to obtain a feasible operating point, based on the topology of the system.

The OPF problem of the first step is similar to the one used in the standard HLII assessment, but the lower voltage limit is significantly reduced. This is defined as Step 1 in Figure 5.2. The lower voltage limit is reduced to not take into considerations reactive power shortages, which will be investigated in the following steps.

Another difference is that the order of the injection step and the curtailment step is changed. This can be observed in the flowchart in Figure 5.2, where Step 2 is the curtailment step and Step 3 is the injection step. The change is due to the generation rescheduling capability of the system, where the voltage violations from Step 1 can in some cases be alleviated by rescheduling of generation. If that is the case, it is not necessary to run both Step 2 and Step 3. Since rescheduling of generation is more time efficient at the curtailment step due to tolerance levels, a change of order is advantageous. The tolerance levels will be explained further in Chapter 6.

In Step 2, shown in Figure 5.2, another OPF problem is solved to determine the curtailments due to reactive power shortage. If necessary, the curtailments are performed at the buses with voltage violations defined in Step 1. As written earlier, the curtailments are not done proportionally at the voltage violated buses, but based on minimising the

curtailments and thus curtailment costs.

In Step 3, the OPF problem is defined to only inject reactive power at the voltage violated buses to alleviate the voltage violations. Thus, no active or reactive power curtailments are performed. It should be noted that the injections can be performed at all buses, also the ones without load. In the approach of this thesis the injections are performed with the goal of minimising curtailments.

In [2], there is an uncertainty concerning the reactive power injection routine. It is stated that 1 % of the reactive power load is injected in each iteration until the voltage violations are alleviated. This is not applicable when the algorithm also allows for injections at buses without any load. In addition, it is not mentioned how the injections are performed at buses without load, but the results show that there are also injections at the buses with no load. Thus, it is expected that the results utilising the method including adaptations will deviate from the benchmark results.

5.4 Step-by-step Algorithmic Approach

The following algorithmic description is meant to provide a sufficient understanding of the approach without the need for deeper knowledge of the Python syntax or the non-linear optimisation solver used. The objective is for the reader to be able to understand the approach from a theoretical perspective. This description acts as a explanatory support to the flowchart shown in Figure 5.2.

It can also be noted that the MCS sampling method and the identification of isolated buses are not explained in this section. This is because they are performed in the same manner as for the standard HLII assessment. The reader is therefore referred to Section 4.4 for further algorithmic explanation.

The approach is divided into three steps, where each step utilises a numerical OPF solver on a sampled contingency state of a system. In each step, the solver is used to find the minimal solution to an objective function with set boundaries for the decision and control variables, as well as constraints. As for the standard HLII assessment algorithm, the objective function is minimised based on the cost of curtailment, where rescheduling

of generation and adjusting the bus voltage magnitudes and voltage angles within set boundaries are deemed to have no cost.

Step 1: OPF without lower voltage limit

Each contingency state is investigated in an OPF solver, where there are changes in some of the parameters compared to the standard HLII assessment.

- Purpose: The purpose of this step is to identify the active and reactive curtailment due to active power shortage ($EENS_P$ and $EVNS_P$), and to identify possible buses with voltage violations.
- Objective function: The objective function is based on minimising the cost of curtailment. This is so because rescheduling of generation and adjusting bus voltages are deemed to have no cost.
- Decision variables: Regular boundaries for the active and reactive power generation and curtailment on each bus are applied. The lower limit of the voltage magnitude is significantly reduced to provoke voltage violations in the system.
- Constraints: The applied constraints include the line ratings, active and reactive power balance equations and constant power factor at the load buses.

The resulting curtailment from the OPF solver (if any) is recorded, and used as initial level of curtailment in Step 2 and Step 3. In addition, the buses with voltage violation are identified. The algorithm proceeds to Step 2 if there are any voltage violations. If there are no voltage violations, the next contingency state is considered.

Step 2: OPF, curtail active and reactive power to alleviate voltage violations

In this step curtailments at the voltage violated buses are performed to alleviate the voltage violations in the system. A modified OPF solver is utilised.

- Purpose: The purpose of this step is to identify the active and reactive power not supplied due to reactive power shortage at the voltage violated buses ($EENS_Q$ and $EVNS_Q$, respectively).

- Objective function: The objective function is cost based, with the goal of minimising curtailment costs. Rescheduling of generation and adjusting bus voltages are deemed to have no cost.
- Decision variables: Regular boundaries are applied for the active and reactive power generation, and voltage magnitudes and angles. Also regular boundaries for curtailment at the voltage violated buses are applied. The curtailment at buses without voltage violations is locked at the curtailment found in Step 1.
- Constraints: All constraints from Step 1 are applied. This includes line ratings, power balance equations and power factor at load buses.

The resulting curtailment from the solver investigation is recorded. This does not include the initial curtailment from Step 1. If it is observed that the voltage violations can be alleviated simply by rescheduling of generation, it is not necessary to proceed to Step 3, and the next curtailment state should be considered.

Step 3: OPF, inject Q to alleviate voltage violations

In this step the reactive power injection technique proposed by [2] is utilised. A modified OPF solver is used to evaluate the reactive power shortage.

- Purpose: The purpose of this step is to identify reactive power shortage at buses with voltage violation. This is done by injecting reactive power at the voltage violated buses identified in Step 1. The injected reactive power contributes to the the expected Var shortage due to voltage violations ($EVarS$).
- Objective function: The objective function is still cost based, with the goal of minimising reactive power injection costs. Rescheduling of generation and adjusting bus voltages are deemed to have no cost.
- Decision/control variables: The active power curtailment is locked at the curtailment from Step 1, so that no further active power curtailment is performed. The reactive power curtailment decision variable is re-represented as the reactive power injection at the voltage violated buses. Regular boundaries for the active and reactive power generation, and voltage magnitudes and angles.

- Constraints: The line rating and power balance constraints are the same as in Step 1 and Step 2, while the constant power factor constraint is removed. This to allow for reactive power to be injected, without affecting active power curtailment from Step 1.

The resulting contribution to the index is recorded.

By completing this step, the full investigation of the contingency state is finished. When all states have been investigated, yearly and cumulative indices are calculated, together with their SD and CV.

6 Code Development and Programming

A major part of the workload dedicated to this thesis has been the development of a PSR tool in Python, with the goal of creating a computational tool for both the standard HLII assessment and the HLII RPC assessment. The code is developed in a highly generalised manner such that most systems can be implemented for the HLII assessment with any number of generators, compensators and transmission lines. The system parameters are required to have the same input format as the test systems utilised in this thesis.

The standard HLII assessment is implemented with an AC OPF formulation, utilising the MCS State Sampling method. The approach is based on the methodological approach of [6], whose in-house MATLAB code was made available to this thesis work as a stepping stone and benchmark comparison for the code development conducted. The developed HLII RPC code is an extension of the standard HLII code, and is a combination of the methodological approach of [6] and [2]. The approach of the standard HLII assessment is explained in Chapter 4 and the approach of HLII RPC assessment is explained in Chapter 5.

One major difference between MATLAB and Python is the programming structure. MATLAB is optimised for an iterative style of programming, and is able to run through large loops rapidly. Python, on the other hand, addresses and stores variables in such a way that an iterative approach is significantly slower. This means that the PSR tool in Python has to be implemented using a different approach than the initial MATLAB code. In order to avoid the iterative approach, bulk of data is treated simultaneously utilising the matrix calculation library *NumPy* for Python [39]. As a consequence, the code in Python is based on an adaptation of the methodology in [6], rather than an adaptation of the in-house MATLAB code itself.

6.0.1 Multi Processing

Since the PSR MCS assessment investigates a large number of system states, an efficient way of improving the total computational time of the code is to introduce multi processing functionality. Modern computers have several cores in their CPU, which means

that several states can be investigated in parallel by utilising all available CPU cores. In Python, the function *concurrent.futures.ProcessPoolExecutor* [40] can be used to implement this functionality. The computational time can roughly estimated to be divided by the number of available CPU cores of the computer utilised.

The *ProcessPoolExecutor* function creates a pool of workers based on the number of CPU cores available, and distributes the contingency states to each worker as they complete the previously assigned contingency state. Because the time to solve each contingency state differs significantly, the investgated states are not completed in chronological order. Since the indices are calculated after all contingency states have been investigated, they have to be mapped back to the original order. This is solved by attaching each contingency state with its original positional index, so the states can be sorted in chronological order after all contingency states are solved.

6.1 Contingency State Filtering Application

In HLII assessment, the computational time is substantially increased compared to the generation adequacy assessment at HLI. Since the contingency solver is the most computationally demanding task in HLII assessment, a way to reduce the computational time is to reduce the amount of states investigated. This can be done by pre-screening the sampled states and filtering out trivial states based on specific criteria. An example of a trivial state is a system state without any components on outage. This state, if investigated by the contingency solver, would not cause any loads to be curtailed and would therefore not have an impact on the system indices.

In [6], three base filtering criteria are introduced as a proposal to reduce the amount of states being investigated by the contingency solver. The criteria are based on three aspects: The load level, the lines on outage and the generators on outage. These filtering criteria are also implemented in the developed Python code, acknowledging the thorough testing conducted and argumentation presented in [6]. However, for one of the test systems, [6] introduces an extra system specific criterion. This will not be implemented in the work of this thesis, due to the objective of generalising the code as much as possible to fit different test systems more easily. The effect of not implementing this criterion will

be investigated in the case studies.

In order to further increase the efficiency of the simulations, another filtering criteria is introduced. This is a duplicate state filtering technique that identifies the states that occur more than once, and will be explained later in this chapter.

6.1.1 Load Level Criterion and Generators on Outage Criterion

The generation level criterion is set to identify the contingency states where the total generation is lower than the total hourly load demand multiplied by a constant k. This is shown in Equation (6.1), where n is the total number of buses. The constant k is largely dependent on the topography of the system and how the generators are distributed.

The other generator criterion is based on the number of generators on outage. If the number of generators on outage is less than a stated limit, the state is filtered out. The combination of these two criteria is found to be an efficient, and does not affect the reliability notably [6].

$$\sum_{i=1}^{n} P_{gi} < k \sum_{i=1}^{n} P_{load_i} \tag{6.1}$$

6.1.2 Lines on Outage Criterion

It is worth mentioning that the two previously described criteria automatically filter out all states where no contingencies occur. The third and last of the criteria presented in [6] is to investigate all states where one or more of the transmission lines are on outage. This strict criteria was found in [6] to only slightly increase the total contingency states to be investigated because the transmission lines in the test systems are more reliable than the generators. This was also observed in the code development process of this thesis.

6.1.3 Duplicate Contingency State Filtering

Due to the simultaneous sampling approach utilised in the Python code, all states are sampled before being investigated by the contingency solver. Through a literature survey in the field of MCS applied to PSR, no previous work was discovered utilising this sampling technique. This somewhat unconventional approach allows for screening and filtering of all the sampled states before being investigated by the solver. Consequently, it opens up a possibility to identify, count and filter out identical contingency states, which in return leads to a decrease in total contingency states that need to be investigated.

The duplicate state filtering technique developed in this thesis work identifies the identical contingency states. These are states where both the load level and the components on outage are the same. Thus, they have the same contribution to the indices when investigated by the contingency solver. One important aspect of filtering out identical contingency states, is to be able to map the solution back to the simulation years where they occur. If not, the yearly indices will be incorrect. This is solved by introducing a "year of state index" array, which contains the simulation years in which each specific contingency state occurs.

To further explain the duplicate state filtering technique, an example is made. A very small system of 2 buses connected by 1 line is considered. Each year has 2 contingency states sampled, as shown in the left part of Table 6.1. The load is equal for all states. It can be observed that state {0, 0, 1} and state {1, 0, 0} are both occurring twice. However, they only need to be considered once, and are assigned with the years where the state occurs, as shown in the right part of Table 6.1. The number of states is reduced from 6 states considered to 4 states considered.

The more components in the system, the more possible unique constellations of contingency states occur. Thus, the effect of the filter is expected to be dependent on the system size. When considering a small system, the probability of repeating states is most often greater than for a larger system. This is due to a lower number of components. Another aspect that has an impact on the efficiency of the duplicate state filter is how efficient the three base filtering criteria are. This is so because these are applied before the duplicate state filtering, and thus some identical states are already filtered out before

Table 6.1: *Duplicate contingency state filtering example.*

System state $\{S_{G1}\ S_{G_2}\ S_{L_1}\}$	Year of state
{0 0 1}	1
{1 0 0}	1
{0 1 1}	2
{1 0 0}	2
{0 1 0}	3
{0 0 1}	3

System state $\{S_{G1}\ S_{G_2}\ S_{L_1}\}$	Year(s) of state
{0 0 1}	1, 3
{1 0 0}	1, 2
{0 1 1}	2
{0 1 0}	3

being identified by the duplicate state filter.

In general, the individual efficiency and effect when combining the different state filtering techniques is expected to differ depending on what system is being investigated and the following filter parameters that are set.

6.2 Solver Options and Parameters When Addressing the Optimisation Problem

6.2.1 Solver Alternatives in Python

To solve the OPF problem, the SciPy [41] function *optimize.minimize* is chosen as the alternative to the *fmincon* solver in the MATLAB code of [6]. The *optimize.minimize* function was found to be very versatile, where it provides the option to choose between different algorithmic methods that are tailored to the type of optimisation problem that is addressed. This improves the efficiency of the solver, which could reduce the computational time significantly.

Through a literature survey followed by testing, the SciPy *SLSQP* method in the *optimize.minimize* function was shown to be the most efficient for the OPF problem addressed in this thesis. The *SLSQP* is a sequential least squares programming algorithm based on a FORTRAN code developed by Dieter Kraft [42]. The programming specific description

of the method can be found in [43]. As an option in the *SLSQP* algortithm, the Jacobian for the optimisation problem's constraints and objective function can be implemented. If not implemented, the algorithm will approximate the Jacobian numerically, which showed itself to increase the computational time by a tenfold for each state investigated. This is also observed in literature [21]. As a result, it was decided to generalise the Jacobian for the optimisation problem in the code. The calculation of the Jacobian matrices is described in Section 4.3.4.

6.2.2 Tolerance Criterion

The solver tolerance criterion is the set threshold for the numerical size of the objective function. If this parameter is set too high, it would technically allow for more curtailment. If the tolerance is set too low, on the other hand, the solver will run through all iterations unnecessarily if a better solution is not found, which can be time consuming. Consequently, the tolerance parameter needs to be tuned finely to properly fit the system under consideration. It should also be mentioned that a more indirect way of adjusting this tolerance would, for the OPF problem addressed in this thesis, be to equally change the cost of curtailment on all buses.

6.2.3 Iterations

The optimisation method *SLSQP* has various options and parameters that can be tuned to increase the efficiency and the accuracy of the solver. One of them is the number of iterations used to find a local optimal solution. By default, the number of iterations is set to 100. However, during testing it was found that this number should be increased to 300 iterations or more, depending on the considered system and the wanted accuracy.

For the majority of the contingency states where the initial solving process failed to find a solution, increasing the iterations to above 300 does not result in more states being successfully solved. In most cases, an increase in the number of iterations only increases the total computational time.

If the solver reaches the iteration set point without finding an optimal solution, it will

return a Boolean variable stating that the success of the optimisation is false. In these cases, alternative measures should be executed, which will be descried in the following section.

6.2.4 Initial Starting Point and Alternative Measures

Convergence issues is a common problem in OPF and conventional power flow calculations, where the success is strongly dependent on the selection of initial starting point [21]. If the selected initial values of the control variables deviate too much from the actual solution, the power flow equations might converge towards a false solution.

A common practice in OPF is to conduct a "flat start", where active and reactive power generation are set to zero, bus voltage magnitudes are set to $1\,p.u.$ and the corresponding voltage angles are set to zero. Another option is to select the previous solution of the OPF as a starting point, which is known as a "warm start". This can, in some situations, decrease the number of iterations needed to reach convergence [21]. In this thesis, however, a "semi-flat start" adopted from [6] is utilised, where the general "flat start" parameters for the reactive power generation, voltage magnitudes and voltage angles are combined with active power generation set to maximum available capacity. Through testing, this has been shown to be the most efficient strategy when solving the majority of the contingency states.

As mentioned, when no solution to the OPF problem is found, alternative measures have to be conducted. The alternative measures strategies are developed through a trial and error phase when testing the OPF solver on different contingency states. The SLSQP method depends solely on the set tolerance of the sum of the objective function, and returns the success of the trial in terms of pass or fail. Through testing, it was found to be both efficient and accurate for the test systems utilised in this thesis to perform a three stage measure strategy with a decreasing tolerance level for each stage. The measures are conducted when the initial run fails to find a solution to the contingency state.

Each stage of the measure scheme utilises the solution from the previous. Consequently, the investigated contingency states can be processed several times in order to find the

most optimal solution. If all measure stages are tried without finding a solution, the state is considered a failed state. The resulting actions will be explained in more detail in the following section.

6.2.5 Failed States

If all measures are conducted on a contingency state without finding an optimal solution, it is considered a failed state. With further investigation it has been found that the solution is in most cases not unfeasible, but rather fails to meet the set tolerance for the sum of the objective function. The reason behind the state not necessarily being unfeasible, is that the *SLSQP* solver method sticks strictly within the set boundaries of the decision variables. This prevents it from being an "illegal" or a "false" state. Thus, the approximate solution of the failed state is accepted.

However, when testing the solver on the three steps in the HLII RPC assessment, it was discovered that the solution from Step 2 and Step 3 in a few rare cases did not obey the constraints. Thus, the approximate solution from these failed states cannot be accepted, because they are considered false solutions. In addition, the false solutions from Step 3 result in very high reactive power injections at the buses, which might compromise the main results.

As a remedial measure, the false solutions where the sum of the active and reactive power flow constraints exceed 0.05 are removed. It is, however, important to note that these states happen extremely rarely, and even with several simulation runs no false solutions were identified contributing to the reliability indices.

7 Case Studies

The developed standard HLII software and the HLII RPC software are tested and verified in this chapter. First, the test systems are described, including the system specific parameters utilised in the contingency state filtering stage and the contingency solver. This is followed by a description of the load model and the computer used in the simulations.

The objective of the first case study is to verify the developed standard HLII software, applied to RBTS and IEEE RTS. In the second case study the HLII RPC software is tested and verified, utilising the IEEE 30-bus system. Both case studies are divided into several cases.

7.1 Test Systems

Three different test systems are investigated in this thesis work. Each of them serves a purpose, either to strengthen the theoretical understanding, or to provide a proof of concept of the methods investigated. This section presents each system, with the goal to make it as clear as possible which parameters are used and the reasoning behind them.

7.1.1 Roy Billinton Test System (RBTS)

The RBTS is a simple system with 6 buses originally developed for educational purposes [11]. The YPL of the system is 185 MW, and the power factor is equal to 0.2 at all buses. The system consists of 11 generators with capacity ranging from 5 to 40 MW, adding up to a total generation capacity of 240 MW. The 6 buses are connected through 9 transmission lines. The system data can be found in Appendix D, where the tables include generator data, bus specifications, network parameters and outage data. The grid topology is shown in Figure 7.1.

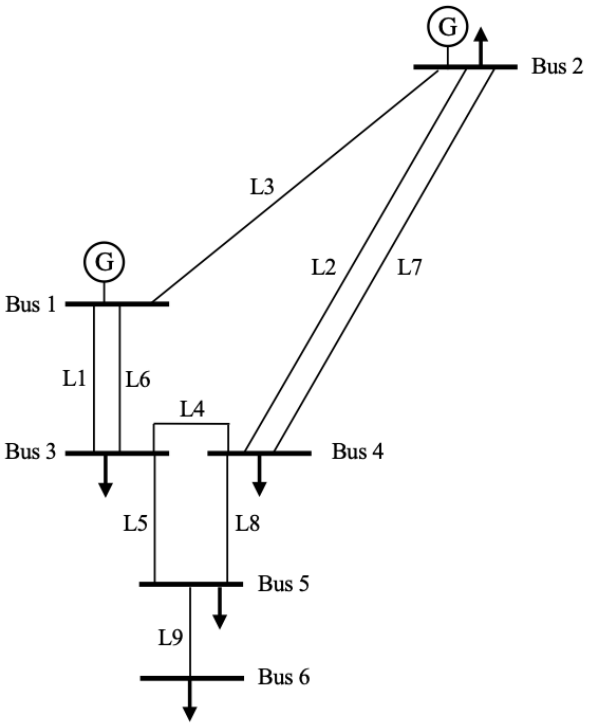

Figure 7.1: *Singe line diagram of the RBTS grid. Figure adapted from [11].*

System Specific Parameters

The parameters for the contingency state filtering criteria, described in Section 6.1, can be seen in Table 7.1. These are identical to the benchmark criteria [6], due to the direct comparison in Case 1 of the standard HLII assessment in Section 7.4.1. In addition, the duplicate contingency state filter is applied.

Table 7.1: *Filtering criteria [6] and duplicate filter applied to the RBTS for the standard HLII assessment.*

Test system	Generation capacity to load	Max lines on outage	Max generators on outage	Duplicate filter
RBTS	1.04 × Total load	0	2	Yes

Through testing, it was found that a change of alternative measures, compared to [6], was necessary. This is so because the benchmark measure scheme is highly inefficient with the OPF solver used in this thesis. A new strategy with subsequent reduction of the solver tolerance is therefore introduced, presented in Table 7.2. The measures are

based on utilising a starting point from the previous solution, which is found to be more accurate and more computationally efficient with the utilised OPF solver.

Table 7.2: *The initial starting point and subsequent measures when solving contingency states, with the standard HLII assessment applied on the IEEE RTS and the RBTS; and Steps 1 and 2 in the HLII RPC assessment applied on the IEEE 30-bus system.*

	P_{gen}	Q_{gen}	$Curt_P$	$Curt_Q$	V	δ	Iter	ftol
Initial	Max	0	0	0	1	0	300	10^{-4}
Measure 1	X_{init}	X_{init}	X_{init}	X_{init}	X_{init}	X_{init}	300	10^{-3}
Measure 2	X_{M1}	X_{M1}	X_{M1}	X_{M1}	X_{M1}	X_{M1}	300	10^{-2}
Measure 3	X_{M2}	X_{M2}	X_{M2}	X_{M2}	X_{M2}	X_{M2}	300	10^{-1}

7.1.2 IEEE Reliability Test System (IEEE RTS)

The IEEE RTS is a 24-bus system also developed for educational purposes, but is more complex than the RBTS [38]. The YPL of the system is 2850 MW, and the power factor is equal to 0.2 at all buses. The system consists of 32 generating units, ranging from 12 to 400 MW, adding up to a total generation capacity of 3405 MW. There are also voltage regulating units consisting of one synchronous condenser, one reactor and autotransformers. In addition, a total of 38 lines are connecting the buses. The system data can be found in Appendix E, which includes generator data, bus specifications, network parameters and outage data. The grid topology is shown in Figure 7.2.

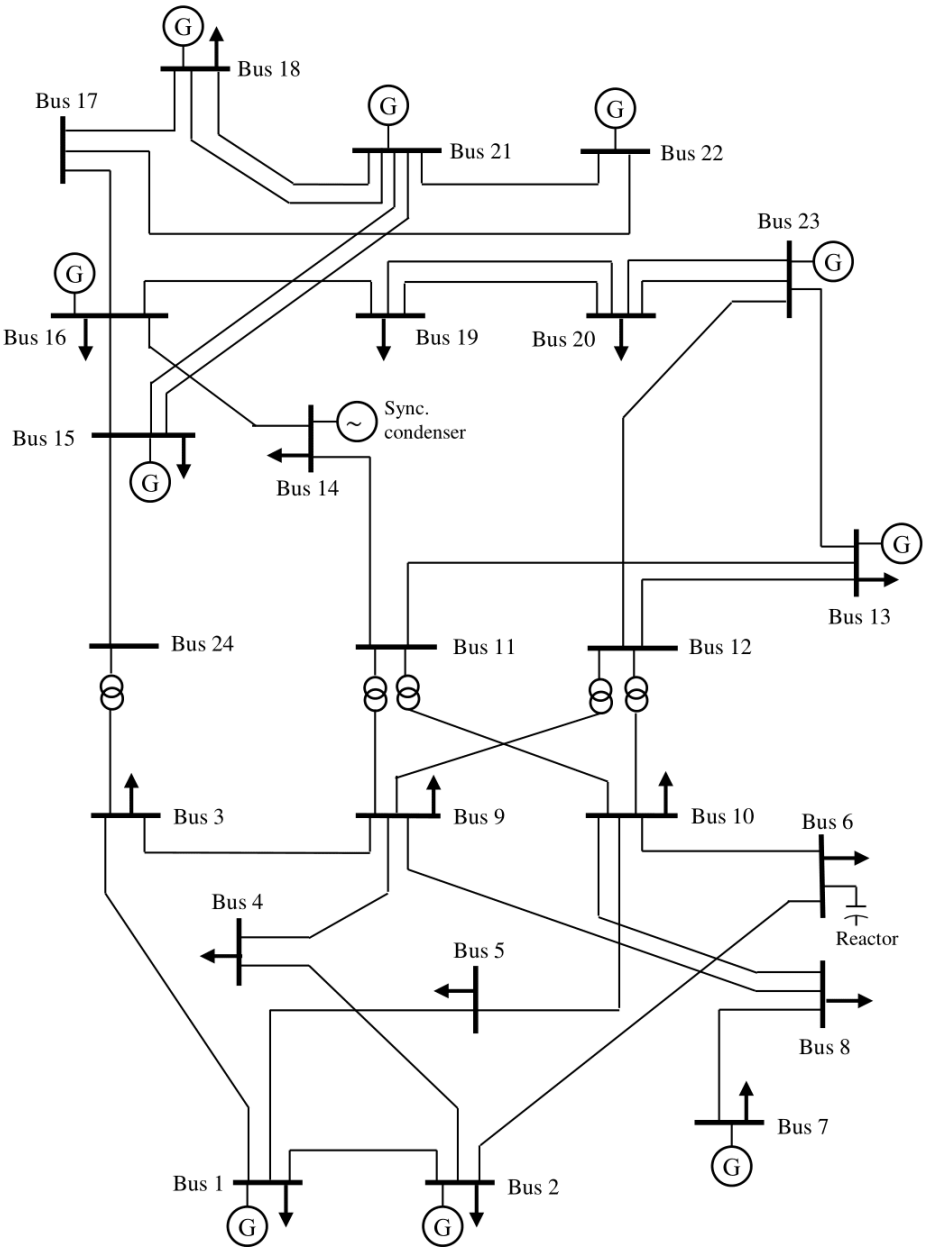

Figure 7.2: *Singe line diagram of the IEEE RTS grid. Figure adapted from [38].*

System Specific Parameters

The parameters for the contingency state filtering criteria, described in Section 6.1, are presented in Table 7.3. The first base criteria are chosen to be the same as the benchmark [6], due to the direct comparison of results. The filter criterion in [6] that investigates contingency states with the three generators on outage at Bus 7 is not applied. This is a decision made based on the objective of generalising the code. In addition, the duplicate contingency state filter is applied.

Table 7.3: *Filtering criteria [6] and duplicate filter applied to the IEEE RTS for the standard HLII assessment.*

Test system	Generation capacity to load	Max lines on outage	Max generators on outage	Duplicate filter
IEEE RTS	1.10 × Total load	0	5	Yes

The alternative measures used for the IEEE RTS are the same as for the RBTS, which are presented in Table 7.2. This measure scheme was also shown to be computationally efficient when applying it to the IEEE RTS.

7.1.3 Modified IEEE 30-bus System

When validating the code conversion of the method in [6] for the standard HLII assessment, applying it on the two test systems RBTS and IEEE RTS is crucial for proving the validity of the adaptation. In the testing phase of the HLII RPC code, however, both the RBTS and the IEEE RTS were found to be too robust. In practice, the voltage violations can in most cases be relieved by rescheduling of generation, causing no significant curtailments due to voltage violations. Thus, another test system needs to be implemented.

In [2], the reasoning behind choosing the modified IEEE 30-bus system reflects on the same points. The relatively long distance of power transmission due to the dense concentration of generation in the system, and high reactive power demand, makes it less robust and more prone to voltage issues. This is in direct contrast to the IEEE RTS system, where the generation capacity is distributed throughout the system. This thesis' scope is as a result narrowed down to only implement the IEEE 30-bus system found in [23], with modifications as stated in [2]. Thus, a comparison with the results from the source of the HLII RPC method [2] is seen as more valuable.

The topology of the modified system can be seen in Figure 7.3. It has 4 generation units of 60 MW at Bus 1 and 3 generation units of 20 MW at Bus 2. The active and reactive peak load is 283.4 MW and 126.2 MVar, respectively, with bus specific power factors shown

in Appendix F. The system also has 4 synchronous condensers and 6 shunt-capacitors distributed at different buses. In this thesis the 6 shunt-capacitors have perfect reliability and are also perfectly adjustable to full capacity, which is believed to differ from the benchmark method [2]. There are also tap-changing transformers with fixed tap settings. This, along with the generator data, bus specifications, the general network parameters and outage data, can be found in Appendix F.

The cost of curtailment at buses is set equally high at all buses to fit the solver tolerance parameter and the non-prioritised curtailment policy in [2]. The cost of curtailment is chosen based on experiences with the IEEE RTS.

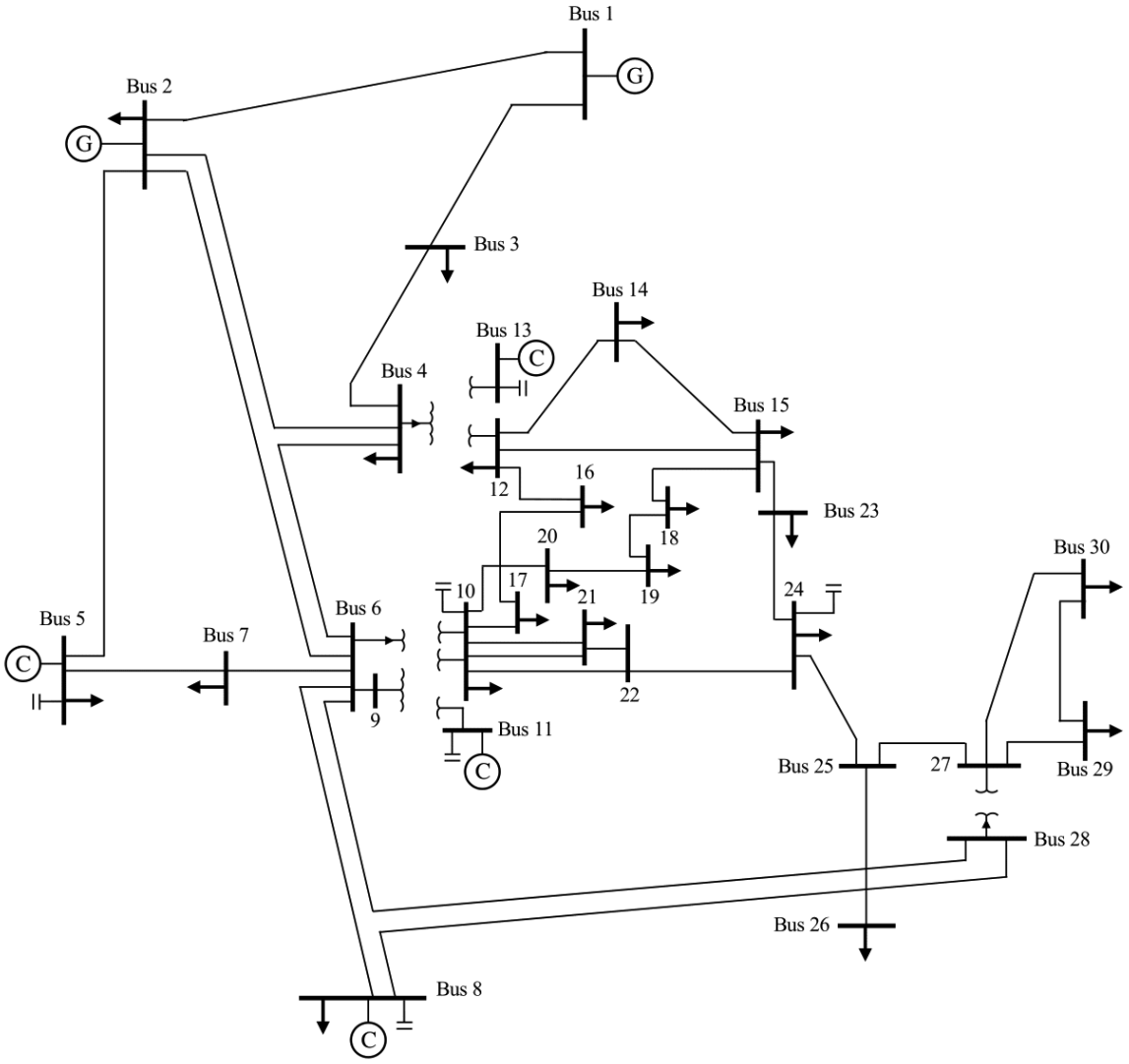

Figure 7.3: *Singe line diagram of the IEEE 30-bus system. Figure adapted from [23]*

System Specific Parameters

When comparing the IEEE RTS in Section 7.1.2 with the modified IEEE 30-bus system, both systems have similar amounts of transmission lines and buses. The key difference, from a composite system adequacy point of view, is the number of generators and how they are distributed throughout the system. The IEEE 30-bus system has all of its 7 active power generating units concentrated on 2 buses, causing it to be vulnerable for lower order contingency states. Thus, a strict generators on outage criterion is set, which can be seen in Table 7.4. It can also be observed that the generation capacity to load criterion is the same as for the IEEE RTS, as this has little to no measurable effect due to the very strict generator on outage criterion. The maximum lines on outage criterion is also the same as for the IEEE RTS, and the duplicate contingency state filter is applied.

Table 7.4: *Filtering criteria and duplicate filter applied to the modified IEEE 30-bus system for the RPC HLII assessment.*

Test system	Generation capacity to load	Max lines on outage	Max generators on outage	Duplicate filter
IEEE 30-bus	1.10 × Total load	0	2	Yes

The measure scheme for Steps 1 and 2 are the same as the one for the RBTS and the IEEE RTS, which is presented in Table 7.2. A more strict tolerance criteria is set for Step 3, as shown in Table 7.5. This is due to the significant reduction of states investigated by the solver in Step 3. Thus, the strict tolerance criterion is set to increase the accuracy of the result. As an example, in Table 7.6 it can be observed that out of the 273 773 initial investigated states in Step 1, only 3415 of them are investigated in Step 3.

Table 7.5: *The initial starting point and subsequent measures when solving contingency states in Step 3, for the RPC HLII State Sampling method applied on the modified IEEE 30-bus system.*

	P_{gen}	Q_{gen}	$Curt_P$	$Curt_Q$	V	δ	Iter	ftol
Initial	Max	0	0	0	1	0	500	10^{-6}
Measure 1	X_{init}	X_{init}	X_{init}	X_{init}	X_{init}	X_{init}	300	10^{-5}
Measure 2	X_{M1}	X_{M1}	X_{M1}	X_{M1}	X_{M1}	X_{M1}	300	10^{-4}
Measure 3	X_{M2}	X_{M2}	X_{M2}	X_{M2}	X_{M2}	X_{M2}	300	10^{-3}

Table 7.6: *The number of states at each step in the RPC HLII State Sampling method, after 500 years simulated.*

	Step 1	Step 2	Step 3
Initial	273 773	7365	3415
Measure 1	5065	394	351
Measure 2	3300	29	764
Measure 3	10	2	10
Failed states	0	17	59

7.2 Load Model

In the case studies, an hourly load model is utilised. Further explanation on hourly load model can be found in Section 2.4. The load data are found in Appendix C, based on data from [38]. The HPL at time t can be calculated as shown in Equation (7.1). $L_{weekly,t}$ is given as percentages of YPL, $L_{daily,t}$ is given as percentages of $L_{weekly,t}$ and $L_{hourly,t}$ is given as percentages of $L_{daily,t}$. The load model has seasonal, weekly, daily and hourly variations [38]. It must also be noted that using this approach to find the load for the hourly time increments results in $52 \cdot 7 \cdot 24 = 8736$ hours in a year.

$$HPL_t = YPL \cdot L_{weekly,t} \cdot L_{daily,t} \cdot L_{hourly,t} \tag{7.1}$$

7.3 NTNU Server Farm

In order to compare the performance in computational time, both the MATLAB code and the Python code are executed using the NTNU's Software Farm, Intel Xeon CPU E5-2690 v4 2.60GHz. This has a total of 28 cores. The number of available cores depends on the number of users that are connected at the same time.

The computational time performance is highly dependent on which computer hardware is being used and it is acknowledged that differences in software support on platforms can have an impact on the overall performance. In addition, the computational time is dependent on the available capacity of the computer being used. With that being said, a large difference in computational time can still be a clear indication that an actual improvement in performance is achieved.

7.4 Standard HLII Case Studies

As an important stepping stone towards the reactive power implementation, a verification of the standard HLII assessment code in Python is necessary to avoid any consequential errors. Since this thesis has adapted the methodological approach of [6], the results should be compared.

All simulations in the following case studies have been executed using the MCS State Sampling method, as explained in Chapter 4. The simulations are executed for 500 simulation years, utilising the NTNU server farm. As mentioned, the computational time may vary depending on the available capacity at the time of the simulation. In order to compare the computational time of the Python code and the MATLAB code, the latter has also been run using the NTNU server farm.

The standard HLII case studies will be presented in the following order:

- Case 1: Standard HLII assessment utilising the RBTS. The results from the simulations are presented, as well as a comparison with the benchmark results [6].
- Case 2: Standard HLII assessment utilising the IEEE RTS. The results from the

simulations are presented, as well as a comparison with the benchmark results [6].

7.4.1 Case 1: RBTS

The standard HLII assessment using State Sampling method on the RBTS is executed for 500 simulation years. The computational time for the simulation in MATLAB was approximately 20 minutes, while Python utilised approximately 2 minutes. Consequently, the execution in Python is around 10 times faster. The resulting indices for the Python code are presented in Table 7.7. The system CVs for the Python results and the MATLAB results are 1.40 % and 1.41 %, respectively. This means that the same degree of convergence is reached. A complete list of the CVs for each bus can be found in Table G.1 in Appendix G.

As expected, the highest curtailment is at Bus 6, because this part of the system does not comply with the N-1 criterion[1], which more often leads to the bus being isolated. In addition, there is a noticeable curtailment at Bus 3 due to the low curtailment cost at the bus.

Table 7.7: *The indices from the HLII State Sampling of the RBTS with 500 simulation years in Python. Buses without load are not included.*

Bus	LOLE [hours/year]	LOL SD [hours/year]	LOLP	EENS [MWh/year]	ENS SD [MWh/year]
2	0	0	0	0	0
3	1.948	1.365	0.000223	17.5218	16.8207
4	0.002	0.047	0	0.0001	0.0032
5	0.012	0.109	0.000001	0.0860	1.0788
6	10.822	3.322	0.001239	124.9821	41.4889
System:	12.552	3.456	0.001437	142.5891	44.6573

Figure 7.8 is made to compare the Python results and the MATLAB benchmark results. It can be observed that the system indices are almost identical, where the Python $EENS$

[1]The N-1 criterion states that if a component in the system is on outage, it should not cause losses in energy supply [44].

is only 0.6 % higher than the MATLAB EENS. This is to be expected, as the code adaptation developed in Python utilises the same method as [6].

Further, it can be seen that the bus indices differ slightly more. The curtailment at Bus 3 in Python is 11.7 % higher and the curtailment at Bus 6 is 2.1 % lower than the MATLAB results. It can also be noted that in the Python results there is a small curtailment at Bus 4, compared to no curtailment in the MATLAB results.

Due to the random nature of MCS, the results will never be exactly the same. For example, the curtailment on Bus 4 can be a consequence of a few very rare states that are sampled in the Python simulations but not in the MATLAB simulations. In general, it is not desirable to look for exact same results, but rather that the tendencies are the same, which is the case in these simulation results.

Table 7.8: *Comparison of the indices from the Python code and the MATLAB code [6] using the RBTS. Buses without load are not included.*

Bus	Python LOLE [hours/year]	MATLAB[6] LOLE [hours/year]	Python LOLP	MATLAB[6] LOLP	Python EENS [MWh/year]	MATLAB[6] EENS [MWh/year]
2	0	0	0	0	0	0
3	1.948	1.8220	0.000223	0.000209	17.5218	15.6874
4	0.002	0	0	0	0.0001	0
5	0.012	0.0060	0.000001	0.000001	0.0860	0.0736
6	10.822	11.4620	0.001239	0.001312	124.9821	127.6475
System:	12.552	12.5640	0.001437	0.001438	142.5891	143.4085

7.4.2 Case 2: IEEE RTS

The MCS using State Sampling method on the IEEE RTS is executed for 500 simulation years. The computational time for the simulation in MATLAB was approximately 245 minutes, while Python utilised approximately 55 minutes. Consequently, the execution in Python is more than 4 times faster. The system CV using Python is 1.47 %, whereas in the MATLAB results the system CV is 1.51 %. Thus, the same level of convergence is

reached. The CVs of the bus indices can be found in Table G.2 Appendix G.

The resulting indices from the Python code is presented in Figure 7.7. It can be observed that the largest $EENS$ values are at Bus 7, Bus 9 and Bus 14. The large curtailment at Bus 7 is due to the N-1 criterion not being fulfilled, and the curtailment at Bus 9 is due to its lowest curtailment cost. Bus 14 has the second to lowest curtailment cost.

Table 7.9: *The indices from the HLII State Sampling of the IEEE RTS with 500 simulation years in Python. Buses without load are not included.*

Bus	LOLE [hours/year]	LOL SD [hours/year]	LOLP	EENS [MWh/year]	ENS SD [MWh/year]
1	0.5600	0.7499	0.000064	0.5282	5.4560
2	0.4440	0.6774	0.000051	0.2649	2.5997
3	0.4220	0.6511	0.000048	0.7519	5.2887
4	0.3840	0.6169	0.000044	0.2418	2.8075
5	0.4040	0.6362	0.000046	0.1533	1.7310
6	3.3040	1.9266	0.000378	41.6690	29.2754
7	3.3560	1.7622	0.000384	225.2893	126.5689
8	0.3980	0.6384	0.000046	0.6885	7.2674
9	12.2920	3.2776	0.001407	1071.3724	347.2021
10	0.5400	0.7378	0.000062	9.9534	32.8875
13	0.4040	0.6235	0.000046	0.0025	0.0366
14	4.0580	1.9785	0.000465	314.3406	197.4549
15	0.4300	0.6302	0.000049	0.0092	0.1394
16	0.3860	0.6364	0.000044	0.0057	0.0800
18	0.4660	0.7049	0.000053	1.1076	14.2603
19	1.2580	1.1382	0.000144	64.5627	90.2010
20	0.4040	0.6487	0.000046	0.0452	0.5329
System:	18.0540	4.0639	0.002067	1730.9864	569.9086

The bus indices and the system indices of the Python code and the MATLAB code are presented in Table 7.10. It can be observed that the the system indices are similar, which is expected due to the equal methodological approach. The total EENS of the Python

results is 1.4 % lower than the total MATLAB EENS.

A main difference in the results is that in the MATLAB results $EENS$ at Buses 1, 2, 4, 13 and 16 are equal to zero. In the Python results, however, there are curtailments at all buses. This might be a consequence of the different measures used on the states where a solution is not initially found. Another possible explanation is how load shedding is performed when no solution is found and the approximate solution is used. Also factors like numerical precision can cause minor differences in the results.

Another major difference is the $LOLE$ at Bus 14 and Bus 19. It can, for example, be observed that the $LOLE$ at Bus 14 in the Python results is 1.2580 hours/year, compared to 11.5740 hours/year in the MATLAB results. A similar trend can be observed at Bus 14. However, the EENS results are similar. It can be difficult to point out exact reason for this difference. Since the solvers used in the two programming languages are different, the dissimilarity might be due to the different solver routines, how the solvers are prioritizing, or the tolerance level used. In addition, there are many possible solutions to the OPF problems of the contingency states, which can affect the resulting indices.

A remark should be made regarding a difference in the approach of the two codes. In [6], Bus 13 is defined as slack bus, which is renumbered as the new Bus 1. In addition, all other buses have been reorganized with new bus numbers as well. By looking at the generator data in Appendix E, it can be observed that making Bus 13 the slack bus can be a reasonable choice based on conventions due to its large generation capacity. However, when implementing HLII assessment in Python, Bus 1 was chosen as the slack bus. This is based on testing, where having Bus 1 as slack bus gave similar results as when having Bus 13 as slack bus. Also, since the goal was to generalise the code for utilisation on different systems, it was chosen to not investigate this matter further.

Another difference in the two approaches is that [6] investigates all states where all generation capacity at Bus 7 is on outage. This measure is not included in the Python code, in order to generalise the code as much as possible. The results show that the curtailment at Bus 7 in Python is 9.5 % lower than the curtailment in the MATLAB result. Thus, not including this measure might have an influence on the results.

Table 7.10: *Comparison of the indices from the Python code and the MATLAB code [6] using the IEEE RTS. Buses without load are not included.*

Bus	Python LOLE [hours/year]	MATLAB[6] LOLE [hours/year]	Python LOLP	MATLAB[6] LOLP	Python EENS [MWh/year]	MATLAB[6] EENS [MWh/year]
1	0.5600	0	0.000064	0	0.5282	0
2	0.4440	0	0.000051	0	0.2649	0
3	0.4220	0.1600	0.000048	0.000018	0.7519	0.4460
4	0.3840	0	0.000044	0	0.2418	0
5	0.4040	0.0020	0.000046	0.000000	0.1533	0.0969
6	3.3040	3.3880	0.000378	0.0000388	41.6690	45.1686
7	3.3560	3.4340	0.000384	0.000393	225.2893	249.0532
8	0.3980	0.0080	0.000046	0.000001	0.6885	0.2547
9	12.2920	11.6520	0.001407	0.001334	1071.3724	1060.7666
10	0.5400	3.5800	0.000062	0.000410	9.9534	9.8586
13	0.4040	0	0.000046	0	0.0025	0
14	4.0580	11.6340	0.000465	0.001332	314.3406	320.4070
15	0.4300	0.1440	0.000049	0.000016	0.0092	0.0148
16	0.3860	0	0.000044	0	0.0057	0
18	0.4660	0.6980	0.000053	0.000080	1.1076	1.0284
19	1.2580	11.5740	0.000144	0.001325	64.5627	68.8798
20	0.4040	0.1140	0.000046	0.000016	0.0452	0.0188
System:	18.0540	18.4500	0.002067	0.002067	1730.9864	1755.9935

7.5 HLII RPC Case Studies

The HLII RPC simulations have been executed for 500 simulation years. The states are sampled using MCS State Sampling method, and unnecessary states are filtered out using the techniques explained in Section 6.1.

As the HLII RPC approach contains three sequential OPF solver stages, it is expected that the total computational time increases compared to standard HLII assessment. The HLII RPC simulations take approximately 8 hours, utilising the NTNU server farm. However, as mentioned earlier, the computational time may vary depending how much capacity that is available at the time of the simulation.

To verify the method of [2], simulations have been performed on three different cases:

- Case 1: The first part of the case study presents the results from the HLII RPC assessment on the IEEE 30-bus System. The utilised MCS State Sampling method is explained in Section 4.2.1, and the RPC algorithmic approach utilised is presented in Section 5.4. The relevant results will be compared with the results of the benchmark paper [2], and the differences will be commented upon.
- Case 2: In the second case, $EENS$ from standard HLII assessment using the IEEE 30-Bus System is compared against $EENS_P$ and $EENS_Q$. The sum of $EENS_P$ and $EENS_Q$ should be close to the value of $EENS$. This is to validate if the active power curtailment due to active power shortage can be differentiated from the active power curtailment due by reactive power shortage.
- Case 3: The last case aims to validate that the index $EVarS$ can give information on where and how much reactive power compensation is needed to possibly reduce load shedding. This is done by placing a shunt capacitor at the bus with the most injection in Case 1, to create a reduction in the $EVarS$. This is tested for two shunt capacitors of different capacity levels, 2 MVar and 4 MVar, respectively. The shunt capacitors are assumed to have perfect reliability and are adjustable.

7.5.1 Case 1: HLII RPC Assessment and Benchmark Comparison

The bus and system SD for the indices can be found in Table H.1 in Appendix H. The system CVs for the different RPC indices are shown in Table 7.11, and the CVs for each bus can be found in Table H.2 in Appendix H. It can be observed that the system CV of $EENS_P$ is the lowest, whereas the CVs of $EENS_Q$ and $EVarS$ are slightly higher. However, as written in Section 4.2.3, a CV of 1-2 % can be considered fully converged, which means that the indices have in this case converged sufficiently.

Table 7.11: *System CVs for the different RPC indices.*

	$EENS_P$	$EENS_Q$	$EVarS$
CV [%]	0.81	1.7	2.70

$\mathbf{EENS_P}$

In Table 7.12 the resulting indices from the HLII RPC assessment are presented, where $EENS_P$ is the expected energy not supplied due to active power shortage. The $EENS_P$ shows high curtailment at Buses 5, 26 and 30. The curtailment at Bus 5 might be caused by the bus having the largest load in the system, where curtailment at high load levels is inevitable if one of the two connecting lines is on outage. Bus 26 is the bus that is the most prone to isolation, due to not fulfilling the N-1 criterion.

Further, it can be observed that Bus 30 has the highest curtailment of all buses in the system. This might be due to its remote placement in the system, furthest away from the sources of generation. In addition, it can be observed that Bus 30 has a higher curtailment than Bus 29. This is a consequence of Bus 30 having a share of load 4 times larger than Bus 29, which should result in larger curtailment.

$\mathbf{EENS_Q}$

The index $EENS_Q$ represents the expected energy not served due to reactive power shortage, and indicates where in the system voltage violations are most likely to occur. In Table 7.12 it can be observed that Buses 26, 29 and 30 are most prone to the voltage violations that lead to curtailment. This is to be expected, as the closest shunt capacitor

is placed quite far away, at Bus 24. This argument is also pointed out in [2]. In addition, these are the most remotely placed buses with respect to the generating units in the system.

$\mathbf{EVNS_P}$ and $\mathbf{EVNS_Q}$

The $EVNS_P$ and $EVNS_Q$ in Table 7.12 are functions of $EENS_P$ and $EENS_Q$, respectively. This is because of the fixed power factor at the load buses. It can be seen that their values correspond to the power factor relationship, which indicates that the solver complies with the method used in this thesis.

EVarS

The expected reactive power shortage due to voltage violations, $EVarS$, reflects the values of the corresponding bus indices of $EENS_Q$. As seen in Table 7.12, the $EVarS$ is the highest at Bus 30. This is also the bus with the highest $EENS_Q$. It would not be inaccurate to expect that an increase in reactive power capacity at this bus is also beneficial for the voltage levels at the surrounding buses. This would explain why $EVarS$ is much higher at Bus 30 than at the other buses in near proximity. In general, the $EVarS$ in correlation with the $EENS_Q$ is an indication on what curtailment that could have been avoided if more reactive power was available at the buses.

It must be pointed out that the method allows for reactive power injections at buses without any load, which can be seen by the absence of values for other indices in Table 7.12. The result of this gives an interesting effect, with a higher $EVarS$ at bus 28 than 29. Bus 28 has no load and whereas Bus 29 has a significant $EENS_Q$. This might have been caused by the reactive power transportation from Bus 8, where it would be more beneficial to compensate closer to the area with voltage violations for some contingency states. If reactive power injections were only allowed on voltage violated buses with load, the $EVarS$ would most probably have increased at Bus 29.

Table 7.12: *Energy based indices for HLII RPC using the IEEE 30-bus system.*

Bus	$EENS_P$ [MWh/year]	$EENS_Q$ [MWh/year]	$EVNS_P$ [MVarh/year]	$EVNS_Q$ [MVarh/year]	$EVarS$ [MVarh/year]
1	–	–	–	–	0
2	0.95323	0	0.5579	0	0
3	0.1520	0	0.0760	0	0
4	1.7069	0	0.3594	0	0
5	164.1098	0	33.1007	0	0
6	–	–	–	–	0
7	12.3183	0.0005	5.8890	0.0003	0.0125
8	75.0160	0.0029	75.0160	0.0029	0
9	–	–	–	–	0
10	19.0334	0	6.5633	0	0
11	–	–	–	–	0
12	0.3256	0.0003	0.2180	0.0002	0
13	–	–	–	–	0
14	19.7113	0.0178	5.0868	0.0046	0.0181
15	5.6927	0.0011	1.7356	0.0003	0.0573
16	0.4612	0.0015	0.2372	0.0008	0
17	1.1959	0.0185	0.7707	0.0119	0.2057
18	13.1283	0.0073	3.6923	0.0021	0.1129
19	5.8056	0.0548	2.0778	0.0196	0.1237
20	6.1278	0.0167	1.9498	0.0053	0.0251
21	4.1079	0.2164	2.6291	0.1385	0.1283
22	–	–	–	–	0.0001
23	0.6651	0.0544	0.3326	0.0272	0.0461
24	0.5961	0.0411	0.4590	0.0316	0.0151
25	–	–	–	–	0.0210
26	108.7888	0.5570	71.4898	0.3661	0.0858
27	–	–	–	–	0.0241
28	–	–	–	–	0.7538
29	15.5219	3.7586	5.8207	1.4095	0.3977
30	184.5210	16.3157	33.0745	2.9245	7.3850
System:	639.9385	21.0646	251.1358	4.9453	9.4212

$\mathbf{ELC_P}$

The expected curtailment due to active power shortage, ELC_P, seen in Table 7.13, corresponds well with the $EENS_P$ in Table 7.12. At Bus 5 the ELC_P is expected to be high due to the large load at the bus. ELC_P at Bus 30 is also relatively high. However, Bus 30 has a close but higher $EENS_P$ than Bus 5, but less than half of the ELC_P. This can indicate that when there is curtailment at Bus 5, the curtailment is larger.

$\mathbf{ELC_Q}$

The expected curtailment due to reactive power shortage ELC_Q, presented in Table 7.13, coincides with the $EENS_Q$ in Table 7.12. ELC_Q is largest at Buses 29 and 30, which are the buses that also have the highest $EENS_Q$. It must be pointed out that the $EENS_Q$ and ELC_Q have equal values at Bus 7 to Bus 20, as well as Bus 24. This is most probably caused by only one contingency state in the whole 500 year simulation run. The high bus CV, which is presented in Appendix H.2, further confirms that these bus specific values have not converged properly. This ultimately shows the importance of also evaluating the indices based on their individual bus CV.

$\mathbf{EQC_P}$ and $\mathbf{EQC_Q}$

The EQC_P and EQC_Q in Table 7.13 are functions of ELC_P and ELC_Q, respectively, and are based on the set power factor at each bus. It can be observed that their values correspond to this power factor relationship, which indicates that the solver complies with the method used in this thesis.

Table 7.13: *Capacity based indices for HLII RPC using the IEEE 30-bus System. Buses without load are not included.*

Bus	ELC_P [MW/year]	ELC_Q [MW/year]	EQC_P [MVar/year]	EQC_Q [MVar/year]
2	0.3268	0	0.1989	0
3	0.0651	0	0.0331	0
4	0.5059	0	0.1172	0
5	12.7910	0	2.6578	0
7	2.5548	0.0005	1.2481	0.0002
8	3.8867	0.0029	3.8867	0.0029
10	2.5233	0	0.9010	0
12	0.1503	0.0003	0.1028	0.0002
14	1.8641	0.0178	0.4948	0.0046
15	1.0936	0.0011	0.3559	0.0003
16	0.2120	0.0015	0.1146	0.0008
17	0.4668	0.0185	0.3103	0.0119
18	1.2496	0.0073	0.3603	0.0021
19	1.1307	0.0548	0.4248	0.0196
20	0.9188	0.0167	0.3020	0.0053
21	1.3448	0.2129	0.8717	0.1363
23	0.2909	0.0499	0.1539	0.0250
24	0.1580	0.0411	0.1227	0.0316
26	1.9337	0.4074	1.2734	0.2677
29	0.8761	0.8005	0.3313	0.3003
30	4.9748	2.1251	0.8972	0.3809
System:	39.3177	3.7583	15.1583	1.1896

Comparison With the Benchmark Method

A direct comparison with [2] for the following indices $EENS_P$, $EENS_P$, ELC_P and ELC_Q will not be conducted because of the differences in the curtailment method. It is important to restate that this thesis' load shedding policy with its equal cost of curtail-

ment is neither priority based nor is it curtailing equally at buses during a contingency state. In other words, the resulting curtailment is based on the amount of load at each bus and the topography of the grid. This is a clear difference, which in most cases is expected to give different results.

It is also important to point out that [2] only provides bus specific values utilising a CYPL model, and by that the values are expected to be higher than this thesis' results, where a HPL model is utilised. In addition, the filtering techniques differ substantially, which also affects the results.

$\mathbf{EENS_Q}$ and $\mathbf{ELC_Q}$

Table 7.14 shows a comparison of the $EENS_Q$ and ELC_Q with the results from the benchmark method [2]. The $EENS_Q$ is overall lower, as expected, and the comparison indicates that voltage violations occur in the same areas of the system.

The largest deviation can be observed at Bus 5, which has a high $EENS_Q$ in the benchmark results [2]. In the results from this thesis, however, there is no curtailment at Bus 5. This might be due to the difference in the curtailment method. The method of [2] is to curtail proportionally at all voltage violated buses until all voltage violations are alleviated. This can lead to large curtailments at buses with only minor voltage violations, which might be the case for Bus 5.

In the method used in this thesis, however, the objective of the OPF is to minimise the curtailment. Thus, curtailment is only performed at the buses where curtailments are strictly necessary to alleviate the voltage violations. It is also possible that [2] do not consider the possibility of rescheduling generation, which in the method utilised in this thesis might solve the initial voltage violations at Bus 5.

Another explanation for the differences in the results might be how the utilisation of the shunt capacitors is interpreted, this is explained in Section 5.3. Consequently, the interpretation made by this thesis could be expected to have less voltage issues in the test system, leading lower values for the related indices compared to the results of [2]. It might also explain the large $EENS_Q$ at Bus 5 in the benchmark results, and why it is absent in this thesis' results.

Table 7.14: *Obtained indices compared with the benchmark indices [2], where the benchmark uses a CYPL model. The buses without load are not included.*

Bus	$EENS_Q$ [MWh/year]	$EENS_Q$[2] [MWh/year]	ELC_Q [MW/year]	ELC_Q[2] [MW/year]
2	0	0	0	0
3	0	0	0	0
4	0	0	0	0
5	0	12.3818	0	1.7146
7	0.0005	0.9068	0.0005	0.1256
8	0.0029	1.264	0.0029	0.1806
10	0	0	0	0
12	0.0003	0.7405	0.0003	0.1046
14	0.0178	0.3305	0.0178	0.0467
15	0.0011	0	0.0011	0
16	0.0015	0	0.0015	0
17	0.0185	0.2465	0.0185	0.0533
18	0.0073	0	0.0073	0
19	0.0548	0.0811	0.0548	0.0176
20	0.0167	0.0011	0.0167	0.0002
21	0.2164	1.033	0.2129	0.223
23	0.0544	0.0884	0.0499	0.0191
24	0.0411	0.0741	0.0411	0.0161
26	0.5570	4.9766	0.4074	0.7218
29	3.7586	28.1153	0.8005	3.6058
30	16.3157	17.1324	2.1251	2.298
System:	21.0646	67.4098	3.7583	9.127

In the results of [2], the $EENS_Q$ of Bus 29 is larger than the $EENS_Q$ at Bus 30. In this thesis' results, however, it is the other way around. It could be expected, based on the method of [2], that Bus 30 would have more curtailment than Bus 29 as the load is approximately four times larger and the loads are shed proportionally. In addition,

Bus 30 is the most remote bus in the system, so the largest curtailment value might be expected at this bus.

Another argument in favor of this thesis' results is that the lines connecting Buses 29 and 30 to Bus 27 and to each other, have the same capacity and FOR value. This should not lead to more contingency states where Bus 29 is the most remote bus, and thus have larger curtailment.

The ELC_Q in Table 7.14 confirms the same trends as their corresponding $EENS_Q$ index for both results.

EVarS

The expected reactive power shortage due to voltage violations, $EVarS$, is compared with the $EVarS$ of the benchmark [2] in Table 7.15. Again, it should be mentioned that the benchmark results are based on a CYPL model, while this thesis uses a HPL model. Thus, the values of [2] are in general higher. In general, it can be observed that the $EVarS$ reflects the $EENS_Q$ in Table 7.14 for the results of [2] as well as the results of this thesis.

It can be observed that the buses with a high $EENS_Q$ also have a high $EVarS$. Also in this case, the $EVarS$ at Bus 30 is larger than at Bus 29, as opposed to the results of [2]. This is not discussed further, as the arguments are the same as for $EENS_Q$.

In addition, it can also be noticed that the benchmark results has $EVarS$ at Bus 27 instead of Bus 28, which has more $EVarS$ in this thesis' result. This might indicate that the reactive power injection routine in the benchmark method [2] acts differently from the OPF approach in this thesis.

Table 7.15: *The comparison of the $EVarS$ with the benchmark [2], where the benchmark load model is based on a CYPL. Buses where both indices are equal to zero are not included.*

Bus	$EVarS$ [MVarh/year]	$EVarS$[2] [MVarh/year]
5	0	10.012
7	0.0125	1.2564
8	0	1.4203
12	0	0.8645
14	0.0181	0.2732
15	0.0573	0
17	0.2057	0.3228
18	0.1129	0
19	0.1237	0.0762
20	0.0251	0.0021
21	0.1283	1.2594
22	0.0001	0
23	0.0461	0.0799
24	0.0151	0.104
25	0.021	1.8098
26	0.0858	4.4569
27	0.0241	8.6035
28	0.7538	0
29	0.3977	23.153
30	7.385	14.345
System	9.4212	68.039

Hourly Load Model Results

The results of using HPL model should also be discussed. In the benchmark paper [2], only the system indices when using HPL is presented. Also, as written earlier, [2] utilises an approximate HPL model.

The HPL results are shown in Table 7.16. It can be observed that the indices in the benchmark results are much lower than the results of this thesis. Through testing, it was found that the curtailment caused by isolated buses alone would almost be as high as the total $EENS_P$ in [2]. This significant difference in the indices might be due to the contingency states considered. The benchmark paper [2] only considers 1378 of all up to second order contingency states, whereas this thesis has the possibility to investigate all possible contingency states due to the MCS approach. The results in this thesis are therefore based on a larger variety of contingency states, including the extreme states that often have a larger impact on the final results.

Table 7.16: *The total system indices for the HLII RPC and the benchmark [2] using the IEEE 30-bus system.*

	$EENS_{P+Q}$ [MWh/year]	$EVarS$ [MVarh/year]	ELC_{P+Q} [MW/year]	EQC_{P+Q} [MVar/year]
RPC HLII	661.0031	9.4212	43.0760	16.3992
Benchmark [2]	152.15	1.96	0.2893	0.0864

Comment on Including Additional Shunt Capacitors

As written in Section 5.2, there in an uncertainty regarding the system when PV buses are changed to PQ buses. The interpretation used in this thesis ultimately provides an increased reactive power capacity in the system. However, not including this capacity can also be an interpretation of the method in [2].

Therefore, the RPC script has been run without including the additional shunt capacitors, and the results are shown in Table H.3 in Appendix H. This results in more curtailment due to reactive power shortage and larger reactive power injections, which is to be expected due to less available reactive power in the system under consideration. This matter will not be investigated further, but is worth noting. Case 2 and Case 3 will be based on the system including the shunt capacitors.

7.5.2 Case 2: Comparison of Standard HLII and HLII RPC

The standard HLII assessment is performed to make a comparison with the HLII RPC assessment, where both are conducted using the same set of MCS states. The objective is to investigate if the active power curtailment due to active power shortage can be differentiated from the curtailment caused by reactive power shortage.

In Table 7.17, the sum of $EENS_P$ and $EENS_Q$ from Case 1 and standard HLII $EENS$ are presented. The difference in the total expected energy not supplied is only 0.2 %. The bus values are also similar.

The disparity between the $EENS_{P+Q}$ of Case 1 and $EENS$ of standard HLII can be explained by, among others, the CV of the indices. In Table 7.18 it can be observed that the CV of $EENS_Q$ is higher than the two other indices. Thus, $EENS_{P+Q}$ is "less" converged than $EENS$ of standard HLII, which means that the values vary more. Factors such as numerical precision can also have an influence on the variation of results.

Table 7.18: *System CVs for the indices of Case 2.*

	$EENS_P$	$EENS_Q$	$EENS$
CV [%]	0.81	1.7	0.79

7.5.3 Case 3: Adding Shunt Capacitors

The two shunt capacitors of 2 MVar and 4 MVar that are added to Bus 30 are deemed to have perfect reliability and are adjustable. This is done so that the reliability of these components does not affect the standard reliability indices. The placement of the shunt capacitor is based on the results from Case 1, where Bus 30 had the highest expected Var shortage, $EVarS$. The objective is to investigate whether shunt capacitors can be strategically placed to reduce the reactive power shortage in the system.

Table 7.19 shows the resulting bus and system $EVarS$ at Buses 23-30. The second and third columns show the $EVarS$ of each bus when adding shunt capacitors of 2 MVar and 4 MVar, respectively. A table including values at all buses can be found in Table H.4

Table 7.17: *$EENS_{P+Q}$ (Sum of $EENS_P$ and $EENS_Q$) for HLII RPC, and $EENS$ from standard HLII applied on the IEEE 30-Bus system. Buses with no load are not included.*

Bus	$EENS_{P+Q}$ [MWh/year]	$EENS$ [MWh/year]
2	0.9533	0.8075
3	0.1520	0.1412
4	1.7069	1.7068
5	164.1098	163.2079
7	12.3187	12.3292
8	75.0188	74.7980
10	19.0334	19.0334
12	0.3259	0.2937
14	19.7290	19.6938
15	5.6938	5.6735
16	0.4627	0.4019
17	1.214	1.2430
18	13.136	13.1256
19	5.8604	5.9065
20	6.1445	6.1592
21	4.3243	4.4082
23	0.7195	0.4701
24	0.6371	0.6019
26	109.3458	109.2063
29	19.2805	18.4769
30	200.8366	201.7837
System:	661.0031	659.4680

Appendix H. The reduction of injected reactive power at Bus 30 is 81.8 % when adding a shunt capacitor of 2 MVar, and 99.7 % when adding a shunt capacitor of 4 MVar.

Table 7.19: *$EVarS$ at Bus 23-30 when adding shunt capacitors of 2 MVar and 4 MVar at Bus 30, using the IEEE 30-Bus system in HLII RPC assessment.*

Bus	$EVarS$ Case 1 [MVarh/year]	$EVarS$ +2 MVar [MVarh/year]	$EVarS$ +4 MVar [MVarh/year]
⋮	⋮	⋮	⋮
23	0.0461	0.0134	0.0120
24	0.0151	0.0044	0.0493
25	0.0300	0.0010	0.0109
26	0.0858	0.1517	0.1154
27	0.0241	0	0.0028
28	0.7538	0.5940	0.4247
29	0.3977	0.0903	0.0119
30	7.3850	1.3415	0.0208
System:	9.4212	2.44367	1.1651

In addition, as shown in Table H.4 in Appendix H, the curtailments decrease as well when adding an extra shunt capacitor. This is probably caused by the reduction of states with voltage violations. In Table 7.20, it can be seen that the states with voltage violations decrease significantly when adding a shunt capacitor at Bus 30.

However, it can also be observed that the CV increases. As many states that previously had voltage violations are no longer considered, the cases that lead to higher injections are more prominent. These often have a higher variance, and thus a higher CV. More simulation years should therefore be considered to obtain a lower CV.

Table 7.20: *Number of states considered at Step 2 and Step 3, and the resulting system CVs.*

	Case 1	+2 MVar	+4 MVar
Number of states Step 1	273 773	270 538	269 740
Number of states Step 2	7365	2487	745
Number of states Step 3	3415	1242	336
CV_{EVarS} [%]	2.7	5.7	13.3

7.6 Duplicate Contingency State Filtering Application in MCS

For composite system adequacy assessment, the most computational demanding part pertains to the contingency solver. The number of contingency states usually increases with the number of components in the system. In addition, the number of contingency states sampled also increases with the number of simulation years. As a result, the total computational time will increase considerably.

As written in Section 6.1, three base contingency state filtering criteria are introduced in [6]. This includes load level criterion, and generators and lines on outage criteria. For simplicity, these are referred to as the benchmark filter in this section. As an extension, a duplicate state filtering technique is introduced in this thesis. Thus, an evaluation of the proposed technique should be conducted.

7.6.1 RBTS

In Figure 7.4a, the effect of the benchmark filter for the RBTS is represented by the yellow line. It can be observed that the total number of contingency states without any filtering increases rapidly, reaching more than 1.8 million sampled contingency states at 1000 years simulated. The effect of the three benchmark criteria from [6] reduces the number of sampled states to 200 000, which can be observed in the figure.

By introducing the duplicate filter, represented by the red line in Figure 7.4b, the total number of investigated contingency states is further reduced to around 40 % of the

benchmark criteria states at 1000 years simulated. An interesting observation is that the contingency states after the duplicate filter seem to flatten out after 1000 years of simulation, while the benchmark filter continues to increase linearly. This can also be interpreted as: the number of unique states being sampled is decreasing with an increasing number of simulation years.

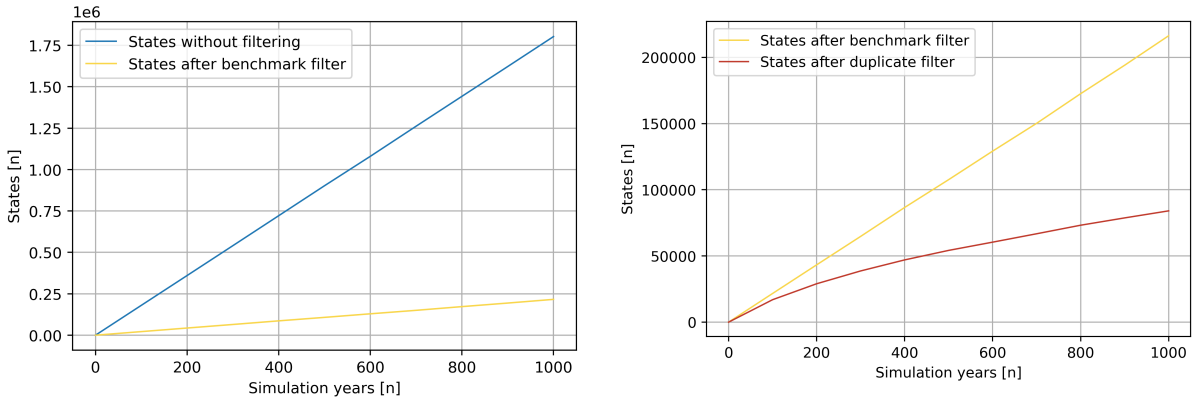

(a) **(b)**

Figure 7.4: *The number of sampled states for the RBTS, before and after the benchmark criteria and duplicate filtering.*

7.6.2 IEEE RTS

In Figure 7.5a it can be observed that the benchmark filter reduces the total amount of states from 7 million to around 200 000 at 1000 years simulated. By comparing Figure 7.5b for the IEEE RTS and Figure 7.4b for the RBTS, it can be observed that the effect of the duplicate filter is much smaller when applied to the IEEE RTS. This is most likely due to the IEEE RTS being a much larger system with more components. Consequently, the number of unique states increases tremendously, resulting in a significant decrease in the occurrences of duplicate states. At 1000 simulation years, the reduction of duplicate states is 5.6 % of the sampled states compared to the benchmark filter, and at 500 simulation years the reduction is only 3.3 %.

In addition, the number of generators on outage criterion is much stricter for the IEEE RTS than for the RBTS, where more than 5 generators have to be on outage for the state to be investigated. Because the FOR for the generators are much higher than for

the transmission lines, it is expected that more contingency states with only generators on outage will be sampled. When there are more contingency states with generators on outage, the probability of repeating states is also increased. However, these states are filtered out by the benchmark filter before the duplicate contingency state filter is applied, which in turn will reduce the effect of the duplicate filter.

It should be noted that the increase in computational time for filtering duplicate contingency states is only in the range of seconds. Thus, the benefit of having a reduced amount of investigated contingency states will decrease the total computational time by much more, even for the IEEE RTS.

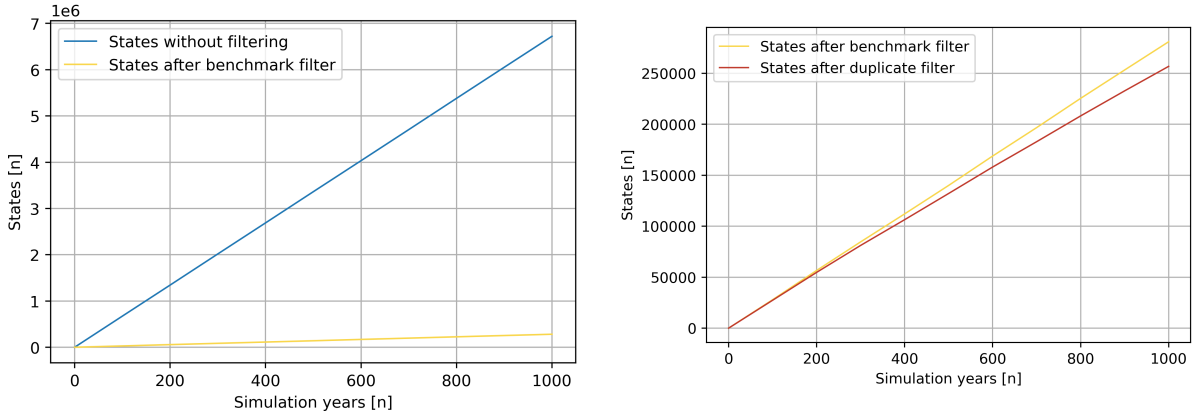

(a) **(b)**

Figure 7.5: *The number of sampled states for the IEEE RTS, before and after the benchmark criteria and duplicate filtering.*

7.6.3 IEEE 30-Bus System

Due to the strict generator on outage criterion for the IEEE 30-bus system, the number of contingency states after applying the benchmark filter is high. However, the system has few generating units compared to the IEEE RTS, which should result in a greater number of recurring contingency states. Thus, the duplicate contingency state filter is expected to have a greater effect on the IEEE 30-bus system than on the IEEE RTS.

As shown in Figure 7.6a, the number of initial states at 1000 simulation years is almost 3 million. The number of contingency states after the benchmark filter is less than 1

million. This shows that the benchmark filter is less effective when applied on the IEEE 30-bus system, compared with the effect on the IEEE RTS.

In Figure 7.6b at 1000 simulation years, the number of investigated contingency states is further reduced by around 47 %, when the duplicate filter is applied. This results in 274 046 contingency states being investigated by the contingency solver. Thus, showing that the duplicate contingency state filter can reduce the amount of investigated states significantly.

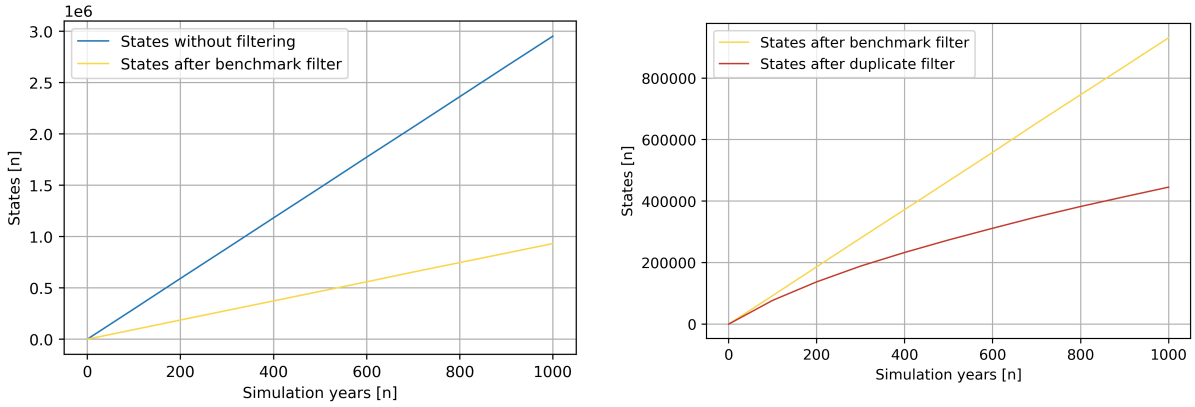

(a) **(b)**

Figure 7.6: *The number of sampled states for the modified IEEE 30-bus system, before and after the benchmark criteria and duplicate filtering.*

8 Conclusions and Further Work

8.1 Conclusions

This thesis adapted the MCS State Sampling method [10] and the AC-based optimal power flow approach of [6] to conduct composite system adequacy assessment. To further implement reactive power considerations, the standard HLII approach was combined with the so-called RPC method and proposed reliability indices of [2]. Two in-house Python scripts were developed for the applied methods: one for the standard HLII assessment and one for HLII RPC assessment. Also, a duplicate contingency state filtering technique for the MCS State Sampling method was developed to reduce computational time for both assessments.

By building on top of the previous work conducted by [6], this thesis aimed, through reproduction of the benchmark results, to verify the composite system adequacy assessment tool developed in Python. In addition to creating a foundation of its own for the continued work using Python in PSR studies, an important objective has been to present the work in a transparent and pedagogical manner. This was endeavoured by making the algorithmic approach as detailed and self-explanatory as possible, enabling a full replication of the results.

The adaptation of the methodological approach of [6] was found to be successful when applied to the RBTS and the IEEE RTS; this was concluded through the observed similarities of the main adequacy indices, as well as their satisfactory CVs. The results are a proof of the ability of reproduction of the adapted method. The deviation between some of the indices might be explained by the different contingency solvers applied, as well as the absence of system specific filtering criteria in the approach used in this thesis. This indicates a future necessity of implementing system specific criteria.

The adaptation of the RPC method of [2] in combination with an MCS OPF approach was shown to be feasible. By comparing the relevant indices with the results of [2], a difference in contingency state solver routines was observed. This resulted in curtailments and voltage violations at slightly different system locations. This also showed that new

insights into the system can be gained with the MCS and OPF-based approach when working with RPC in HLII reliability assessment.

The results of the RPC HLII assessment indicated that it is possible to differentiate the curtailments due to reactive power shortage from the curtailments caused by active power shortage. This is an important contribution to the verification of the RPC method. It must, however, be noted that this was only verified using the modified IEEE 30-bus system.

The results from the reactive power injection method indicate that the indices can give valuable information on where to strategically locate additional reactive power compensation. A step-wise implementation of larger reactive power compensation at the bus with the highest initial reactive power injection, reduced the corresponding reliability indices. This revealed that the voltage conditions in the system considered were significantly improved.

The duplicate contingency state filtering technique showed itself to be highly beneficial when sampling system states, in that a large reduction of states could be observed. This result also supports the algorithmic decision to sample all system states before the contingency solver investigation. The implementation of the duplicate contingency state filter for both the standard HLII assessment and HLII RPC assessment resulted in an additional reduction of the computational time, compared to the standard HLII benchmark results [6].

8.2 Further Work

A natural continuation of this thesis work would be to investigate the MCS State Transition method, explained in Section 3.1.3, in combination with the RPC method. This is so as to achieve frequency based indices, which could give new insight in the rate at which contingency states with voltage violations occur.

Applying the RPC method from this thesis on other test systems for further validation could also be valuable. However, it is then advised to investigate systems similar to the modified IEEE 30-bus system. This to be able to provoke voltage violations that can only be alleviated through load shedding instead of rescheduling of generation.

The method in [2] also investigates the effect of utilising a generator model based on its PQ-curve, where a reduction in the voltage violations due to reactive power shortages was observed. An implementation of this generator model could give a more realistic representation of the generation capability, both for the standard HLII assessment and the HLII RPC assessment.

Reactive power considerations in PSR with respect to renewable power generation has previously been investigated, for example in [45]. However, only an analytic approach similar to the one in [2] is applied. The HLII RPC tool utilising an OPF approach developed in this thesis gives a foundation to investigate what impact renewable power sources have on voltage issues and reactive power shortages. Renewable power sources like wind power and solar power could for example be implemented.

Voltage stability issues in the distribution grid is a growing concern, where the location of reactive power compensation is one of the main aspects of improvement [4]. Thus, it would be interesting to implement the RPC method and the associated reliability indices in reliability assessment at the distribution level.

Solving contingency states in composite system assessment in PSR is the most computationally demanding task. Thus, a further improvement in code efficiency to reduce computational time is a relevant extension of the work conducted in this thesis.

Contingency state filtering techniques have in this thesis shown to reduce the amount of

states investigated in the contingency solver, heavily impacting the over all computational time. Other filtering techniques have been suggested [46, 47], and an investigation of this topic for application to the MCS methods could reduce the computational time even further. This would allow for even larger systems to be investigated with the RPC method, while at the same time maintaining a reasonable time duration of the simulations.

References

[1] IEA. (2020, Oct) World Energy Outlook 2020. IEA. Paris. [Online]. Available: https://www.iea.org/reports/world-energy-outlook-2020

[2] W. Qin, P. Wang, X. Han, and X. Du, "Reactive Power Aspects in Reliability Assessment of Power Systems," IEEE Transactions on Power Systems, vol. 26, no. 1, pp. 85–92, Feb 2011.

[3] IEA. (2020, Apr) Global Energy Review 2020. IEA. Paris. [Online]. Available: https://www.iea.org/reports/global-energy-review-2020

[4] S. Hu, Y. Xiang, X. Zhang, and et.al., "Reactive Power Operability of Distributed Energy Resources for Voltage Stability of Distribution Networks," Mod. Power Syst. Clean Energy, no. 7, p. 851–861, Jan 2019.

[5] M. Benidris, S. Sulaeman, Y. Tian, and J. Mitra, "Reactive Power Compensation for Reliability Improvement of Power Systems," in 2016 IEEE/PES Transmission and Distribution Conference and Exposition (T&D), May 2016, pp. 1–5.

[6] O. S. Laengen, "Application of Monte Carlo Simulation to Power System Adequacy Assessment," NTNU, Trondheim, 2018, Master thesis.

[7] R. Billinton and R. N. Allan, "Power-system Reliability in Perspective," Electronics and Power, vol. 30, no. 3, pp. 231–236, Mar 1984.

[8] R. Billinton and R. N. Allan, Reliability Evaluation of Power Systems, 2nd ed. Plenum Press, 1994.

[9] CIGRE and IEEE Task Force, "Definition and Classification of Power System Stability," IEEE Transactions on Power Systems, vol. 19, no. 3, pp. 1387–1401, Aug 2004.

[10] R. Billinton and W. Li, Reliability Assessment of Electric Power Systems Using Monte Carlo Methods, 1st ed. Plenum Press, 1994.

[11] R. Billinton, R. Allan, I. Sjarief, L. Goel, and K. S. So, "A Reliability Test System for Educational Purposes - Basic Data," IEEE Transactions on Power Systems, vol. 6, no. 2, pp. 813–820, May 1991.

[12] Probability Methods Subcommittee, "IEEE Reliability Test System," IEEE Transactions on Power Apparatus and Systems, vol. PAS-98, no. 6, pp. 2047–2054, Nov 1979.

[13] Department of Energy & Climate Change, UK, "EMR Panel of Technical Experts' Final Report on National Grid's Electricity Capacity Report," 2015.

[14] A. Verma, S. Ajit, and D. Karanki, Reliability and Safety Engineering, 1st ed. Springer, 2010.

[15] R. Billinton and S. Kumar, "Indices for Use in Composite Generation and Transmission System Adequacy Evaluation," International Journal of Electrical Power & Energy Systems, vol. 12, no. 3, pp. 147–155, Jul 1990.

[16] R. Allan, "Power System Reliability Assessment - A Conceptual and Historical Review," Reliability Engineering & System Safety, vol. 46, no. 1, pp. 3–13, 1994.

[17] Power Systems Engineering Committee, "Reliability Indices for Use in Bulk Power Supply Adequacy Evaluation," IEEE Transactions on Power Apparatus and Systems, vol. PAS-97, no. 4, pp. 1097–1103, Jul 1978.

[18] W. Li and J. Zhou, "Probabilistic Reliability Assessment of Power System Operations," Electric Power Components and Systems, vol. 36, no. 10, pp. 1102–1114, Sep 2008.

[19] R. Billinton and R. N. Allan, Reliability Evaluation of Engineering Systems, 2nd ed. Plenum Press, 1992.

[20] R. Walpole, R. Myers, S. Myers, and K. Ye, Probability and Statistics for Engineers and Scientists, 9th ed. Pearson, 2012.

[21] S. Frank and S. Rebennack, "An Introduction to Optimal Fower Flow: Theory, Formulation, and Examples," IIE Transactions, vol. 48, no. 12, pp. 1172–1197, Aug 2016.

[22] B. Subhonmesh, S. Low, and K. Chandy, "Equivalence of Branch Flow and Bus Injection Models," in 50th Annual Allerton Conference on Communication, Control, and Computing, Oct 2012, pp. 1893–1899.

[23] H. Saadat, Power System Analysis, 3rd ed. PSA Publishing, 2010.

[24] W. Zhang, F. Li, and L. Tolbert, "Review of Reactive Power Planning: Objectives, Constraints, and Algorithms," IEEE Transactions on Power Systems, vol. 22, no. 4, pp. 2177 – 2186, Nov 2007.

[25] X. Yu and C. Singh, "Power System Reliability Analysis Considering Protection Failures," in IEEE Power Engineering Society Summer Meeting, vol. 2, 2002, pp. 963–968.

[26] W. Wangdee, "Bulk Electric System Reliability Simulation and Application," University of Saskatchewan, Saskatoon, 2005, PhD Thesis.

[27] R. Billinton and D. Huang, "Basic Concepts in Generating Capacity Adequacy Evaluation," in International Conference on Probabilistic Methods Appplied to Power Systems, 2006, pp. 1–6.

[28] V. Radziukynas and I. Radziukyniene, Optimization Methods Application to Optimal Power Flow in Electric Power Systems, 1st ed. Springer, 2009.

[29] Y. Zhang and Z. Ren, "Optimal Reactive Power Dispatch Considering Costs of Adjusting the Control Devices," IEEE Transactions on Power Systems, vol. 20, no. 3, pp. 1349 – 1356, Aug 2005.

[30] R. Billinton and W. Wangdee, "Impact of Load Shedding Philosophies on Bulk Electric System Reliability Analysis Using Sequential Monte Carlo Simulation," Electric Power Components and Systems, vol. 34, no. 3, pp. 355–368, 2006.

[31] L. Goel and R. Billinton, "A Procedure for Evaluating Interrupted Energy Assessment Rates in an Overall Electric Power System," IEEE Transactions on Power Systems, vol. 6, no. 4, pp. 1396 – 1403, Nov 1991.

[32] B. Leonardi and V. Ajjarapu, "Investigation of Various Generator Reactive Power Reserve (GRPR) Definitions for Online Voltage Stability/Security Assessment," in 2008 IEEE Power and Energy Society General Meeting - Conversion and Delivery of Electrical Energy in the 21st Century, 2008, pp. 1–7.

[33] R. Bayindir, S. Demirbas, E. Irmak, U. Cetinkaya, A. Ova, and M. Yesil, "Effects of Renewable Energy Sources on the Power System," in 2016 IEEE International Power Electronics and Motion Control Conference (PEMC), 2016, pp. 388–393.

[34] M. Benidris and J. Mitra, "Consideration of the Effects of Voltage and Reactive Power Constraints of Composite System Reliability," in 2014 North American Power Symposium (NAPS), Sep 2014, pp. 1–6.

[35] P. Noferi and L. Paris, "Effects of Voltage and Reactive Power Constraints on Power System Reliability," IEEE Transactions on Power Apparatus and Systems, vol. 94, no. 2, pp. 482–490, Mar 1975.

[36] W. Qin, P. Wang, X. Han, Y. Ding, and X. Du, "Reliability Assessment of Power Systems Considering Reactive Power Sources," in 2009 IEEE Power & Energy Society General Meeting, Jul 2009, pp. 1–7.

[37] F. Chen, H. Liu, J. Li, and Z. Huang, "Reactive Power Adequacy Assessment of Composite Power System Based on Interior Point Method and Genetic Algorithm," in 2016 International Conference on Probabilistic Methods Applied to Power Systems (PMAPS), Oct 2016, pp. 1–5.

[38] Reliability Test System Task Force, "IEEE Reliability Test System," IEEE Transactions on Power Apparatus and Systems, vol. PAS-98, no. 6, pp. 2047 – 2054, Nov 1979.

[39] C. R. Harris, K. J. Millman, S. J. van der Walt, R. Gommers, P. Virtanen, D. Cournapeau, E. Wieser, J. Taylor, S. Berg, N. J. Smith, R. Kern, M. Picus, S. Hoyer, M. H. van Kerkwijk, M. Brett, A. Haldane, J. Fernández del Río, M. Wiebe, P. Peterson, P. Gérard-Marchant, K. Sheppard, T. Reddy, W. Weckesser, H. Abbasi, C. Gohlke, and T. E. Oliphant, "Array programming with NumPy," Nature, vol. 585, p. 357–362, 2020.

[40] miscellaneous. (2021) concurrent.futures — Launching parallel tasks. Python Software Foundation. [Online]. Available: https://docs.python.org/3/library/concurrent.futures.html

[41] P. Virtanen, R. Gommers, T. E. Oliphant, M. Haberland, T. Reddy, D. Cournapeau, E. Burovski, P. Peterson, W. Weckesser, J. Bright, S. J. van der Walt, M. Brett, J. Wilson, K. J. Millman, N. Mayorov, A. R. J. Nelson, E. Jones, R. Kern, E. Larson, C. J. Carey, İ. Polat, Y. Feng, E. W. Moore, J. VanderPlas, D. Laxalde, J. Perktold, R. Cimrman, I. Henriksen, E. A. Quintero, C. R. Harris, A. M. Archibald, A. H. Ribeiro, F. Pedregosa, P. van Mulbregt, and SciPy 1.0 Contributors, "SciPy 1.0: Fundamental Algorithms for Scientific Computing in Python," Nature Methods, vol. 17, pp. 261–272, 2020.

[42] D. Kraft, "A Software Package for Sequential Quadratic Programming," DFVLR, Oberpfaffenhofen, 1988, Research report.

[43] miscellaneous. (2021, Feb) Optimization (scipy.optimize). SciPy. [Online]. Available: https://docs.scipy.org/doc/scipy/reference/tutorial/optimize.html#sequential-least-squares-programming-slsqp-algorithm-method-slsqp

[44] O. Gjernde. (2017, Jan) Electricity supply security – N-1 isn't always enough. Sintef. Trondheim. [Online]. Available: https://blog.sintef.com/sintefenergy/energy-systems/electricity-supply-security-n-1-isnt-always-enough/

[45] D. Gaikwad and S. Mehraeen, "Reactive Power Considerations in Reliability Analysis of Photovoltaic Systems," in 2012 IEEE Green Technologies Conference, Apr 2012, pp. 1–6.

[46] G. C. Ejebe and B. F. Wollenberg, "Automatic Contingency Selection," IEEE Transactions on Power Apparatus and Systems, vol. PAS-98, no. 1, pp. 97–109, Jan 1979.

[47] G. C. Ejebe, H. P. Van Meeteren, and B. F. Wollenberg, "Fast Contingency Screening and Evaluation For Voltage Security Analysis," IEEE Transactions on Power Systems, vol. 3, no. 4, pp. 1582–1590, Nov 1988.

Appendices

A Deduction of Equations for the Jacobian Matrices

A.1 Elements of the Jacobian Matrix for the Line Constraints

$$I_n = \Big(V_i \cdot \cos\delta_i - V_j \cdot \cos\delta_j\Big)^2 + \Big(V_i \cdot \sin\delta_i - V_j \cdot \sin\delta_j\Big)^2 - \Big(\frac{I_{ij}^{max}}{y_{ij}}\Big)^2 \tag{A.1}$$

$$\begin{aligned}
\frac{\partial I_n}{\partial V_i} &= 2\,cos(\delta_i) \cdot \big[V_i\,cos(\delta_i) - V_j\,cos(\delta_j)\big] + 2\,sin(\delta_i) \cdot \big[V_i\,sin(\delta_i) - V_j\,sin(\delta_j)\big] \\
&= 2\,\big[(V_i\,cos^2(\delta_i) - V_j\,cos(\delta_j)\,cos(\delta_i) + V_i\,sin^2(\delta_i) - V_j\,sin(\delta_j)\,sin(\delta_i)\big] \\
&= 2\,[\,V_i\,\underbrace{(cos^2(\delta_i) + sin^2(\delta_i))}_{1} - V_j\,\underbrace{(cos(\delta_j)\,cos(\delta_i) + sin(\delta_j)\,sin(\delta_i))}_{cos(\delta_i - \delta_j)}] \\
&= 2\,\big[V_i - V_j\,cos(\delta_i - \delta_j)\big]
\end{aligned} \tag{A.2}$$

$$\begin{aligned}
\frac{\partial I_n}{\partial V_j} &= -2\,cos(\delta_j)\,[V_i\,cos(\delta_i) - V_j\,cos(\delta_j)] + 2\,sin(\delta_j)\,[(V_i\,sin(\delta_i) - V_j\,sin(\delta_j)] \\
&= 2\,[V_j\,cos^2(\delta_j) - V_i\,cos(\delta_i)\,cos(\delta_j) - V_j\,sin^2(\delta_j) + V_i\,sin(\delta_i)\,sin(\delta_j)] \\
&= 2\,[\,V_j\,\underbrace{(cos^2(\delta_j) - sin^2(\delta_j))}_{cos(2\delta_j)} + V_i\,\underbrace{(sin(\delta_i)\,sin(\delta_j) - cos(\delta_i)\,cos(\delta_j))}_{-cos(\delta_i - \delta_j)}] \\
&= 2\,[V_j\,cos(2\delta_j) - V_i\,cos(\delta_i - \delta_j)]
\end{aligned} \tag{A.3}$$

$$\begin{aligned}
\frac{\partial I_n}{\partial \delta_i} &= -2\,V_i\,sin(\delta_i) \cdot \big[V_i\,cos(\delta_i) - V_j\,cos(\delta_j)\big] + 2\,V_i\,cos(\delta_i) \cdot \big[V_i\,sin(\delta_i) - V_j\,sin(\delta_j)\big] \\
&= 2\,V_i\,V_j\,[\cancel{-V_i^2\,cos(\delta_i)\,sin(\delta_i)} + cos(\delta_j)\,sin(\delta_i) + \cancel{V_i^2\,cos(\delta_i)\,sin(\delta_i)} - cos(\delta_i)\,sin(\delta_j)] \\
&= 2\,V_i\,V_j\,\underbrace{[cos(\delta_j)\,sin(\delta_i) - cos(\delta_i)\,sin(\delta_j)]}_{sin(\delta_i - \delta_j)} \\
&= 2\,V_i\,V_j\,sin(\delta_i - \delta_j)
\end{aligned} \tag{A.4}$$

$$
\begin{aligned}
\frac{\partial I_n}{\partial \delta_j} &= -2\,V_j\,sin(\delta_j)\cdot\left[V_i\,cos(\delta_i) - V_j\,cos(\delta_j)\right] + 2\,V_j\,cos(\delta_j)\cdot\left[V_i\,sin(\delta_i) - V_j\,sin(\delta_j)\right] \\
&= 2\,V_i\,V_j\,[\cancel{-V_j^2\,cos(\delta_j)\,sin(\delta_j)} + cos(\delta_i)\,sin(\delta_j) + \cancel{V_j^2\,cos(\delta_j)\,sin(\delta_j)} - cos(\delta_j)\,sin(\delta_i)] \\
&= 2\,V_i\,V_j\,\underbrace{[cos(\delta_i)\,sin(\delta_j) - cos(\delta_j)\,sin(\delta_i)]}_{sin(\delta_j - \delta_i)} \\
&= 2\,V_i\,V_j\,sin(\delta_j - \delta_i)
\end{aligned}
\tag{A.5}
$$

B HLII RPC Methodology

B.1 Bus Indices Ratio

Table B.1: *The $EENS_P$ from [2], the ratio between the bus $EENS_P$ and the cumulative system $EENS_P$, as well as the IEEE 30 Bus System share of load.*

Bus	$EENS_P$ [2] [MW/year]	$EENS_{Pi}/EENS_P^{tot}$ [2]	Share of Load
2	274.73	0.07295454	0.07657022
3	30.4	0.00807272	0.0084686
4	96.22	0.02555122	0.02681722
5	1194.05	0.31707991	0.33239238
7	289.01	0.07674659	0.08045166
8	380.39	0.10101254	0.10585745
10	73.43	0.01949933	0.02046577
12	141.8	0.03765498	0.03952011
14	78.6	0.02087223	0.02187721
15	103.82	0.02756939	0.02893437
16	44.57	0.01183556	0.01235004
17	114.46	0.03039485	0.03175723
18	40.68	0.01080257	0.01129146
19	120.93	0.03211295	0.03352152
20	27.93	0.00741681	0.00776288
21	224.89	0.05971953	0.06175018
23	40.7	0.01080788	0.01129146
24	110.15	0.02925033	0.03069866
26	208.51	0.05536982	0.01235004
29	31.48	0.00835951	0.0084686
30	139.03	0.03691941	0.03740296
Total	3765.77	1.000002655	1

C Load Data

Table C.1: *Weekly peak load in percent of annual peak [38].*

Week	Peak load [%]	Week	Peak load [%]
1	86.2	27	75.5
2	90.0	28	81.6
3	87.8	29	80.1
4	83.4	30	88.0
5	88.0	31	72.2
6	84.1	32	77.6
7	83.2	33	80.0
8	80.6	34	72.9
9	74.0	35	72.6
10	73.7	36	70.5
11	71.5	37	78.0
12	72.7	38	69.5
13	70.4	39	72.4
14	75.0	40	72.4
15	72.1	41	74.3
16	80.0	42	74.4
17	75.4	43	80.0
18	83.7	44	88.1
19	87.0	45	88.5
20	88.0	46	90.9
21	85.6	47	94.0
22	81.1	48	89.0
23	90.0	49	94.2
24	88.7	50	97.0
25	89.6	51	100.0
26	86.1	52	95.2

Table C.2: *Daily peak load in percent of weekly peak [38].*

Day	Peak load [%]
Monday	93
Tuesday	100
Wednesday	98
Thursday	96
Friday	94
Saturday	77
Sunday	75

Table C.3: *Hourly peak load in percent of daily peak [38].*

	Winter weeks 1-8 & 44-52		Summer weeks 18-30		Spring/Fall Weeks 9-17 & 31-43	
Hour	Weekday	Weekend	Weekday	Weekend	Weekday	Weekend
00-01	67	78	64	74	63	75
01-02	63	72	60	70	62	73
02-03	60	68	58	66	60	69
03-04	59	66	56	65	58	66
04-05	59	64	56	64	59	65
05-06	60	65	58	62	65	65
06-07	74	66	64	62	72	68
07-08	86	70	76	66	85	74
08-09	95	80	87	81	95	83
09-10	96	88	95	86	99	89
10-11	96	90	99	91	100	92
11-12	95	91	100	93	99	94
12-13	95	90	99	93	93	91
13-14	95	88	100	92	92	90
14-15	93	87	100	91	90	90
15-16	94	87	97	91	88	86
16-17	99	91	96	92	90	85
17-18	100	100	96	94	92	88
18-19	100	99	93	95	96	92
19-20	96	97	92	95	98	100
20-21	91	94	92	100	96	97
21-22	83	92	93	93	90	95
22-23	73	87	87	88	80	90
23-00	63	81	72	80	70	85

D RBTS Data

Table D.1: *The generator data for the RBTS [11].*

Capacity [MW]	Bus	Q_{min} [MVar]	Q_{max} [MVar]	FOR
10	1	0	7	0.020
20	1	-7	12	0.025
40	1	-15	17	0.030
40	1	-15	17	0.030
5	2	0	5	0.010
5	2	0	5	0.010
20	2	-7	12	0.015
20	2	-7	12	0.015
20	2	-7	12	0.015
20	2	-7	12	0.015
40	2	-15	17	0.020

Table D.2: *Bus specifications for the RBTS [11] including IEAR [30].*

Bus	Share of load	V_{min} [pu]	V_{max} [pu]	IEAR [$/kWh]	Priority
1	0	0.97	1.05	0	–
2	0.1081	0.97	1.05	9.6325	1
3	0.4595	0.97	1.05	4.3769	5
3	0.2162	0.97	1.05	8.0267	3
4	0.1081	0.97	1.05	8.6323	2
4	0.1081	0.97	1.05	5.5132	0

Table D.3: *Network parameters and outage data for the RBTS [11].*

Line	From	To	R [pu]	X [pu]	B/2 [pu]	Current rating [pu]	FOR
1	1	3	0.0342	0.18	0.0106	0.85	0.00171
2	2	4	0.1140	0.60	0.0352	0.71	0.00568
3	1	2	0.0912	0.48	0.0282	0.71	0.00455
4	3	4	0.0228	0.12	0.0071	0.71	0.00114
5	3	5	0.0228	0.12	0.0071	0.71	0.00114
6	1	3	0.0342	0.18	0.0106	0.85	0.00171
7	2	4	0.1140	0.60	0.0352	0.71	0.00568
8	4	5	0.0228	0.12	0.0071	0.71	0.00114
9	5	6	0.0228	0.12	0.0071	0.71	0.00114

E IEEE RTS Data

Table E.1: *Generator data for the IEEE RTS [38].*

Capacity [MW]	Bus	Q_{min} [MVar]	Q_{max} [MVar]	FOR
12	15	0	7	0.02
12	15	0	7	0.02
12	15	0	7	0.02
12	15	0	7	0.02
12	15	0	7	0.02
20	1	0	10	0.1
20	1	0	10	0.1
20	2	0	10	0.1
20	2	0	10	0.1
50	22	-10	16	0.01
50	22	-10	16	0.01
50	22	-10	16	0.01
50	22	-10	16	0.01
50	22	-10	16	0.01
50	22	-10	16	0.01
76	1	-25	30	0.02
76	1	-25	30	0.02
76	2	-25	30	0.02
76	2	-25	30	0.02
100	7	0	60	0.04
100	7	0	60	0.04
100	7	0	60	0.04
155	15	-50	80	0.04
155	16	-50	80	0.04
155	23	-50	80	0.04
155	23	-50	80	0.04
197	13	0	80	0.05
197	13	0	80	0.05
197	13	0	80	0.05
350	23	-25	150	0.08
400	18	-50	200	0.12
400	21	-50	200	0.12
0	14	-50	200	0
0	6	-100	0	0

Table E.2: *Bus specifications for the IEEE RTS [38] including IEAR [30].*

Bus	Share of load	V_{min} [pu]	V_{max} [pu]	IEAR [$/kWh]	Priority
1	0.038	0.97	1.05	8.9815	3
2	0.034	0.97	1.05	7.3606	5
3	0.063	0.97	1.05	5.8990	11
4	0.026	0.97	1.05	9.5992	1
5	0.025	0.97	1.05	9.2323	2
6	0.048	0.97	1.05	6.5238	9
7	0.044	0.97	1.05	7.0291	8
8	0.060	0.97	1.05	7.7742	4
9	0.061	0.97	1.05	3.6623	17
10	0.068	0.97	1.05	5.1940	14
11	0	0.97	1.05	0	–
12	0	0.97	1.05	0	–
13	0.093	0.97	1.05	7.2813	6
14	0.068	0.97	1.05	4.3717	16
15	0.111	0.97	1.05	5.9744	10
16	0.035	0.97	1.05	7.2305	7
17	0	0.97	1.05	0	–
18	0.117	0.97	1.05	5.6149	13
19	0.064	0.97	1.05	4.5430	15
20	0.045	0.97	1.05	5.6836	12
21	0	0.97	1.05	0	–
22	0	0.97	1.05	0	–
23	0	0.97	1.05	0	–
24	0	0.97	1.05	0	–

Table E.3: *Network parameters and outage data for the IEEE RTS [38].*

Line	From	To	R [pu]	X [pu]	B/2 [pu]	Current rating [pu]	FOR
1	1	2	0.0026	0.0139	0.23055	1.93	0.000438164
2	1	3	0.0546	0.2112	0.0286	2.08	0.000581853
3	1	5	0.0218	0.0845	0.01145	2.08	0.00037657
4	2	4	0.0328	0.1267	0.01715	2.08	0.000445007
5	2	6	0.0497	0.1920	0.0260	2.08	0.000547645
6	3	9	0.0308	0.1190	0.0161	2.08	0.000433602
7	3	24	0.0023	0.0839	0	5.1	0.001750356
8	4	9	0.0268	0.1037	0.01405	2.08	0.00041079
9	5	10	0.0228	0.0883	0.01195	2.08	0.000387977
10	6	10	0.0139	0.0605	1.2295	1.93	0.001316757
11	7	8	0.0159	0.0614	0.0083	2.08	0.000342349
12	8	9	0.0427	0.1651	0.02235	2.08	0.000502031
13	8	10	0.0427	0.1651	0.02235	2.08	0.000502031
14	9	11	0.0023	0.0839	0	5.1	0.001750356
15	9	12	0.0023	0.0839	0	5.1	0.001750356
16	10	11	0.0023	0.0839	0	5.1	0.001750356
17	10	12	0.0023	0.0839	0	5.1	0.001750356
18	11	13	0.0061	0.0476	0.04995	6	0.000502031
19	11	14	0.0054	0.0418	0.04395	6	0.000489486
20	12	13	0.0061	0.0476	0.04995	6	0.000502031
21	12	23	0.0124	0.0966	0.1015	6	0.000652542
22	13	23	0.0111	0.0865	0.0909	6	0.000614918
23	14	16	0.0050	0.0389	0.0409	6	0.000476941
24	14	16	0.0022	0.0173	0.0182	6	0.000414212
25	15	21	0.0063	0.0490	0.0515	6	0.000514575
26	15	21	0.0063	0.0490	0.0515	6	0.000514575
27	15	24	0.0067	0.0519	0.05455	6	0.000514575
28	16	17	0.0033	0.0259	0.02725	6	0.000439305
29	16	19	0.0030	0.0231	0.02425	6	0.000426758
30	17	18	0.0018	0.0144	0.01515	6	0.000401665
31	17	22	0.0135	0.1053	0.1106	6	0.000677623
32	18	21	0.0033	0.0259	0.02725	6	0.000439305
33	18	21	0.0033	0.0259	0.02725	6	0.000439305
34	19	20	0.0051	0.0396	0.04165	6	0.000476941
35	19	20	0.0051	0.0396	0.04165	6	0.000476941
36	20	23	0.0028	0.0216	0.02275	6	0.000426758
37	20	23	0.0028	0.0216	0.02275	6	0.000426758
38	21	22	0.0087	0.0678	0.0712	6	0.000564749

F IEEE 30-bus Data

Table F.1: *Generator data for the IEEE 30-bus system [2].*

Capacity [MW]	Bus	Q_{min} [MVar]	Q_{max} [MVar]	FOR
60	1	-20	25	0.02989984
60	1	-20	25	0.02989984
60	1	-20	25	0.02989984
60	1	-20	25	0.02989984
40	2	-20	20	0.02013423
40	2	-20	20	0.02013423
40	2	-20	20	0.02013423

Table F.2: *Synchronous condenser data for the IEEE 30-bus system [2].*

Capacity [MW]	Bus	Q_{min} [MVar]	Q_{max} [MVar]	FOR
0	5	-20	25	0.02989984
0	8	-10	25	0.02989984
0	11	-6	20	0.02989984
0	13	-6	20	0.02989984

Table F.3: *Shunt capacitor data for the IEEE 30-bus system [2].*

Capacity [MW]	Bus	Q_{min} [MVar]	Q_{max} [MVar]	FOR
0	5	0	12	0.02989984
0	8	0	12	0.02989984
0	10	0	10	0.02989984
0	11	0	10	0.02989984
0	13	0	10	0.02989984
0	24	0	2	0.02989984

Table F.4: *Bus specifications for the IEEE 30-bus [23].*

Bus	Share of load	V_{min} [pu]	V_{max} [pu]	IEAR [$/kWh]	Power Factor
1	0	0.9	1.05	10	–
2	0.076570219	0.9	1.05	10	0.585253456
3	0.008468596	0.9	1.05	10	0.5
4	0.026817219	0.9	1.05	10	0.210526316
5	0.332392378	0.9	1.05	10	0.201698514
6	0	0.9	1.05	10	–
7	0.080451658	0.9	1.05	10	0.478070175
8	0.105857445	0.9	1.05	10	1
9	0	0.9	1.05	10	–
10	0.020465773	0.9	1.05	10	0.344827586
11	0	0.9	1.05	10	–
12	0.039520113	0.9	1.05	10	0.669642857
13	0	0.9	1.05	10	–
14	0.021877205	0.9	1.05	10	0.258064516
15	0.028934368	0.9	1.05	10	0.304878049
16	0.012350035	0.9	1.05	10	0.514285714
17	0.031757234	0.9	1.05	10	0.644444444
18	0.011291461	0.9	1.05	10	0.28125
19	0.033521524	0.9	1.05	10	0.357894737
20	0.007762879	0.9	1.05	10	0.318181818
21	0.061750176	0.9	1.05	10	0.64
22	0	0.9	1.05	10	–
23	0.011291461	0.9	1.05	10	0.5
24	0.030698659	0.9	1.05	10	0.770114943
25	0	0.9	1.05	10	–
26	0.012350035	0.9	1.05	10	0.657142857
27	0	0.9	1.05	10	–
28	0	0.9	1.05	10	–
29	0.008468596	0.9	1.05	10	0.375
30	0.037402964	0.9	1.05	10	0.179245283

Table F.5: *Network parameters and outage data for the IEEE 30-bus [23].*

Line	From	To	R [pu]	X [pu]	B/2 [pu]	Current rating [pu]	FOR	Tap Setting
1	1	2	0.0192	0.0575	0.0264	1.3	0.00114025	1
2	1	3	0.0452	0.1852	0.0204	1.3	0.00114025	1
3	2	4	0.057	0.1737	0.0184	0.65	0.00114025	1
4	3	4	0.0132	0.0379	0.042	1.3	0.00114025	1
5	2	5	0.0472	0.1983	0.0209	1.3	0.00114025	1
6	2	6	0.0581	0.1763	0.0187	0.65	0.00114025	1
7	4	6	0.0119	0.0414	0.0045	0.9	0.00114025	1
8	5	7	0.046	0.116	0.0102	0.7	0.00114025	1
9	6	7	0.0267	0.082	0.0085	1.3	0.00114025	1
10	6	8	0.012	0.042	0.0045	0.32	0.00114025	1
11	6	9	0	0.208	0	0.65	0.00114025	0.978
12	6	10	0	0.556	0	0.32	0.00114025	0.969
13	9	11	0	0.208	0	0.65	0.00114025	1
14	9	10	0	0.11	0	0.65	0.00114025	1
15	4	12	0	0.256	0	0.65	0.00114025	0.932
16	12	13	0	0.14	0	0.65	0.00114025	1
17	12	14	0.1231	0.2559	0	0.32	0.0017094	1
18	12	15	0.0662	0.1304	0	0.32	0.0017094	1
19	12	16	0.0945	0.1987	0	0.32	0.0017094	1
20	14	15	0.221	0.1997	0	0.16	0.0017094	1
21	16	17	0.0824	0.1923	0	0.16	0.0017094	1
22	15	18	0.1073	0.2185	0	0.16	0.0017094	1
23	18	19	0.0639	0.1292	0	0.16	0.0017094	1
24	19	20	0.034	0.068	0	0.32	0.0017094	1
25	10	20	0.0936	0.209	0	0.32	0.0017094	1
26	10	17	0.0324	0.0845	0	0.32	0.00567537	1
27	10	21	0.0348	0.0749	0	0.32	0.00567537	1
28	10	22	0.0727	0.1499	0	0.32	0.00567537	1
29	21	22	0.0116	0.0236	0	0.32	0.00567537	1
30	15	23	0.1	0.202	0	0.16	0.00567537	1
31	22	24	0.115	0.179	0	0.16	0.0017094	1
32	23	24	0.132	0.27	0	0.16	0.0017094	1
33	24	25	0.1885	0.3292	0	0.16	0.0017094	1

Table F.6: *Network parameters and outage data for the IEEE 30-bus [23].*

Line	From	To	R [pu]	X [pu]	B/2 [pu]	Current rating [pu]	FOR	Tap Setting
34	25	26	0.2544	0.38	0	0.16	0.00567537	1
35	25	27	0.1093	0.2087	0	0.16	0.00567537	1
36	28	27	0	0.396	0	0.65	0.0017094	0.968
37	27	29	0.2198	0.4153	0	0.16	0.00567537	1
38	27	30	0.3202	0.6027	0	0.16	0.00567537	1
39	29	30	0.2399	0.4533	0	0.16	0.00567537	1
40	8	28	0.0636	0.2	0.0214	0.32	0.00567537	1
41	6	28	0.0169	0.0599	0.065	0.32	0.00567537	1

G Additional Results from the Standard HLII Case Study

G.1 Additional Results Using the RBTS

Table G.1: *CV of bus indices and system indices using the RBTS. Buses without load are not included.*

Bus	CV_{LOLE}	CV_{EENS}
3	0.0314	0.0429
4	0.9990	0.9990
5	0.4058	0.5611
6	0.0137	0.0148
System:	0.0123	0.0140

G.2 Additional Results Using the IEEE RTS

Table G.2: *CV of bus indices and system indices using the IEEE RTS. Buses without load are not included.*

Bus	CV_{LOLE}	CV_{EENS}
1	0.0462	0.2244
2	0.0507	0.2696
3	0.0546	0.2756
4	0.0570	0.4310
5	0.0557	0.2969
6	0.0239	0.0321
7	0.0238	0.0274
8	0.0574	0.5520
9	0.0126	0.0152
10	0.0492	0.1427
13	0.0556	0.4836
14	0.0210	0.0278
15	0.0550	0.4327
16	0.0560	0.4659
18	0.0524	0.3695
19	0.0351	0.0591
20	0.0559	0.5859
System:	0.0099	0.0147

H Additional Results from the HLII RPC Case Study

H.1 Case 1

Table H.1: *SD for bus and system indices for HLII RPC utilising the IEEE 30-bus system.*

Bus	SD_{EENS_P}	SD_{EENS_Q}	SD_{EVarS}
1	–	–	0
2	3.1024	0	0
3	0.4689	0	0
4	2.4535	0	0
5	68.8574	0	0
6	–	–	0
7	11.1662	0.0115	0.1979
8	20.8063	0.0452	0
9	–	–	0
10	9.1513	0	0
11	–	–	0
12	1.3593	0.0042	0.0004
13	–	–	0.0005
14	8.6731	0.1996	0.3079
15	4.8850	0.0177	0.7813
16	1.0573	0.0187	0.0001
17	2.4567	0.1232	1.8685
18	5.1613	0.1155	1.2671
19	5.1451	0.4221	1.0816
20	3.0520	0.1540	0.3512
21	6.7837	0.7178	0.5047
22	–	–	0.0019
23	1.1622	0.3321	0.6041
24	1.1155	0.2767	0.1376
25	–	–	0.6694
26	15.4456	1.0517	0.4387
27	–	–	0.4513
28	–	–	1.6373
29	4.7913	2.0409	1.2979
30	35.4517	6.7481	3.7086
System:	115.8932	7.7771	5.6963

Table H.2: *CVs for bus and system indices. CV_{EVNS_P} and CV_{EVNS_Q} not included as they are the same as CV_{EENS_P} and CV_{EENS_Q}, respectively.*

Bus	CV_{EENS_P}	CV_{EENS_Q}	CV_{EVarS}
1	–	–	–
2	0.1455	–	–
3	0.1380	–	–
4	0.0643	–	–
5	0.0188	–	–
6	–	–	–
7	0.0405	0.9990	0.7060
8	0.0124	0.7096	–
9	–	–	–
10	0.0215	–	–
11	–	–	–
12	0.1867	0.7058	0.7914
13	–	–	0.9892
14	0.0197	0.5024	0.7628
15	0.0384	0.7018	0.6101
16	0.1025	0.5566	0.6704
17	0.0919	0.2976	0.4062
18	0.0176	0.7037	0.5021
19	0.0396	0.3443	0.3912
20	0.0223	0.4114	0.6258
21	0.0739	0.1483	0.1759
22	–	–	0.9560
23	0.0781	0.2733	0.5862
24	0.0837	0.3012	0.4073
25	–	–	0.9990
26	0.0063	0.0844	0.2287
27	–	–	0.8380
28	–	–	0.0971
29	0.0138	0.0243	0.1459
30	0.0086	0.0185	0.0225
System:	0.0081	0.0165	0.0270

Table H.3: *$EENS_P$, $EENS_Q$ and $EVarS$ when no additional shunt capacitors are added to Buses 5, 8, 10, 11, 13 and 24.*

Bus	$EENS_P$ [MWh/year]	$EENS_Q$ [MWh/year]	$EVarS$ [MVarh/year]
1	–	–	0
2	0.6548	0	0
3	0.1137	0	0
4	3.1801	0	0
5	244.6468	0.7074	0.7556
6	–	–	0
7	2.9434	0.57856	0.5468
8	138.7630	0.0832	0.0023
9	–	–	0
10	18.6345	0.0068	0.1052
11	–	–	0
12	1.3842	0.5506	0.2041
13	–	–	0.0217
14	30.9863	0.9029	1.0271
15	13.8646	0.3668	0.4035
16	1.2306	0.1176	0.1087
17	3.3388	2.4011	3.6753
18	21.5341	2.7889	9.8239
19	39.5727	17.0026	17.7232
20	10.2563	1.9527	3.2843
21	11.4587	12.0434	10.1778
22	–	–	1.8662
23	2.6334	5.8867	6.8353
24	7.2592	27.8410	29.8001
25	–	–	2.2122
26	102.7726	33.6665	50.7905
27	–	–	0.3550
28	–	–	2.2822
29	21.2521	16.8898	14.9458
30	270.5045	113.3670	79.7793
System:	946.9844	237.1535	236.7263

H.2 Case 3

Table H.4: *EVarS when adding compensators of 2 MVar and 4 MVar, using the IEEE 30-Bus system in HLII RPC assessment.*

Bus	Case 1		+2 MVar		+4 MVar	
	$EVarS$ [MVarh/year]	$EENS_Q$ [MVarh/year]	$EVarS$ [MVarh/year]	$EENS_Q$ [MVarh/year]	$EVarS$ [MVarh/year]	$EENS_Q$ [MVarh/year]
1	0	0	0	0	0	0
2	0	0	0	0	0	0
3	0	0	0	0	0	0
4	0	0	0	0	0	0
5	0	0	0	0.0001	0	0
6	0	–	0	–	0	–
7	0.0125	0.0005	0.0180	0.0086	0.0076	0.0072
8	0	0.0029	0	0	0	0.0005
9	0	–	0	–	0	–
10	0	0	0	0	0	0
11	0	–	0	–	0	–
12	0	0.0003	0	0.0002	0.0025	0.0001
13	0	–	0	–	0	–
14	0.0181	0.0178	0.0042	0.0087	0.0076	0.0103
15	0.0573	0.0011	0.0001	0.0003	0.0103	0.0011
16	0	0.0015	0.0005	0.0009	0.0033	0.0021
17	0.2057	0.0185	0.0449	0.0309	0.2617	0.0159
18	0.1129	0.0073	0.0064	0.0052	0.0989	0.0051
19	0.1237	0.0548	0.0481	0.0309	0.0363	0.0436
20	0.0251	0.0167	0.0029	0.0062	0.0028	0.0014
21	0.1283	0.2164	0.1135	0.2085	0.0862	0.1341
22	0.0001	–	0	–	0.0002	–
23	0.0461	0.0544	0.0134	0.0397	0.0120	0.0328
24	0.0151	0.0411	0.0044	0.0063	0.0493	0.0088
25	0.0300	–	0.0010	–	0.0109	–
26	0.0858	0.5570	0.1517	0.2509	0.1154	0.1759
27	0.0241	–	0	–	0.0028	–
28	0.7538	–	0.5940	–	0.4247	–
29	0.3977	3.7596	0.0903	0.6101	0.0119	0.2784
30	7.3850	16.3157	1.3415	3.1075	0.0208	0.7172
System:	9.4212	21.0646	2.44367	4.3147	1.1651	1.4345

I Software Codes

(Restricted Public Access)

Ingvild G. Birkeland and Kristian Bjørgve

Reactive Power Considerations in Reliability Assessment of Power Systems

NTNU
Norwegian University of
Science and Technology